UNIVERSITY OF OKLAHOMA

GRADUATE COLLEGE

SIMULATING CO_2 SEQUESTRATION IN THE ARBUCKLE GROUP OF OKLAHOMA AND EXPLORING THE EXTENT OF APPLICABILITY OF AN ANALYTICAL MODEL IN PREDICTING PRESSURE BUILDUP

A THESIS

SUBMITTED TO THE GRADUATE FACULTY

In partial fulfillment of the requirements for the

Degree of

MASTER OF SCIENCE

By

AYOMIDE ABDULQUADRI HAMZAT

Norman, Oklahoma

2023

SIMULATING CO_2 SEQUESTRATION IN THE ARBUCKLE GROUP OF OKLAHOMA AND EXPLORING THE EXTENT OF APPLICABILITY OF AN ANALYTICAL MODEL IN PREDICTING PRESSURE BUILDUP

A THESIS APPROVED FOR THE MEWBOURNE SCHOOL OF PETROLEUM ENGINEERING

BY THE COMMITTEE CONSISTING OF

Dr. Rouzbeh G. Moghanloo, Chair

Dr. Deepak Devegowda, Member

Dr. Xingru Wu, Member

To Allah, Family, Friends, and the Love of my life, through whom I persevered even in the toughest times.

Acknowledgments

I would like to give thanks to my research advisor, Dr. Rouzbeh Moghanloo, for taking me on when I was far from the finished product. His guidance and advice have constantly propelled me to do more work and always strive for excellence. I also want to thank members of the Carbon Utilization and Storage Partnership (CUSP) through whom I gained lots of useful insights in completing this work. I would also like to express gratitude to Dr. Deepak Devegowda and Dr. Xingru Wu for their time and support in the course of completing this thesis.

Special thanks and gratitude are reserved for Dr. Catalin Teodoriu and Dr. Ahmed Ramadan under whom I worked as a Teaching and Research Assistant during my time at the Mewbourne School of Petroleum and Geological Engineering (MPGE). I appreciate all other members of the faculty including but not limited to Katie Shapiro and Sonya Grant.

I also reserve thanks for Dr. Simon Mathias of the University of Durham who responded to me timely when I required some guidance as to how to employ his analytical models.

Lastly, I want to thank members of my family at home and abroad for all the guidance, prayers, and support they provided. As for my partner, Odunayo Faro, my roommate David Nnamdi, and the great friends I made at OU (especially the Nigerian Community), it is difficult to see how I reach the end of this journey without all of you, and I extend all the gratitude in me to each of you.

Table of Contents

List of Figures

List of Tables

Abstract

This thesis presents the groundwork for a proposed CO_2 sequestration project in Osage County, Oklahoma. It describes the flow simulation of the CO_2 plume in the saline aquifer of the Arbuckle Group, a dolomite formation, proposed as a potential large-scale storage reservoir for CO_2 in the state of Oklahoma. Geological storage of CO_2 is one of the most potent tools today in reducing atmospheric CO_2 and battling climate change. With governments around the world putting policies in place to significantly reduce carbon emissions within the next two decades, there is an expectation for more CO_2 sequestration projects across the world.

This study used Milad et al.'s (2022) geological model that was built by integrating core data and well logs in estimating stratigraphic and petrophysical properties of the formation. A black-oil model with 1 injection well was successfully built to simulate injection for 30 years. Local grid refinement was used around the injection well to improve the level of detail and accuracy of the model in this region. The formation was divided into 10 layers and the injection well was perforated in the bottom four (4) layers of the structure. These layers were selected based on the depth of existing injection wells in the region, some of which are intended to be remodeled for use should the project kick-off. The layers also had a good permeability distribution thus making it suitable for large-scale CO_2 injection at low pressure. Pressure management is important in CO_2 storage because adding large volumes of CO_2 to a reservoir without any fluid removal mechanism runs the risk of potentially rupturing cap-rock seals or generating flow through faults that would otherwise restrict flow. The pressure buildup and CO_2 plume evolution in the 50 years post-injection was also observed, recorded, and analyzed.

The analytical model for predicting pressure buildup developed by Mathias et al. (2011b) was also explored to determine the extent of its applicability. In carrying this out, a single well cylindrical CMG model with specified values of the reservoir properties was built to meet all the assumptions made in the analytical method. The reservoir pore volume was then altered by changing the radial extent of the reservoir to see how well the analytical model performed when compared to a corresponding CMG GEMS model at different injection/pore volume ratios.

After 30 years of injection, the CO_2 plume covered an area of 5827 acres of the 1.2 million acres of the Osage Arbuckle, (less than 0.5%). The dominant CO_2 trapping mechanism was structural trapping with increased residual trapping at the end of injection. Sensitivity analysis revealed that injection had to be carried out with the maximum bottom hole pressure at least 80% of the reservoir fracture pressure and no less than 96 mD permeability to meet the required injection of 50 million metric tons of CO_2. It was observed that the analytical pressure buildup model performed well when the ratio of injected reservoir volume to the pore volume was less than 0.1%. Beyond this number, the slope of the pressure buildup curve calculated analytically deviated from the slope of the corresponding CMG GEMS model. With the aid of a correction factor applied to the time variable, this variation could be corrected.

This thesis provides a reference that would be useful during potential deployment of CO_2 injection in the Arbuckle Group while providing more insight into the use of an analytical model in predicting pressure buildup. It also provides slope correcting factors that could be used in applying the analytical model when the ratio of injected reservoir volume to pore volume in this system exceeds 0.1%. This study could assist decision making during field development in Arbuckle as we work to ensure a sustainable future.

Chapter 1: Introduction

CO_2 is an important part of daily life, plants rely on it to grow, and humans use it in many ways to manufacture food and utilities. It is also a major byproduct of fossil fuel production and utilization and contributes to today's global warming. This is mostly because the degree of utilization of CO_2 exceeds its production, causing a net positive in atmospheric CO_2 material balance. The dilemma today is that addressing climate concerns without compromising ready access to energy is difficult. Global energy demand is expected to rise by 15% by the year 2050 amidst increased development in the global south (ExxonMobil, 2022), and sustaining energy supply to meet this demand at an affordable cost while preserving the environment is paramount. One common method of reducing atmospheric CO_2 is storing it geologically in a process known as CO_2 sequestration.

Oklahoma has significant potential for CO_2 sequestration, and the Arbuckle Group stands out as a potential storage site due to its confined nature. It covers a large part of Oklahoma and mainly comprises dolomite, limestones, and carbonates (Rottmann, 2018). The study was carried out with the Arbuckle Group of the Osage Reservation as the primary area of interest.

1.1 CO_2 and Climate Change

CO_2 is a greenhouse gas, which means it has a greenhouse effect such that it traps heat within the earth. CO_2 is essential for human life, as it is why the earth is not cold enough to freeze all life. As the saying goes, however, too much of everything is not good as excessive atmospheric CO_2 has caused a rapid increase in global temperatures, threatening human existence in a phenomenon known as "Global Warming". Global warming is the main source of climate change today.

The United Nations (2023) defines climate change as long-term shifts in temperature and weather patterns due to natural evolution or human activities. Since the 1800s, climate change has

however seen its main driver switch significantly from nature to human activities owing largely to the burning of fossil fuels like oil, gas, and coal that release CO_2 into the atmosphere (United Nations, 2023). The National Oceanic and Atmospheric Administration has been tracking atmospheric CO_2 levels at their Mauna Loa Observatory in Hawaii and Fig. 1 below shows that atmospheric CO_2 levels have increased by over 80 ppm since the turn of the millennium, with current levels around 420 ppm. In the same time period, global GDP has increased by over 100 trillion USD.

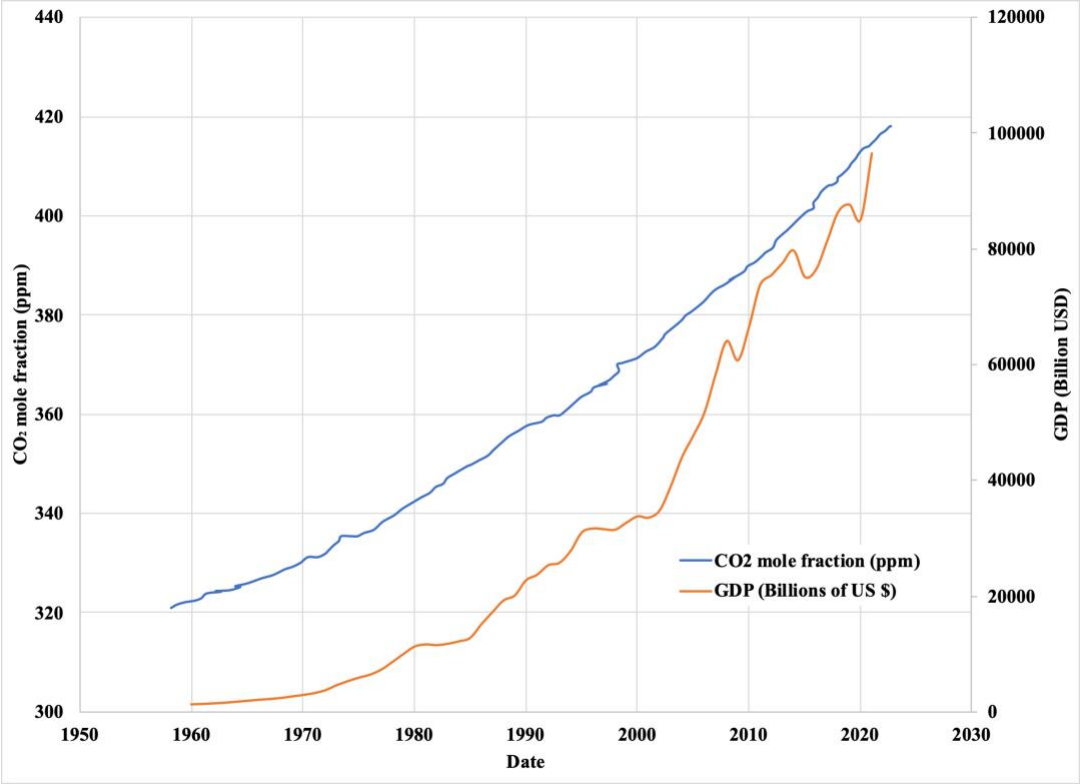

Figure 1: Mauna Loa CO_2 records from 1960 till date (NOAA, 2023) vs world GDP growth in the same period.

The effects of climate change range from rising ocean levels to species extinction. In January 2023, California saw a year's worth of rain in two weeks causing devastating loss of life and property. There has also been an uptick in the spread of wildfires in the western part of the country.

While there is evidence to back up the fact that the increase in ocean CO_2 levels has also contributed to the effects of global warming, as seen in Fig. 2, the onus is on the energy sector to do its part in helping to save the environment from the negative effects of climate change.

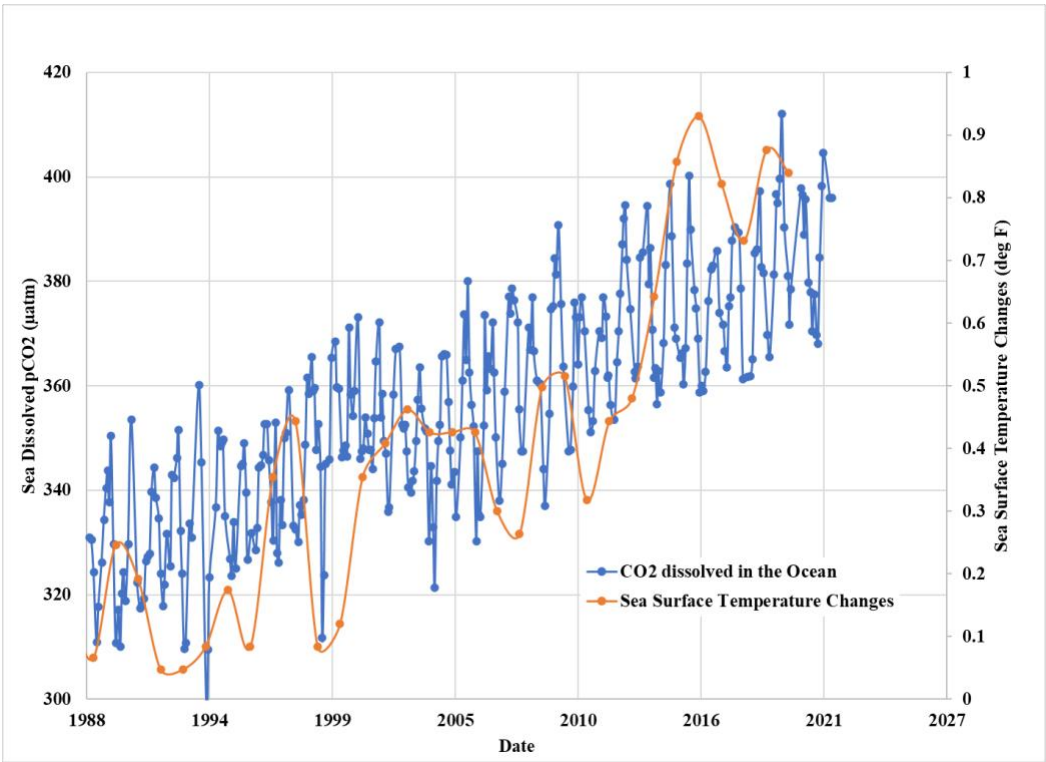

Figure 2: Comparison of Sea CO_2 levels to Sea Surface Temperature Levels (Data from EPA (2023) and Hawaii Ocean Time-Series (2023))

With rising temperatures and CO_2 emissions, different mechanisms have been developed to slow the rise of atmospheric CO_2. Some of these methods include the slow but gradual embracement of electrically powered motor vehicles over their fossil-fueled counterparts, larger scale deployment of wind farms to generate household electricity over the use of gas, CO_2 enhanced oil recovery that sought to create a net-zero oil and gas production system and CO_2 sequestration by geological storage. Of all these methods, geological storage of CO_2 is the most promising as geological formations can in theory, remove higher volumes of CO_2 than any other method.

1.2 CO_2 Geological Storage Mechanisms

CO_2 is stored in a variety of ways including as compressed gas, liquid, or in a supercritical phase. The storage mechanism is mostly dependent on the reservoir condition (Hamzat et al., 2022).

Most CO_2 is initially stored hydrodynamically (Hydrodynamic or Structural trapping). This means the gas is trapped in a mobile phase that can move laterally or upwardly towards the caprock (Zhang and Song, 2014).

Some gas is trapped as residues in what is known as residual or capillary trapping. Residual trapping usually occurs when formation water breaks through the CO_2 plume (Mo et al., 2005). CO_2 displaces brine at the start of injection in a co-current manner but on completion of injection, liquid starts to flow counter-currently, causing the brine to fall downwards because it has a higher density than the gas. This leads to significant amounts of gas being trapped in small clusters of pores.

In the storage of CO_2 in saline aquifer, some of the gas is partially dissolved in the aqueous phase in a process known as solubility trapping (Mo et al., 2005). CO_2 dissolves in water to form carbonated water. This carbonated water is denser than the water itself (Alzayer et al., 2022). The solubility of CO_2 in brine is dependent on salinity, temperature and pressure and the process is typically very slow because the gas has a very small molecular diffusion coefficient (Zhang and Song, 2014).

Mineral trapping of CO_2 occurs when carbonated water reacts with the rocks in formation to deposit minerals on the rock surface. This process takes a very long time to happen (usually hundreds to thousands of years). It is widely known to be the most secure storage system, but it could be detrimental if the reactions enhance CO_2 migration (Alzayer et al., 2022).

1.3 Geologic Setting

The storage geology is comprised of two porous rocks of the Arbuckle Group and the Simpson Group. These groups have two possible confining zones, the Woodford Shale, and the Lower Mississippian Limestone (Fig. 3). The Arbuckle Group is, however, the primary storage reservoir as it was previously confirmed for geological CO_2 storage in Kansas state (Holubnyak et al., 2017). It has also been used for wastewater disposal in the state of Oklahoma over the years (Milad et al., 2022), receiving about 68% of the total saltwater injected in Oklahoma subsurface (Murray, 2015).

The Arbuckle Group is mostly shallow shelf carbonates that were deposited during the Cambrian to early Ordovician age (Johnson, 1991). Its lithology is predominantly dolomite and limestone (Rottmann et al., 2015). It has an aerial extent that spreads across most of Oklahoma and adjacent states like Kansas (Ching and Friedman, 2000). Oklahoma's Arbuckle is comprised of six formations including the West Spring Creek Formation at the top, the Kindblade formation, the Cool Creek formation, the McKenzie Hill formation, the Signal Mountain and the Fort Still formation at the base (Ragland and Donovan, 1991).

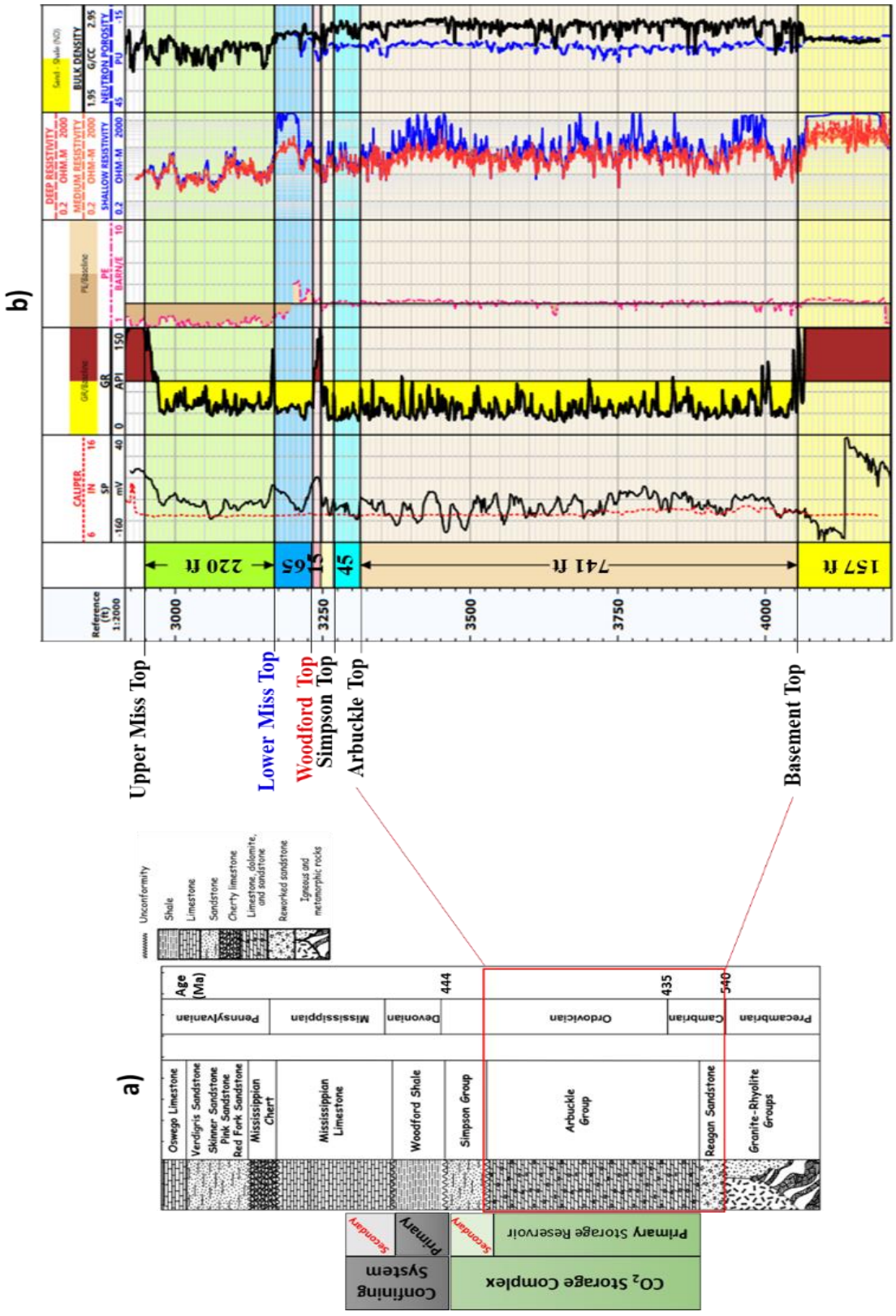

Figure 3: Stratigraphic column and Stratigraphic type log for the Osage Reservation indicating the storage complex and confining zones for the Arbuckle Group (Milad et al., 2022)

The Arbuckle Group makes up the middle southern section of the Great American Carbonate Bank (GACB) and is mostly composed of cyclic carbonates with intertidal and shallow subtidal facies (Fritz et al., 2013).

The Arbuckle Group's thickness ranges from about 1000ft to 2000ft in the Anadarko Shelf to 7000ft in the Anadarko Basin, Ardmore Basin, and Arbuckle Uplift (Johnson 1991, 2008) with the top of the Arbuckle as deep as 30,000 ft below land surface in the Anadarko Basin (Morgan and Murray, 2015).

There are some unconformities within the Arbuckle because the dolomites have been prone to dissolving over periods of uplift and erosion. The Arbuckle Group has extensive karstic features. Due to the recurrent surface exposure of the north-south marine regression sequences, some solution-collapse breccia formed, predominantly in the Arbuckle Group's upper section (Wilson, 1994). The matrix porosity and permeability were significantly influenced by these karst features (Milad et al., 2018).

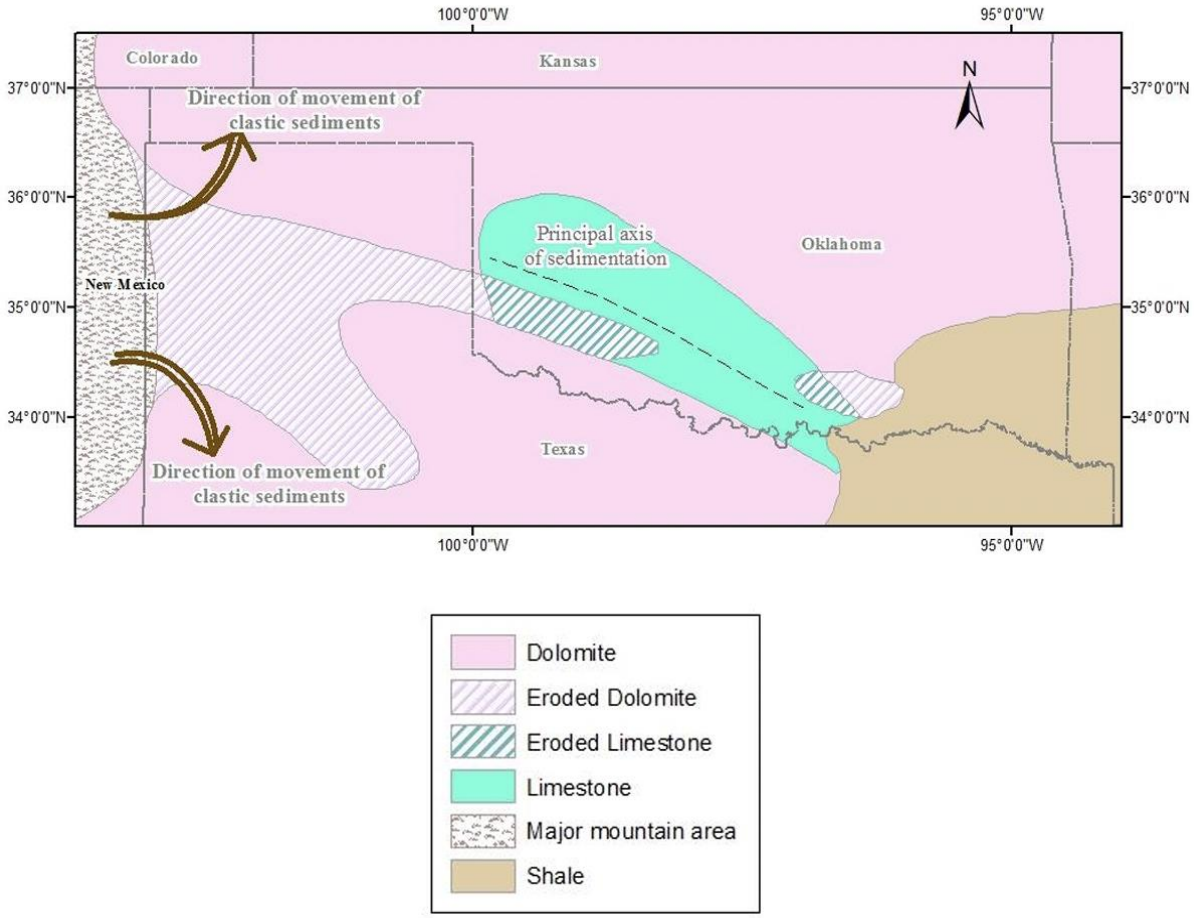

Figure 4: Rock Types of Late Cambrian to Early Ordovician age (Perilla-Castillo, 2017; Modified from Johnson, 2008)

1.4 Study Area

The area of study is the Osage Reservation in north-eastern Oklahoma on the Cherokee platform. The Cherokee platform is bounded by the Ozark uplift from the northeast and the Nemaha uplift from the northwest (Milad et al., 2022). The injection site for CO_2 was in the North Burbank Region in northwestern Osage operated by CapturePoint LLC. Fig. 6 shows nearby CO_2 sources to the area of study, showing the area's viability for potential CO_2 storage.

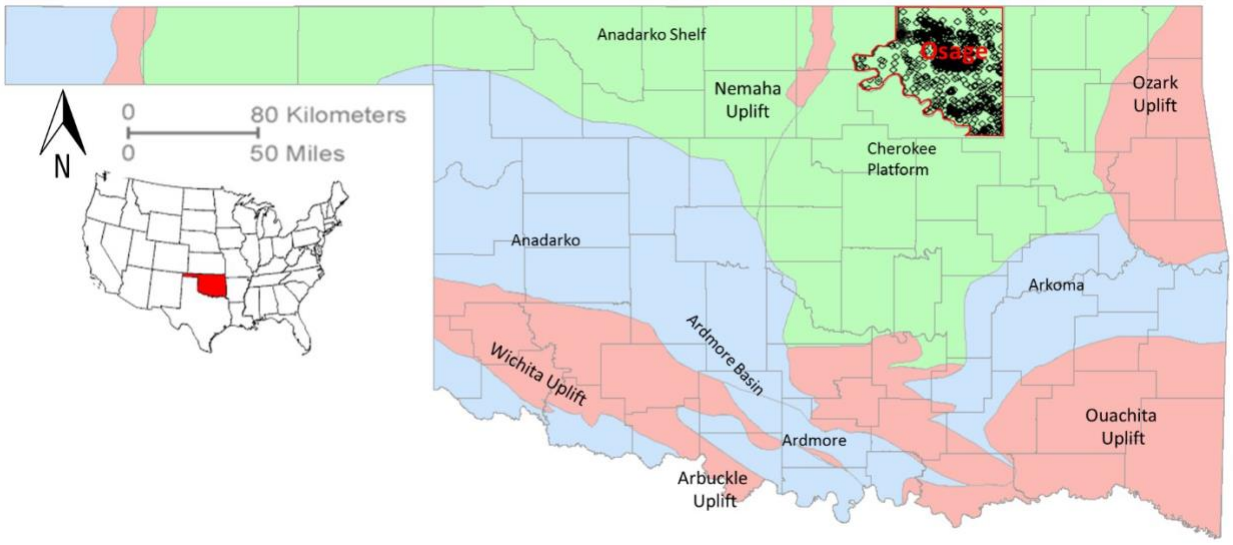

Figure 5: Map showing the major geological provinces in Oklahoma. The red polygon indicates the Osage area of study. (Milad et al., 2022)

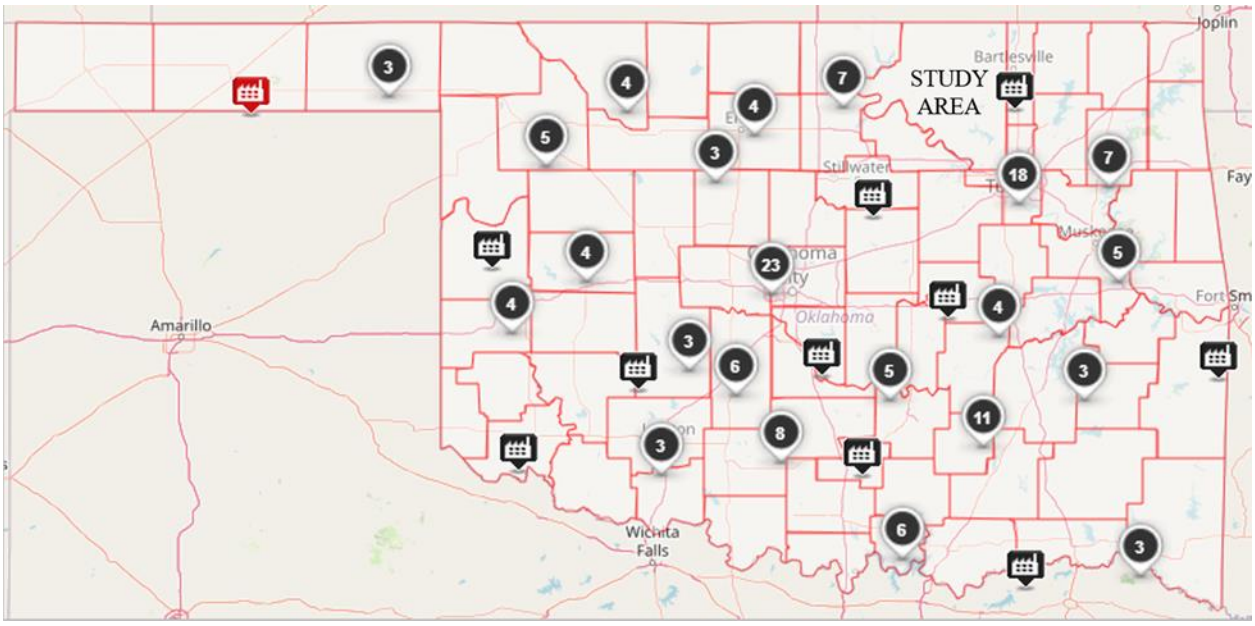

Figure 6: Map showing CO_2 sources near Osage area of study. (Environmental Protection Agency, 2021)

1.5 Research Objectives

CO_2 sequestration was simulated in the Arbuckle group using data from work done by Milad et al. (2022), data provided by CapturePoint LLC, and data available in literature. The Department of Energy has set a requirement of 50 million metric tons of CO_2 for any Phase III and

Phase IV project funding. The evolution of the CO_2 plume and pressure was observed and analyzed given some operational constraints such as proximity to Underground Sources of Drinking Water (USDW) and the reservoir fracture pressure. Some of the objectives of this study were to:

1. Build a numerical simulation model using CMG for CO_2 sequestration in the Osage Reservation Arbuckle Group, modelling structural, solubility and residual trapping.
2. Carry out sensitivity analysis on maximum injection pressure, average reservoir permeability and number of injection wells.
3. Carry out Environmental Impact Assessment (EIA) by comparing proximity of CO_2 plume to USDW.
4. Analyze pressure buildup from continuous injection of CO_2 at a fixed injection rate.
5. Determine the extent of applicability of analytical models developed by Mathias et al. (2011b) for estimating pressure buildup.

This study will help minimize uncertainties associated with storage capacity and injectivity of CO_2 in the Osage Arbuckle Group and provide the right set of parameters to model the pressure buildup in this formation analytically. The sensitivity analysis on bottomhole pressure will help determine the maximum operating bottomhole pressure given the reservoir permeabilities for the injection of 50 million metric tons of CO_2. The study will also help determine the degree to which analytical model of Mathias et al. (2011b) can be used and provide modifications where necessary.

Chapter 2: Literature Review

Due to widespread interest among the public, government, and industry, CO_2 sequestration has been the subject of substantial research over time.

2.1 Geological Carbon Storage (Sequestration)

Finding solutions to reduce greenhouse gas emissions is becoming increasingly crucial as the amount of CO_2 in the atmosphere rises as a result of combustion emissions. Sequestering carbon is one method for doing that. Since the 1920s, the method has been used to separate CO_2 from marketable methane gas in natural gas reservoirs (IEAGHG, 2022). When collected CO_2 was injected into an oil field in Texas to increase productivity from the formation, this idea gained greater traction and became known as enhanced oil recovery (EOR) in the conventional oil and gas business (Battelle, 2018). However, due to its ability to significantly reduce greenhouse gas emissions, carbon sequestration has recently grown in favor. Fig. 7 below shows a general classification of the types of geologic formation for CO_2 sequestration, including shales, saline aquifers, unmineable coal beds, and depleted oil and gas reservoirs.

Perhaps the most promising geologic storage locations for CO_2 are saline aquifers of which the Osage Arbuckle group is one of them. Any CO_2 sequestration project's primary objective is usually to store CO_2 for a very long time. Because injected CO_2 tends to migrate higher since it is less dense than the water in the aquifer, monitoring the CO_2 plume is crucial when storing CO_2 in aquifers (Barrufet, Bacquet, & Falcone, 2010).

The main difficulties with storing CO_2 in aquifers are brine migration and stress changes brought on by pressure increases from sequestration. According to Bandilla et al. (2015), stress

shifts can lead to fault reactivation, enhanced seismicity, formation or caprock fracturing, or surface elevation.

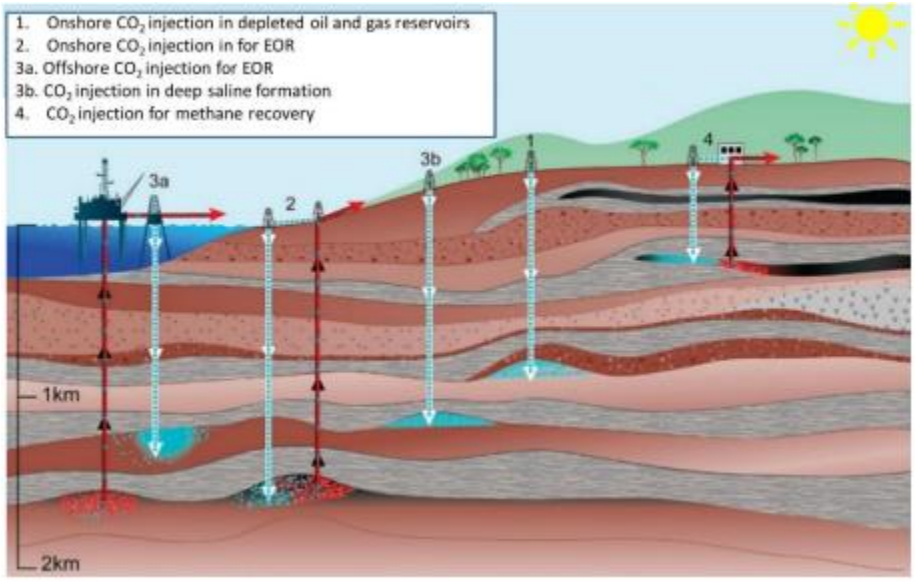

Figure 7: Overview of Geologic Carbon Sequestration. (Ochie, 2022); Modified from (Intergovernmental Panel on Climate Change, 2005

CO_2 can also be stored in hydrocarbon reservoirs since they have in fact stored hydrocarbons for long geological periods. This is significant because CO_2 storage projects can benefit from knowledge gotten from past exploration, exploitation, and production (Chidambaram et al., 2021). Storage in hydrocarbon reservoirs can be done using EOR, which is more popular because it makes money once it is put into use and was being done before CO_2 sequestration was even a viable option for dealing with large CO_2 emissions. Storage could also be done in depleted reservoirs, which is a relatively newer technology (Ochie, 2022).

There is also the option of geological storage in coal beds. CO_2 sequestration in non-mineable coal seams is of interest because of the ability to concurrently recover methane while storing the CO_2 (Gorucu, et al., 2005). This results in decreasing atmospheric CO_2 concentrations while reducing the associated costs of handling CO_2 during methane production. Producing methane is also a source of CO_2 emissions, hence planning for sequestration is also beneficial to

the environment. To study CO_2 storage capacity in coalbed reservoirs, adsorption, and desorption experiments of coal rocks from different regions and coal ranks need to be conducted (Jiang, Dou, Shen, & Sun, 2015).

Despite their abundance, shales are not as widely used for CO_2 storage as other geologic storage sites because they often have very low permeabilities and lack the same level of field development. Fakher et al. (2020) and Fakher & Imqam (2020) highlighted the benefit of using shales to store CO_2 by assuming that absorption is the primary mechanism for storage and by displaying the absorption capacities of several shale plays under various thermodynamic circumstances.

Different storage geologies have different CO_2 trapping mechanisms but as mentioned in the Chapter 1 and earlier in this section, our geologic setting is the Osage Arbuckle Group of Oklahoma which is a deep saline aquifer which traps CO_2 using a combination of structural trapping, solubility trapping, residual trapping, and mineral trapping.

2.2 Life Cycle for CO_2 Storage Project Development

Most storage projects have the following five life cycle phases, according to the Plains CO_2 Reduction (PCOR) Partnership Adaptive Management Approach (AMA):

1. Site selection,
2. Feasibility analysis,
3. Design,
4. Construction and Operation,
5. Closure and Post-closure (Ayash et al., 2016).

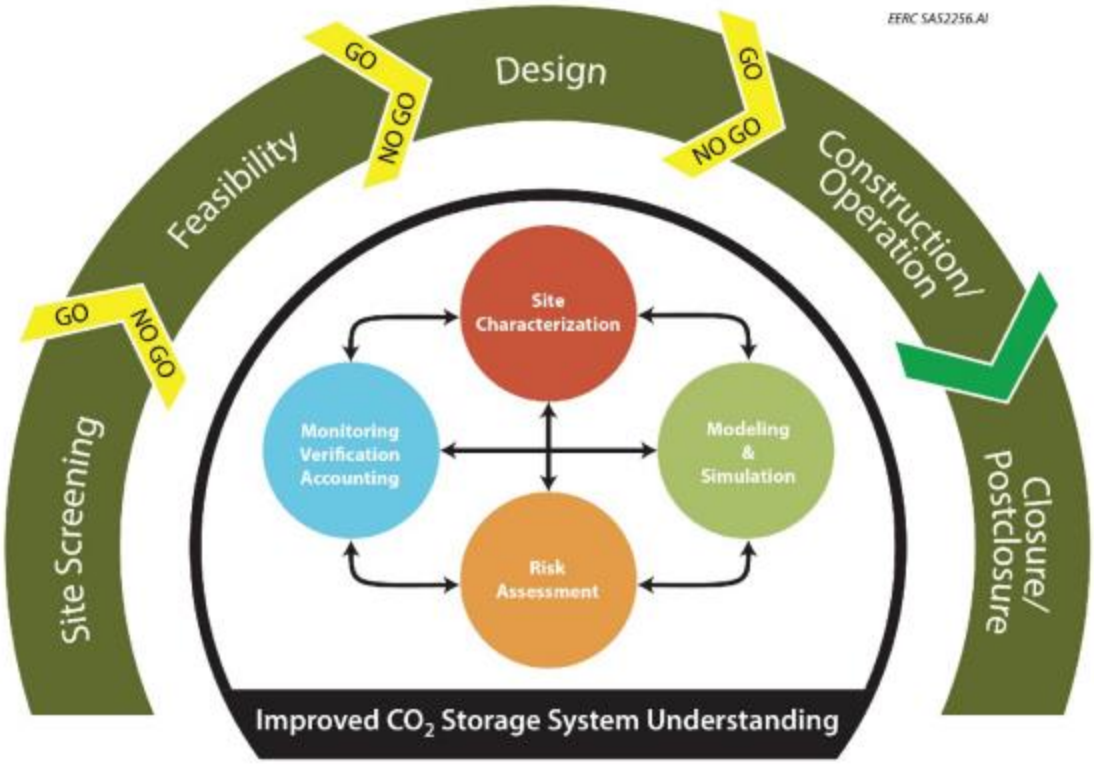

Figure 8: PCOR Partnership AMA for CO_2 storage project development (Ayash et al., 2016)

According to Glazewski et al. (2018), the foundation of the AMA consists of four fundamental technical components, carried out at changing scales and intensities as a project progresses through each of the five phases of the commercial development life cycle. These four components are:

1. **Site Characterization** to understand surface and subsurface characteristics of the storage site.
2. **Modelling and Simulation** to predict the movement and behavior of the injected gas.
3. **Risk Assessment** to spot and monitor project risks.
4. **Monitoring, Verification and Accounting (MVA)** to track injected gas and monitor for changes in surface and subsurface conditions due to injection. Also involves monitoring for any CO_2 leakage.

This study covered modelling and simulation work on the saline aquifer in Arbuckle Group of the Osage Reservation and builds upon the subsurface characterization carried out by Milad et al. (2022). They made use of 124 well logs to determine the stratigraphic thickness of the Arbuckle and combined the well logs and cores in determining the lithology and electrofacies for the estimation of porosity, saturation, and permeability.

2.3 Long-Term CO_2 Geological Storage and Potential Risks

One proposed approach to mitigate global warming is the long-term storage of anthropogenic greenhouse gases like CO_2. Regional aquifers, typically located in sedimentary basins are potential locations for this storage due to their widespread occurrence (Ashfaq, 2017). Geologic carbon storage (GCS) involves injecting CO_2 into porous and permeable rock formations that are 3,000–14,000 ft underground to keep it isolated for long periods (Usually thousands of years). The gas is first captured, concentrated to a supercritical condition, before being injected into an appropriate geologic structure. The injected gas rises due to its buoyancy compared to other formation fluids because it has a lower density and viscosity than oil, water, or other formation fluids (Anderson, 2017).

There are also geo-mechanical risks associated with geological CO_2 storage. Fig. 9 below illustrates how Ringrose, et al. (2013) described the geomechanical concerns connected to geologic carbon sequestration. They emphasize that modifications to the formation can take place even in the CO_2 plume and beyond the point of injection. It has been noted that variations in the temperature and pressure in the area of injection can affect the patterns of stress and mechanical strain as well as the occurrence of faults nearby. Beyond this region, changes in stress and strain can also take place and have an impact on faults, causing seismic occurrences.

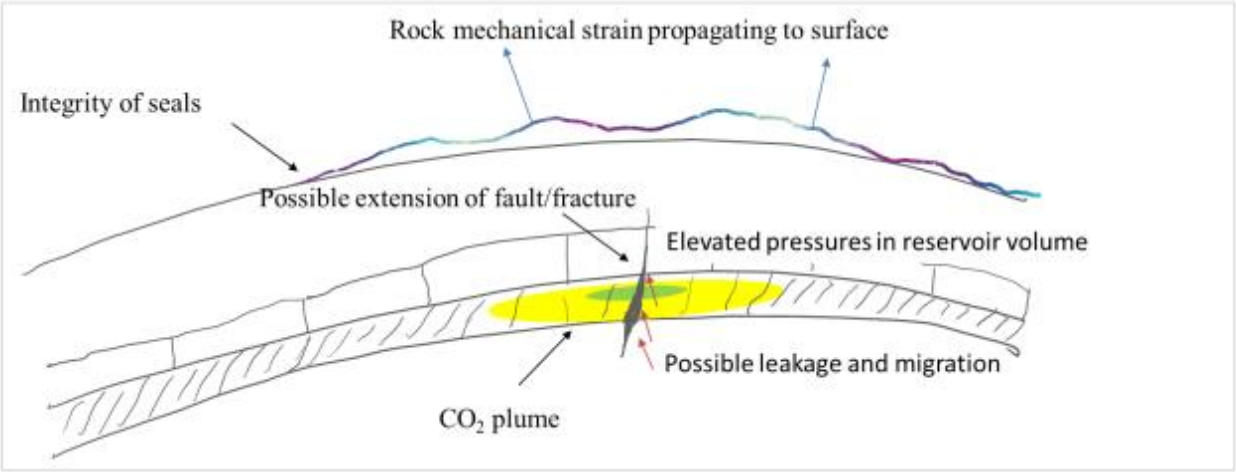

Figure 9: Geo-mechanical risks associated with Geological Carbon Storage in deep sedimentary rock rocks. ((Ochie, 2022); Modified from (Ringrose, et al., 2013)

A sedimentary basin model was utilized in the Powder River Basin of Wyoming to evaluate the duration of stay in possible aquifer storage sites, as well as the movement patterns and velocities away from such locations. The model accounted for the multiphase flow of CO_2, groundwater, and brine (McPherson & Lichtner, 2001) and was also employed to replicate CO_2 transportation through fractures and analyze the allocation of rock matrix and fractures. These models helped to elucidate whether there would be a propensity towards increases or decreases in permeability in the fracture zone due to carbonate reactions. Surface heat flow data was utilized to calibrate hydrologic features on a regional scale, such as the existence of fracture zones. The results suggest that, generally speaking, if the subsurface structure and permeability are accurately assessed or described, sequestering CO_2 in deep aquifers for the long term (over 1000 years) is possible.

Ochie (2022) used data analytics to estimate the likelihood of induced seismicity in the Arbuckle Group using stress data and injection pressures and found that the risk of induced seismicity due to geological CO_2 storage was 12%. This is an example of risk analysis work done

in the formation of interest for this study although their study used site-specific stress data from Kansas and may not be representative in the Osage Reservation of Oklahoma.

According to Ashfaq (2017), despite the potential for long-term CO_2 storage, there are still other risks to consider. One of these risks is the possibility of brine contamination in subsurface sequestration, which may happen if CO_2 escapes from the storage aquifers and enters other aquifers or even the land surface. The potential of unintentional contamination of nearby aquifers by brine displacement from adjacent sealing layers, like marine shales, was evaluated in McPherson and Lichtner (2001). The results indicate that continual CO_2 injection could lead to substantial brine displacement out of neighboring sealing layers, depending on a range of factors such as history of injection, initial composition of brine, and hydrologic properties of the aquifers and the seals. These results highlight the importance of a thorough risk analysis before and during the execution of CO_2 sequestration projects.

Under their current Underground Injection Control (UIC) program, the United States Environmental Protection Agency (EPA) completed U.S. EPA (2010c), and in conjunction with the Class VI rule of September 2011. (U.S. EPA 2011), the Safe Drinking Water Act's (SDWA) was established to protect an Underground Source of Drinking water (USDW) in the course of subterranean CO_2 sequestration in geological structures. According to Rubin et al. (2013), Dixon et al. (2015) and Anderson (2016), some specifications include in the SDWA include:

1. Appropriate characterization and selection of the proposed site,
2. The identification of an Area of Review (A.O.R.) where an operator is required to locate potential leak pathways (such as wells and fault lines) with the potential to cause CO_2 gas or displaced fluids from the formation to enter an Underground Drinking Water Source,

3. reevaluating and potentially upgrading the A.O.R. on a regular basis,
4. designing and building wells to limit fluid intrusion into USDWs,
5. operating injection wells, such that they are monitored during injection and there are restrictions on injection pressures,
6. monitoring the system post-injection and site care.

Requirements for a Class VI permit (EPA, Subpart UU - Injection of Carbon Dioxide, 2021) also necessitate that an operator provides pertinent data on stress, in situ fluid pressures, fractures, rock strength, and ductility. Additionally, they must show that the formation's projected injection pressures and volumes won't cause or spread faults or fractures (EPA, Subpart UU – Injection of Carbon Dioxide, 2021). The injection pressure shouldn't be greater than 90% of the formation fracture pressure, as is the case in (Chiaramonte et al., 2008), and the fracture pressure should be greater than the injection pressure (Zoback, et al., 2003).

The importance of a thorough risk analysis before and during the execution of CO_2 sequestration projects cannot be overemphasized. The importance of the four fundamental technical components listed in section 2.1 becomes very active here as their results feed into any risk analysis to be carried out on a formation.

2.4 CO_2 Sequestration Reservoir Simulations

Numerous studies have been conducted utilizing reservoir simulation software to simulate the sequestration of CO_2 in deep aquifers. There was a study conducted by Holubnyak et al. (2016) where they detailed the process of reservoir simulation for a CO_2 pilot project in the Arbuckle saline aquifer at Wellington Field, Sumner County, Kansas. However, the region of study for this thesis has not yet been the subject of any studies. This research on CO_2 sequestration in the Arbuckle of Oklahoma's Osage Reservation is the first of its kind for this reason.

Chang (1996) studied how much CO_2 can dissolve in water. They used correlations to describe how temperature, pressure, and salinity of water affect the solubility of CO_2. Additionally, they investigated how the water formation volume factor, compressibility, and viscosity correlate with each other. For an accurate model of CO_2 trapping in an aquifer, the model must consider these factors to understand the interrelationship that exists between CO_2 gas and the formation brine.

Kumar et al. (2004) performed a reservoir simulation analysis using compositional modeling to evaluate the potential of CO_2 storage in a deep saline aquifer. The research examined the impact of multiple variables, such as mineralization, temperature, salinity, permeability ratio, residual gas saturation, and aquifer inclination angle, influence the sequestration of CO_2 (Kumar et al., 2004). The study examined three key mechanisms of sequestration, including dissolution, pore-level trapping, and mineralization. Computer Modelling Group (CMG) GEMS was utilized to conduct the study. The results of the study showed that residual gas saturation (S_{gr}) significantly affects the amount of CO_2 trapped as residual gas. Additionally, the horizontal to vertical permeability ratio (anisotropy) and aquifer dip significantly influences the movement of gas, which consequently influences CO_2 solubility in the brine aquifer and the mineralization reactions. The research offers data tables and literature sources that pertain to CO_2 solubility in brine, mineral reactions, and equations for estimating Sgr through porosity measurements. Finally, the study highlighted the importance of data quality in CO_2 sequestration modeling.

Ozah et al. (2005) expanded on Kumar et al.'s (2004) study by introducing new information related to how CO_2 and H_2S mix and using horizontal wells to improve trapping and dissolving without coming into contact with seal formations. Additionally, the study utilized Local Grid Refinement (LGR) to increase the accuracy and reliability of the resulting saturation of gas in the

CO_2 plume and surrounding the injection well (Chaves, 2011). The LGR approach also provided better insight into buoyancy-driven fingering, which is crucial due to the gas's unstable upward flow when injected into the lower section of the aquifer.

Kartikasurja et al. (2008) studied CO_2 sequestration in an aquifer to prevent the release of CO_2 generated from Malaysia's offshore B Field into the atmosphere, meeting the gas sales criterion. The research objective was to evaluate the geology of aquifers and the necessary reservoir engineering for CO_2 injection into formations with insufficient reservoir data. The study provided important selection criteria for choosing an aquifer as a potential formation for CO_2 sequestration. For this project, they used a black-oil simulator, but an indirect approach was used as the simulator did not allow modeling of dissolved gas in the water phase. The indirect method involved giving oil water qualities allowing the dissolution of the gaseous phase during simulation. The study conducted sensitivity analyses to identify the optimal count of gas injection wells needed for a successful project. The study also analyzed the primary characteristics of the reservoir and how they affect CO_2 injection.

Sona et al. (2013) explored the importance of gas solubility in carbon capture and storage (CCS) projects for reducing greenhouse gas emissions. The solubility of gas in liquid depends on the properties of the gas or liquid. The study used numerical simulations to investigate the effects of gas solubility in geological CO_2 storage using CMG STARS software. The study assumes that CO_2 gas is injected into an aquifer at 1001 m (3284 ft) depth and investigated the sensitivity of gas solubility by changing injection pressure and initial reservoir temperature. The results showed that pressure and temperature significantly affect CO_2 gas solubility in the aquifer.

Two publications by Ngheim et al. (2004 & 2009) presented the necessary equations for developing a Geochemical EOS (Equation of State) compositional model (GEMS) that is fully

coupled. The simulator results were verified through validation runs. The researchers utilized experimental data to approximate carbon dioxide storage in aquifers. Their findings indicated that residual trapping and solubility (dissolution) trapping compete in formation, with the former being more prominent where aquifers have low permeability. The addition of water can intensify and expedite residual gas trapping.

Alzayer et al. (2022) discuss the importance of managing carbon emissions so that the oil and gas industry can ensure sustainable energy in a clean environment. CO_2 storage in deep saline aquifers is a way to drive down atmospheric carbon and four trapping mechanisms are used to securely store CO_2. The study used a synthetic anticline model to capture residual and soluble trapping mechanisms and suggested best practices with which to model CO_2 sequestration for optimally secure long-term storage of CO_2 (thousands of years). The ability of CO_2 to dissolve in water is mostly dependent on salinity (ppm) and formation temperature, and as such, these parameters should be accurately captured in any simulation model. This paper serves as a pioneer guide for the industry to accurately simulate the CO_2 sequestration process.

2.5 CO_2 Maximum Injection Capacity

According to predictions, saline aquifers have the potential to store several thousand Giga Tons (Gt) of CO_2 (Ashfaq, 2017). However, filling this capacity is challenging due to several factors. One of these factors is that the formation pressure should not exceed 90% of the fracture pressure (as noted by Chiaramonte et al., 2008), and injecting large volumes of CO_2 rapidly can quickly increase the formation pressure. For any specific reservoir, the amount of CO_2 that may be injected within a specific injection area and time should be determined as the injection capacity. In order to accomplish this, it is necessary to conduct a comprehensive sensitivity analysis of various reservoir features, including formation thickness, the rock compressibility, matrix

permeability and porosity, formation temperature and pressure, aquifer formation fracture pressure, and the quantity and placement of injection wells (Ashfaq, 2017).

Pore pressure may rise after injection in a small drainage area. (Joshi, 2014). The ability of brine to dissolve CO_2 is useful for overcoming spatial challenges. In certain geological scenarios, it may be possible to simulate a confined system with a small catchment area, also called a closed system, by utilizing a modeling approach that assumes no outflow beyond its boundaries. Since the pressurization of closed aquifers spreads deeper into the aquifer, there is a higher risk (Oruganti & Bryant, 2008).

Researchers, van Engelenburg (1993), van der Meer and van Wees (2006), Schembre-McCabe et al. (2007), Anchliya (2009), and Anchliya et al. (2012) have all undertaken studies on the limit of storage and shown reservoir pressurization restrictions in a constrained aquifer. Anchiliya (2009) for instance, compared an open aquifer to a closed one as shown in Fig. 10 below (Ashfaq, 2017):

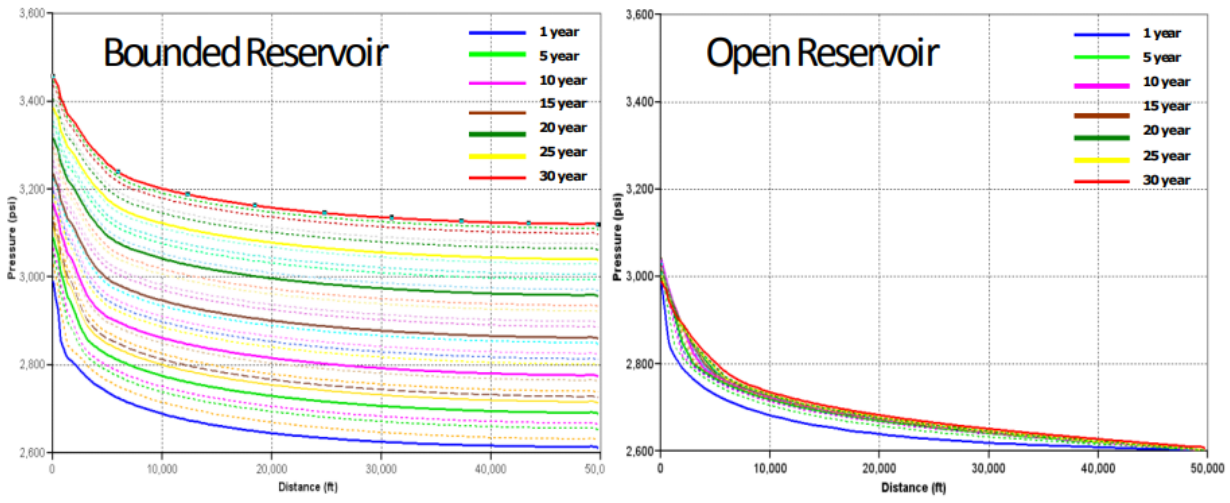

Figure 10: Pressure Profiles for Closed and Open Reservoir systems (Anchiliya, 2009)

2.6 Pressure Buildup Due to Geological CO_2 Storage

As mentioned in the previous section, continuous injection of CO_2 in a bounded reservoir will lead to a buildup in pressure. It is important to monitor this pressure buildup because of its implications for fractures and induced seismicity. Often, CO_2 is injected into high permeability zones to minimize the risk of excessive pressure buildups. Where there are no high permeability zones however, pressure management is usually through local high conductivity features like conductive faults or production wells.

Simulating the injection of supercritical CO_2 into the porous formation is required to estimate the pressure buildup. A numerical multi-phase reservoir simulator can help with this as seen in Rutqvist et al. (2008) and Birkholzer et al., (2009). Yet, acquiring and operating such models can be costly and time-consuming. Hence, there have been simultaneous attempts to create straightforward semi-analytical techniques. The first of them was based on the Buckley-Leverett displacement (Saripalli and McGrail 2002). The Buckley-Leverett equation describes the flow of two phases (immiscible) in one dimension without the influence of capillary pressure. This equation, introduced by Buckley and Leverett (1942), assumes incompressible flow, minimal vertical pressure gradient, and insignificant capillary pressure.

Using the assumptions above, Nordbotten et al. (2005) adopted a similar strategy. When relative permeability is directly proportional to fluid saturation, the governing equations for this scenario are essentially the same as the Buckley-Leverett equation. This method's significant advantage is that it explicitly calculates the saturation distribution. However, the calculation of the pressure distribution requires selecting an arbitrary impact radius.

An alternate approach was developed by Zhou et al. (2008) that takes formation and fluid compressibility into account when calculating storage capacity. The geographical uniformity and

independence of the pressure increase from formation permeability, however, is a crucial limiting assumption in their approach.

Mathias et al. (2009) built on Nordbotten's approach of using matched asymptotic expansions and improved it by incorporating the compressibility of the formation and fluid, resulting in more accurate approximations to the model equations. Afterward, they utilized the methodology proposed by Mathias et al. (2008) to construct a large-time approximation that considers inertial effects by employing the Forchheimer (1901) equation. The acceleration in velocity caused by the flowline convergence around the injection well leads to significant inertial effects in such scenarios, as explained by Mathias et al. (2008) and Mathias and Todman (2010).

Mathias et al. (2011a) did further work to extend their 2009 solution to reservoirs with the finite radial extent and incorporated the reduction in effective relative permeability of the CO_2 due to residual brine saturation.

Mathias et al. (2011b) improved their earlier work by incorporating effects related to the partial miscibility of CO_2 and brine into pressure buildup equations. These included the solubility of CO_2 in brine, the ability of water to evaporate into the CO_2 gas rich phase, and salt precipitation. This was accomplished using a gas saturation distribution function derived from the two-component, two-phase fractional flow theory (Orr, 2007) with linear relative permeability functions. The new pressure buildup equation was created by obtaining and integrating a relative permeability distribution. Their pressure buildup equation is similar in structure to that of Burton et al. (2008). The distinction is that Mathias et al. (2011b) take into account the volume change that occurs during mixing and give closed-form expressions to estimate the positions of the shock fronts in the unique situation where there is a linear relative permeability function, and their equation is applicable in characterizing both open and closed brine aquifers.

Cihan, Birkholzer, and Zhou (2013) conducted a study that demonstrated the utility of a new analytical solution to calculate pressure buildup and the rate of leakage in a multilayered aquifer-aquitard system where there exists both targeted and diffused leakage of brine. The researchers verified the accuracy of the solution by comparing it with a numerical simulation that accounted for the specifics of two-phase flow. They illustrated the effectiveness of the new method in analyzing local pressure buildup in a system with multiple layers and gaining useful insights into how leakage occurs through aquitards, leaky wells, and/or leaky faults by presenting example uses for a CO_2 injection scenario (although two-phase flow was not considered in these examples) (Ashfaq, 2017).

Since then, more work has been done developing analytical solutions to estimate pressure buildup in two-phase systems. More recently, Wu et al. (2017) developed a solution for pressure buildup for two-phase flow with a constant CO_2 injection rate using an infinite-bounded reservoir that has a constant pressure boundary. Where this boundary is placed is time dependent. In order to verify the accuracy and dependability of their solution, they compared the results with the results obtained from TOUGH2/ECO2N simulation for a specified case of CO_2 injection. The results showed good accuracy and revealed that only the flow field close to the front of the CO_2 plume is unstable, with pressure increasing logarithmically with increasing injection time while decreasing as a negative logarithm with increasing radial distance.

Wu et al. (2018) improved on the work of Wu et al. (2017) by considering the role of both partial miscibility and compressibility. Their research established a more precise interpretation of the coefficient of fluid compressibility, and subsequently developed a corresponding power function model (PFM) to tackle the limitations of the conventional coefficient of compressibility. The traditional coefficient was insufficient in capturing the association between CO_2's physical

traits and pressure. The PFM outperformed the conventional exponential function model in terms of accuracy and applicability when compared with a standard data set, confirming the validity of the new concept. In addition, they tackled the challenges involved in calculating fluid saturation in Wu et al. (2017), by proposing the adoption of direct assumptions regarding the averaged relative permeability of each fluid phase across various fluid regions. This approach enhanced the accuracy of the model by circumventing the obstacles associated with determining fluid saturation and eliminating the inaccuracies linked to relative permeability models when assessing reservoir risks. Both Wu et al. (2018) and Wu et al. (2017) however assume an infinite extent of reservoir which will not apply to the study in this thesis.

The method of Mathias et al. (2011b) will be discussed in full in Chapter 3 as it is the subject of analysis aimed at determining the extent of its applicability. This model is particularly useful because of its applicability to closed bounded systems like this study entails.

Chapter 3: Methodology

3.1 Introduction

As mentioned in previous chapters, a combination of the following techniques primarily results in sequestration in deep saltwater aquifers or oil-gas reservoirs.

3.1.1 Structural Trap/Hydrodynamic Trap:

Carbon dioxide can be sequestered in an analogous manner to how gas is stored in a gas-oil reservoir, by confining it as a supercritical fluid under a seal formation. This process, also known as hydrodynamic trapping, is likely the most important method of sequestration in the short term.

3.1.2 Solubility Trap:

This technique entails the solubility of CO_2 into the formation fluids (oil or water). Pressure, temperature, and brine salinity all play a role in this system. Enormous amounts of CO_2 can be trapped; however, this technique is slower than structural trapping.

The following chemical reaction can be used to illustrate the phase equilibrium mechanism that is used to model gas solubility in brine:

$$CO_{2(g)} = CO_{2(aq)}$$

The notations "(g)" and "(aq)" are used to represent the gaseous and aqueous phases, respectively. Since gas dissolves quickly into liquid, it is assumed that these phases are in thermodynamic equilibrium, which means that the fugacity (tendency to escape) is equal in both the gas and aqueous phases.

$$f_{i,g} = f_{i,aq}, i = 1, \ldots n_c$$

The Peng Robinson equation of state (PR _EOS) is used to compute the fugacity "$f_{i,g}$" of component "i" in the gas phase (Chaves 2011) (Peng and Robinson, 1976).

Henry's Law is a formula used to calculate the amount of gas that dissolves in a liquid, based on the pressure of the gas and the solubility of the gas in the liquid. It is expressed as "$f_{i,aq}$" which represents the fugacity of component "i" of the gas in the aqueous phase. This formula was presented in studies conducted by Chaves (2011) and Li and Nghiem (1986).

$$f_{iw} = y_{iw} \times H_i$$

Where H_i represents the pressure, temperature and salinity-dependent Henry's law constants that can be calculated using:

$$\ln H_i = \ln H_i^* + \frac{1}{RT}\int_{p^*}^{p} \overline{v_i}\, dp$$

Where,

H_i is the Henry's Law constant at a pressure, p and temperature, T

R is the Gas Constant value.

$\overline{v_i}$ represents the Partial molar volume of component "i" in the solution.

Henry's constant for several gases, including CO_2, may be calculated using a few correlations that consider temperature, salinity, and the water saturation pressure (Chaves, 2011; Bakker 2003).

3.1.3 Residual Gas Trapping:

Capillary forces cause the CO_2 to be trapped as an immobile phase that has zero relative permeability to gas. This type of storage is influenced by the residual saturation of a non-wetting phase and the relative permeability, which includes hysteresis. These petrophysical factors are essential for successful CO_2 storage (Chaves, 2011).

At the start of sequestration, CO_2 is injected via an injection well, and the gas displaces the water since the water is the wetting phase (also called drainage). When the injection of CO_2 is halted, aqueous brine moves back to the gas injection region (called imbibition), which leads to hysteresis. The gas that remains trapped after the water has imbued into the rock and reached

irreducible water saturation (S_{wir}) and zero capillary pressure is known as residual gas saturation (Chaves, 2011).

There are numerous models for describing CO_2 residual gas trapping. Many simulators (including GEMS) use the traditional Land's model (Land, 1968). This is how the Land's coefficient C is described:

$$C = \frac{1}{S_{gr,max}} - \frac{1}{S_{g,max}}$$

Where, $S_{g,max}$ is the maximum attainable gas saturation and $S_{gr,max}$ is the maximum residual (trapped) gas saturation. The residual gas saturation for any gas can be estimated using:

$$S_{gr}^{*}\left(S_{gi}^{*}\right) = \frac{S_{gi}^{*}}{1 + CS_{gi}^{*}}$$

Where S_{gr}^{*} is the residual gas saturation, S_{gi}^{*} is the gas saturation and C is the Land's coefficient.

It is strongly advised to inject CO_2 close to the aquifer's bottom to encourage residual gas trapping. This will increase the interaction between water and carbon dioxide as the gas rises during structural trapping due to the difference in density.

3.1.4 Mineral Trapping:

This process entails the formation of stable and firm substances such as carbonates by dissolved CO_2 in water with minerals that exist in the formation. The main geochemical factor causing storage is the acidity of the brine brought on by dissolved CO_2 dissociating.

Minerals and aqueous components can interact chemically, as can other elements in the aqueous phase. The chemical processes brought on by CO_2 injection are described in Ortoleva et

al. (1998). The first step involves the dissolution of CO_2 in water to produce weak Carbonic acid (H_2CO_3) that then undergoes a dissociation reaction as follows:

$$CO_{2(aq)} + H_2O \leftrightarrow H_2CO_3$$

$$H_2CO_3 \leftrightarrow HCO^-_{3(aq)} + H^+{}_{(aq)}$$

The principal formation rock minerals dissolve as a result of the increasing acidity, which leads to the complexing of various dissolved cations with the bicarbonate ion, including:

$$HCO^-_{3(aq)} + Ca^{++}{}_{(aq)} \leftrightarrow CaHCO^+_{3(aq)}$$

In certain conditions, it is possible for carbonate ions to undergo reactions with various metal ions that are found in the water of the formation, leading to the formation of minerals composed of carbonate. The most common carbonate minerals are known to react in the following manner (Chaves, 2011):

$$HCO^-_{3(aq)} + Ca^{++}{}_{(aq)} \leftrightarrow CaCO_3(calcite) + H^+_{(aq)}$$

$$2CO^{--}_3{}_{(aq)} + Ca^{++}{}_{(aq)} + Mg^{++}{}_{(aq)} \leftrightarrow CaMg(CO_3)_2(dolomite)$$

$$HCO^-_{3(aq)} + Mg^{++}{}_{(aq)} \leftrightarrow MgCO_3(magnesite) + H^+_{(aq)}$$

$$HCO^-_{3(aq)} + Fe^{++}{}_{(aq)} \leftrightarrow FeCO_3(siderite) + H^+_{(aq)}$$

Table 1 presents common mineral and aqueous processes that capture CO2 by dissolving and precipitating minerals. Nghiem (2004) argues that reservoirs with significant proton sinks, such as feldspar and clay minerals, are more suitable for mineral trapping. Bachu (2009) explains that the minerals react with $H^+_{(aq)}$ and $HCO^-_{3(aq)}$ ions from aqueous chemical equilibrium reactions, leading to an overall reaction of the form:

$$Feldespar + Clays + CO_2 \leftrightarrow Kaolinite + Carbonate\ Minerals + Quartz$$

Table 1: Chemical and Mineral Reactions (Modified from Ngheim, 2009)

GEOCHEMICAL REACTIONS
Aqueous Chemical Equilibrium Reactions
1. $H_2O \leftrightarrow H^+_{(aq)} + OH^-_{(aq)}$
2. $CO_{2(aq)} + H_2O \leftrightarrow H^+_{(aq)} + HCO^-_{3(aq)}$
3. $HCO^-_{3(aq)} \leftrightarrow H^+_{(aq)} + {CO_3^{--}}_{(aq)}$
4. $AlOH^{++}_{(aq)} + H^+_{(aq)} \leftrightarrow Al^{+++}_{(aq)} + H_2O$
Mineral Dissolution/Precipitation Reactions
5. $CaCO_3(calcite) + H^+_{(aq)} \leftrightarrow HCO^-_{3(aq)} + {Ca^{++}}_{(aq)}$
6. $CaMg(CO_3)_2(dolomite) + H^+_{(aq)} \leftrightarrow 2{HCO_3^{--}}_{(aq)} + {Ca^{++}}_{(aq)} + {Mg^{++}}_{(aq)}$
7. $Chalcedony \leftrightarrow SiO_{2(aq)}$
8. $MgCO_3(magnesite) + H^+_{(aq)} \leftrightarrow HCO^-_{3(aq)} + {Mg^{++}}_{(aq)}$
9. $FeCO_3(siderite) + H^+_{(aq)} \leftrightarrow HCO^-_{3(aq)} + {Fe^{++}}_{(aq)}$
10. $Al_2O_3(SiO_2)_2(Kaolinite) + 6H^+_{(aq)} \leftrightarrow 5H_2O + 2SiO_2 + 2Al^{+++}_{(aq)}$
11. $Illite + 8H^+_{(aq)} \leftrightarrow 5H_2O + 0.6K^+_{(aq)} + 0.25{Mg^{++}}_{(aq)} + 2.3Al^{+++}_{(aq)} + 3.5SiO_{2(aq)}$
12. $Annite + 10H^+_{(aq)} \leftrightarrow 3{Fe^{++}}_{(aq)} + K^+_{(aq)} + Al^{+++}_{(aq)} + 3SiO_{2(aq)} + 6H_2O$
13. $Anorthite + 8H^+_{(aq)} \leftrightarrow {Ca^{++}}_{(aq)} + 2Al^{+++}_{(aq)} + 2SiO_{2(aq)} + 4H_2O$

Gunter et al. (2000) and Nghiem (2004) both suggest that sandstone (siliciclastic) aquifers are better suited for mineral trapping of CO_2 than carbonate aquifers. Nghiem (2009) created models to study chemical equilibrium reactions, mineral dissolution, and precipitation reactions, as well as their solutions.

Generally, fluid displacement initially dominates the sequestration of CO_2 in aquifers, but over time, dissolution and reaction take center stage. A large amount of CO_2 can be trapped by the residual trapping, which also plays a vital role. Mineral trapping, however, usually takes hundreds to thousands of years to evolve.

The primary objective of CO_2 sequestration in aquifers is to prevent CO_2 leakage into the atmosphere and maintain long-term storage for hundreds to thousands of years. In structural trapping, there is a higher risk of CO_2 leakage through caprock if there are any microfractures or geomechanical/geochemical failures. Solubility trapping is a secure storage technique since CO_2 can dissolve into brine, and the only way it can escape is through a significant pressure drop, which is unlikely in aquifers. In residual trapping, CO_2 is immobilized in the formation's pores, making it a reliable storage method. Mineral trapping is the most secure mechanism as the CO_2 is transformed into stable carbonate minerals over geological timescales. Fig. 11 illustrates how storage security improves over time. This information is based on Chaves' (2011) study.

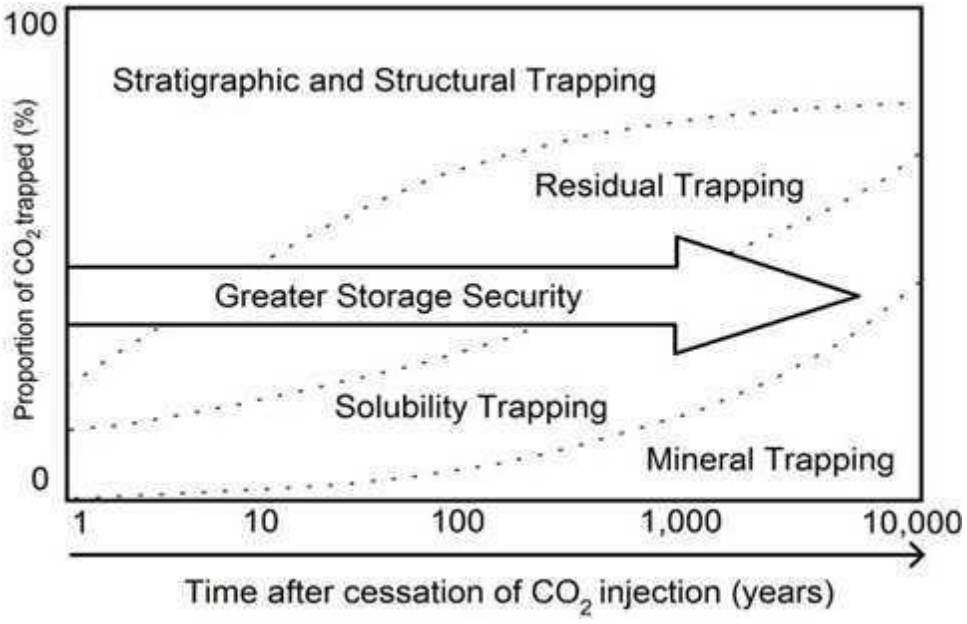

Figure 11: CO_2 Trapping Mechanisms vs time (Chaves, 2011; Faycal et al., 2015)

This study only considers structural, residual and solubility trapping. Mineral trapping should not be a factor over the simulation time period being considered (30 years of injection and 50 years post-injection). The research employs the most reliable and up-to-date data accessible for the specific region being studied.

3.2 Grid Description

The grid was upscaled from the geologic model in Milad et al. (2022) where they used 124 digitized well logs and core data from one well in the study area. Their calculation of the petrophysical properties can be summarized in the Fig. 12 below:

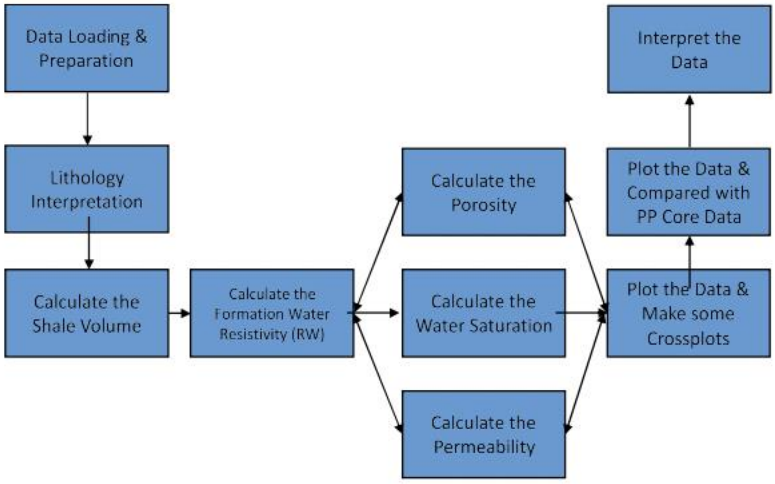

Figure 12: Workflow for petrophysical calculations (Milad et al., 2022)

The area of study has no known faults as seen in the contour map in Fig. 13 below. The grids were generated and upscaled in Petrel. The original grid dimensions were 647 x 601 x 10 (3,888,470 grid blocks). A “skeleton framework” of the new grid was created using pillar gridding before the original grid was upscaled to provide a grid with dimensions of 72 x 67 x 10 (48,240 grid blocks). Upscaling was important because of the infeasibility of running a numerical simulation on over 3 million grid cells in the original geological model. The grid properties were also upscaled in petrel accordingly. After upscaling, the resulting grids were exported into

"RESCUE" files for use in the CMG builder apparatus. Each layer in the grid structure has different thicknesses owing to the varying thickness of the Arbuckle itself as modelled geologically. Fig. 14 shows the grid model and the location of the injection wells. The location of the injection wells is in the North Burbank Unit in the northwestern part of the Osage Reservation.

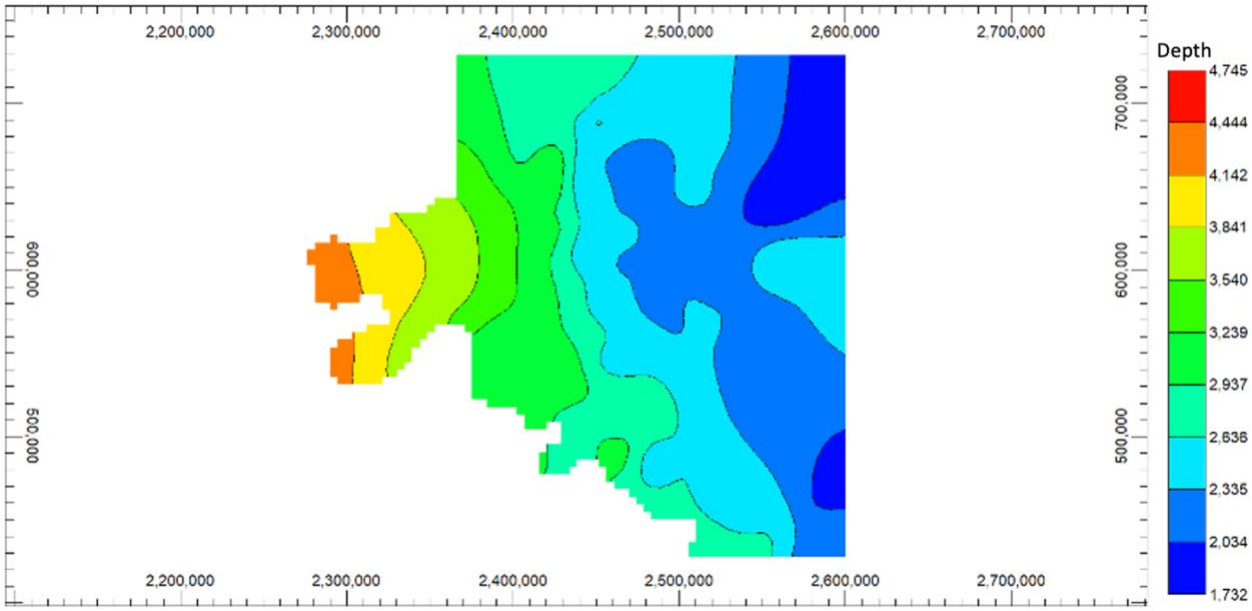

Figure 13: Osage Arbuckle Contour Map (Grid Tops/Depth)

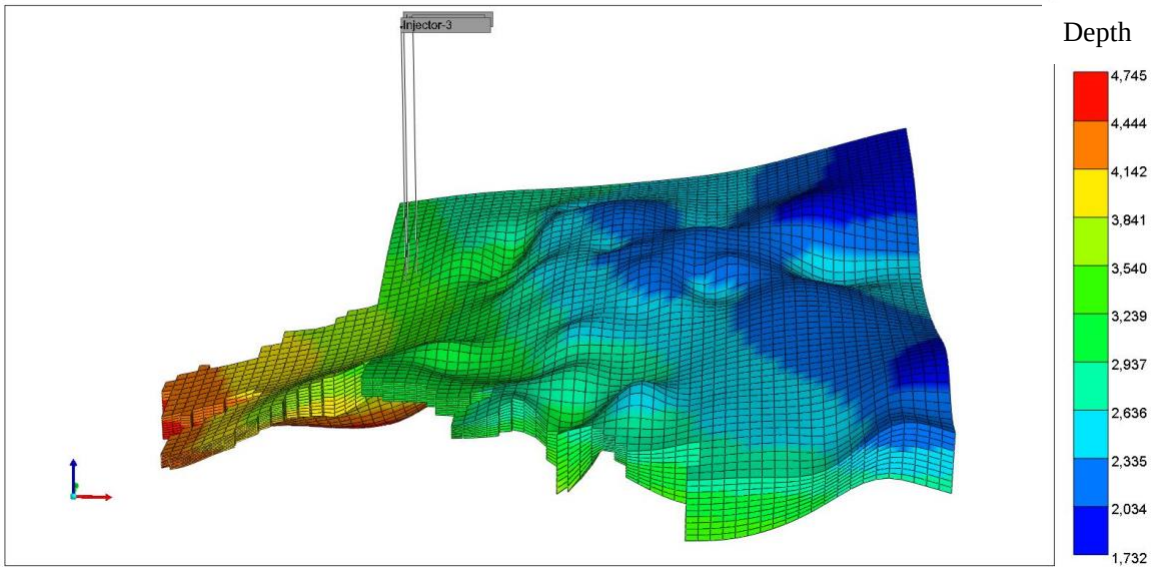

Figure 14: Grid Model, Osage Reservation Arbuckle.

After the grid was created, the model was built using Computer Modelling Group (CMG) Builder. Builder is a tool that makes it easier to create simulation models by offering a framework for data integration and workflow management between CMG's IMEX, GEM, STARS, and external data sources. CMG's GEM is the compositional simulator that was used for this study. It is the most popular Equation-of-State (EoS) reservoir simulator for modeling unconventional, chemical, and compositional reservoirs. It is designed to handle CO_2 injection in saline aquifers thus making it suitable for this study. It provides tools to analyze the individual mechanisms of CO_2 sequestration separately and estimate each mechanism's contribution to the total storage of CO_2 in a reservoir. GEMS also allows for analyzing other important aspects of CO_2 sequestration including pressure buildup.

3.3 Reservoir Properties

A lot of the reservoir information available for this study is based on the work of Milad et al. (2022). They made use of the workflow in Fig. 12 to estimate the petrophysical properties

including porosity and permeability. The porosity map and permeability map they obtained are shown in Fig. 15 and Fig. 16, respectively. Fig. 17 shows the thickness map.

The default CMG water properties were used with a compressibility of 2.99 x 10^{-6} psi [1]. The brine concentration of the Arbuckle ranges between 25,765 ppm in the upper Arbuckle to 125,658 ppm in the lower Arbuckle (Holubnyak, 2017). For this study, the water salinity was assumed to be 100,000 ppm.

The reservoir temperature was held constant at 120° F which lies in the range suggested by Holubnyak (2017). The reference pressure of 1500 psi at 3500 ft (slightly under pressured) was determined using a study by Franseen et al. (2004) where they recorded the final shut-in pressures for thousands of Arbuckle wells in Kansas.

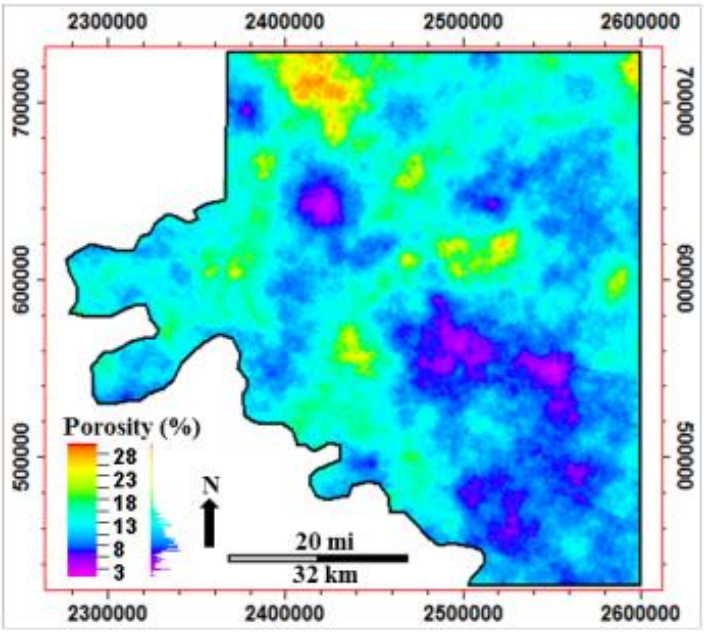

Figure 15: Porosity Map of the Osage Arbuckle (Milad et al., 2022)

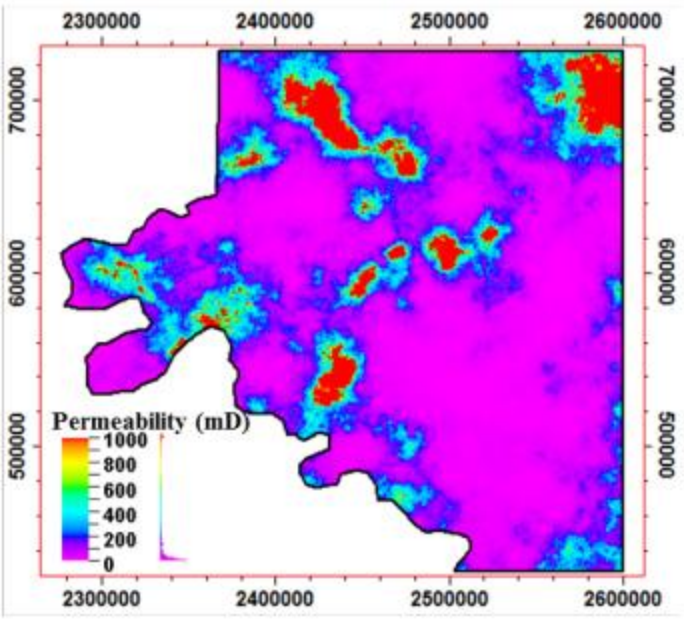

Figure 16: Permeability Map of the Osage Arbuckle (Milad et al., 2022)

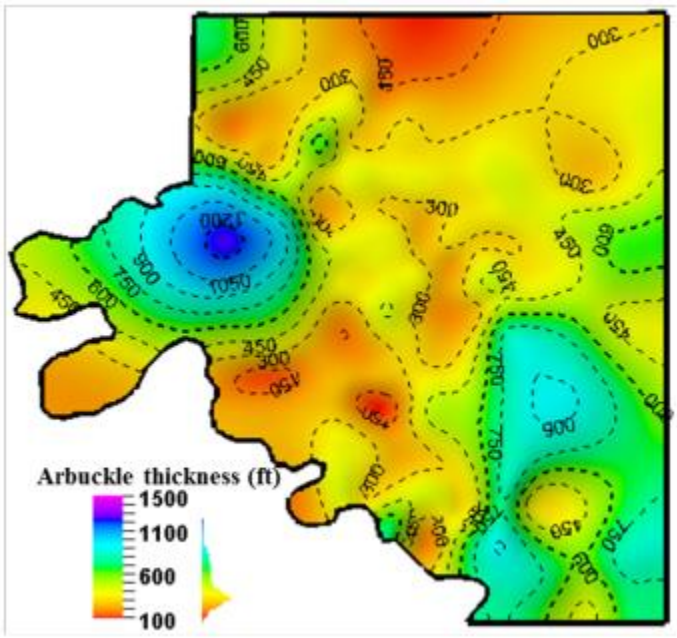

Figure 17: Thickness Map of the Osage Arbuckle (Milad et al., 2022)

The rock compressibility of 3.02 x 10^{-7} psi^{-1} was obtained from Perilla-Castillo (2017) where rock properties of the Arbuckle were derived from the analysis of earth tide strain observed in continuous pressure monitoring in northwestern and north-central Oklahoma.

Table 2: Reservoir Properties

Reservoir Properties	**Value**
Water Density	65 lb/ft^3
Water Compressibility	2.99×10^{-6} psi^{-1}
Water Salinity	100,000 ppm
Rock Compressibility	3.02×10^{-7} psi^{-1}
Reservoir Pressure @ Reference Depth	1500 psi @ 3500 ft
Reservoir Temperature	120° F
Average Permeability	170 mD
Average Porosity	9%

Relative permeability data for the Osage Arbuckle is limited as no study has been carried out till date to determine the Gas-Water relative permeability in the Osage Arbuckle. This study makes use of relative permeability data from the Kansas field Arbuckle as presented by Fazelalavi (2015). The reservoir quality index was calculated using Eq. 3.1 below:

$$RQI = 0.0314 \left(\frac{K}{\emptyset}\right)^{0.5} \qquad (Equation\ 3.1)$$

Using this equation with the average values of Permeability (170 mD) and porosity (0.09) gave an RQI value of 1.23. Fazelalavi' s (2015) report does not have relative permeability data for RQI = 1.23 but has RQI = 1.75. This RQI value (1.75) was adopted and used to select the appropriate relative permeability curves from the report as shown in Fig. 18 and Fig. 19. Fazelalavi also provided capillary pressure data for different RQI values as seen in Fig. 20. These curves were digitized and used for modelling.

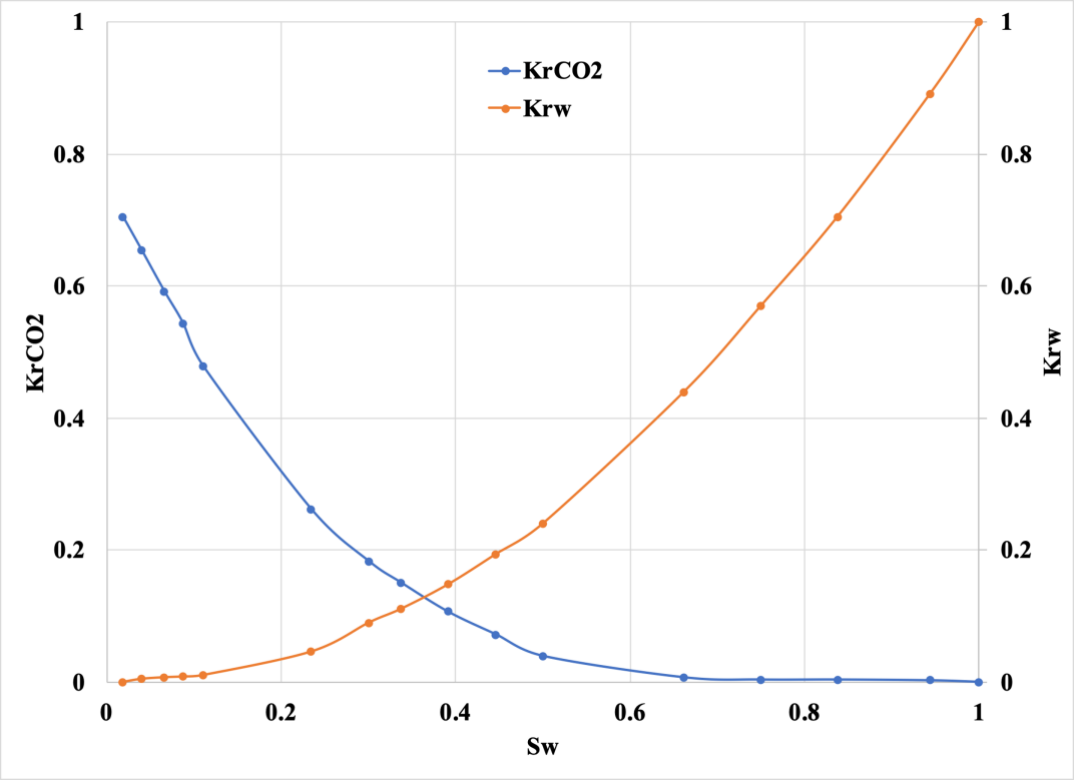

Figure 18: Drainage Relative Permeability Curve for Arbuckle (RQI = 1.75) (Fazelalavi, 2015)

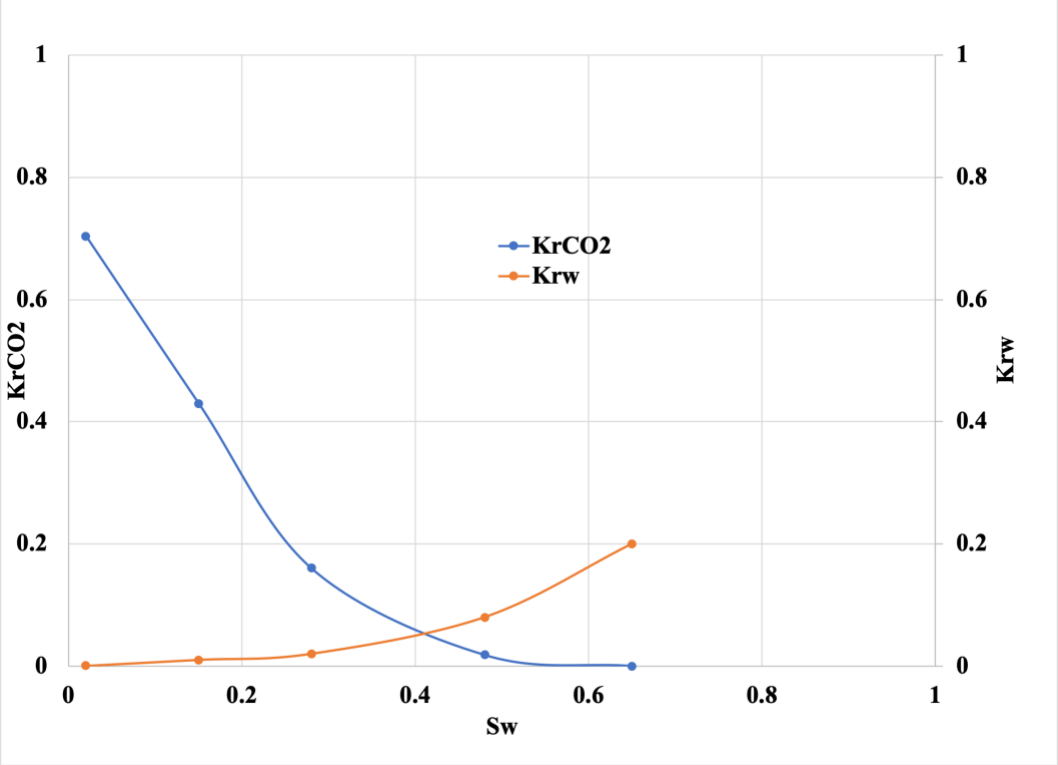

Figure 19: Imbibition Relative Permeability Curve for Arbuckle (RQI = 1.75) (Fazelalavi, 2015)

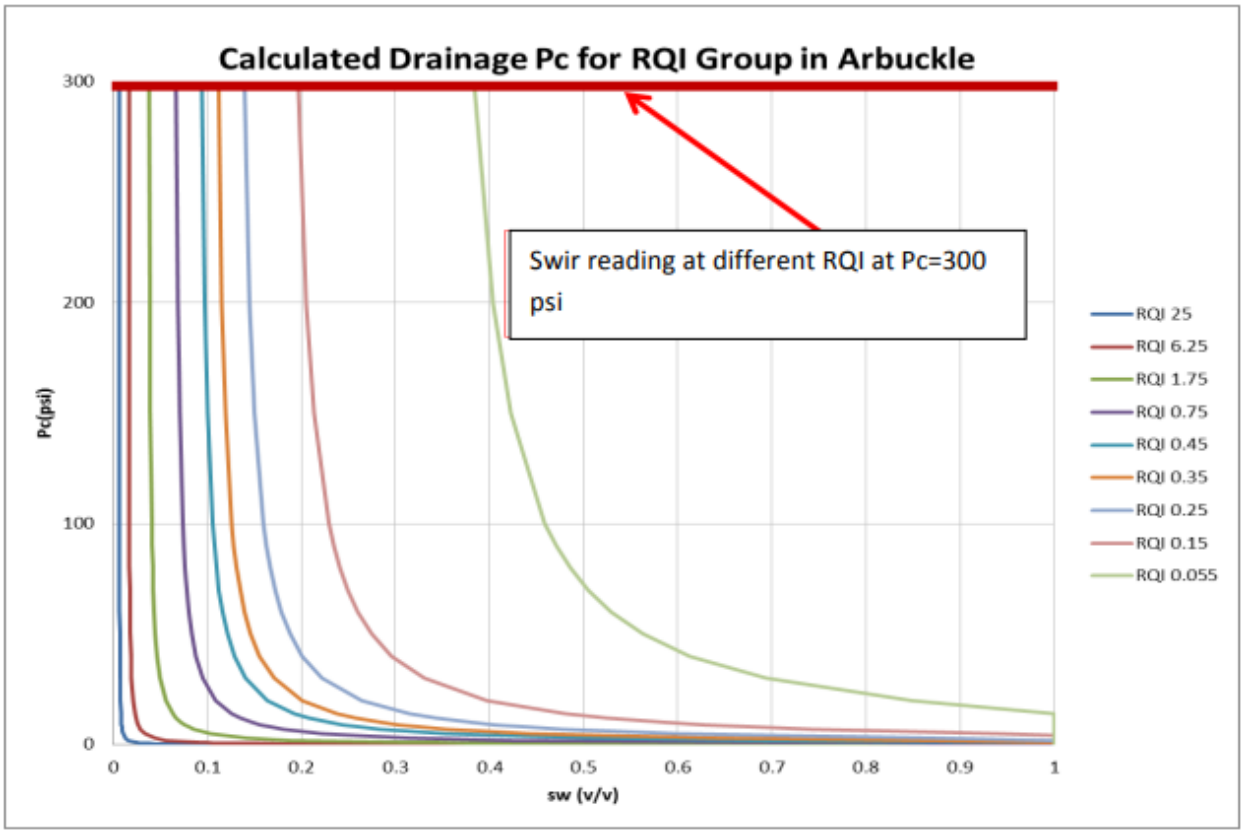

Figure 20: Capillary pressure (Drainage) curves for CO_2 - Brine system in the Arbuckle. (Fazelalavi, 2015)

3.4 CMG GEMS Simulator

The GEM simulator is hosted by the Computer Modeling Group (CMG). Nghiem (2004) created the GEM module for CO_2 sequestration. The compositional simulator using advanced general equations of state is a sophisticated tool that can handle various scenarios, including but not limited to CO_2 injection, dual porosity, volatile oil, gas condensate, horizontal wells, complex phase behavior, and well management (Chaves, 2011). In this work, the CO_2 module of GEMS was utilized to simulate the sequestration of CO_2 into the Arbuckle aquifer formation in Osage Reservation, Oklahoma.

To model CO_2 storage in saline aquifers, it is essential to solving the material balance equations, the thermodynamic equilibrium equations for the gas phase and the aqueous phase, and

the geochemical equations that describe interactions between an aqueous phase and minerals, including dissolution. However, for this study, the geochemistry aspect was excluded because these reactions take a significant amount of time, ranging from hundreds to thousands of years (Ashfaq, 2017).

Two primary methods exist to solve the interconnected set of equations: the sequential method and the simultaneous method. The sequential method involves solving the equations of flow and those that describe the equilibrium of chemical reactions in a specific order, one after the other. The two systems go through iterations until convergence is reached. Newton's method is used in the simultaneous solution approach to solve all equations simultaneously. The fully coupled technique is another name for the simultaneous solution strategy, with which GEMS models the CO_2 sequestration in brine aquifers (Chaves, 2011; Computer Modeling Group User's Guide, 2009).

3.5 Procedure/Workflow

3.5.1 Verification of 100 Psi Maximum Historical Pressure Buildup from Water Disposal

There are a number of uncertainties associated with reservoir simulation studies. One of the goals of this study is to attempt to confirm that the geological model built by Milad et al. (2022) can hold the historical water injection in the formation without significant pressure buildup (<100 psi). Information provided by the operator (CapturePoint LLC) indicates that pressure buildup in the reservoir, in 27 years of water disposal in the formation, is less than 100 psi. The model was simulated using the permeability from Milad et al. (2022) to confirm this. The field injection history is shown in Fig. 21 below (dates have been adjusted to match the simulation start time in GEMS):

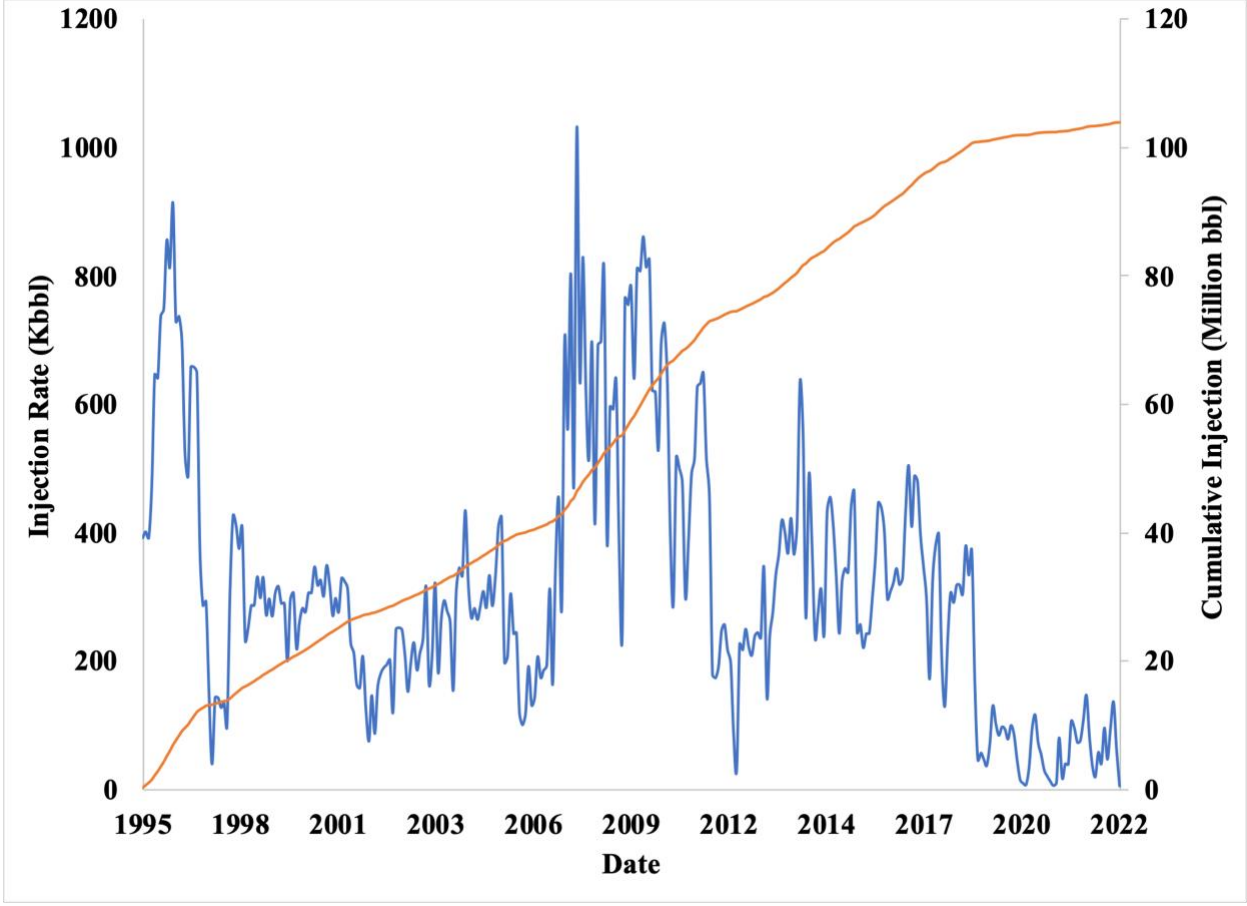

Figure 21: Field Water Injection (Disposal) history

To verify the maximum historical pressure buildup of 100 psi as reported by the operator (CapturePoint LLC.), The geological model presented in Milad et al. (2022) was used in conjunction with water disposal history in seven (7) existing wells. The wells perforated the bottom 4 layers of the Arbuckle and were in grid cells as seen in Appendix. Open flow boundary was simulated by including a horizontal producing pseudo-well constrained to produce at the initial pressure of the blocks it perforates.

The well radius in each was 0.25ft. Injection rates were constrained to match the injection history in Fig. 21.

3.5.2 Simulation of the Injection of CO_2 for 30 years and 50 years of monitoring at the end of injection Using Coarse Grids.

Verifying that the historical pressure buildup from water disposal using the geological model of Milad et al. (2022) provided confidence in the validity of the geological model. The model was afterwards repurposed for CO_2 injection. A simulation case, aimed at injecting at least 50 million metric tons of CO_2 in 30 years was attempted using one (1) injection well at constant bottomhole pressure. The simulation case was also observed for 50 years post-injection.

The radius of the injection well was 0.25ft. The well perforated layers 7 through 10. This was done based on the assumption that an existing water disposal well can be repurposed for sequestration. The maximum injection pressure was set based on work done by Birdie et al. (2022) to determine the average fracture gradient in the Arbuckle formation. They found the average fracture gradient to be 0.6 psi/ft. Given the depth of the injection well (4259 ft) and the 90% of fracture pressure constraint, the fracture pressure, was calculated as:

$$maximum\ injection\ pressure = 0.6 \times 0.9 \times 4259 = 2300\ psi$$

3.5.3 Simulation of the Injection of CO_2 for 30 years and 50 years of monitoring at the end of injection Using Local Grid Refinement (LGR) around Injection Site.

This step involved running the simulation from section 3.5.2 while applying local grid refinement to reduce numerical dispersion and improve simulation results. The injection of at least 50 million metric tons of CO_2 for 30 years and the observation of results for 50 years post-injection was again attempted after some of the grids in the North Burbank Region had been refined. The results were compared to what was obtained in section 3.5.2.

Sensitivity analysis was carried out by varying maximum bottomhole pressure using 80% and 70% of the fracture pressure. This was done to determine the effect of bottomhole pressure limitations on cumulative injection volume.

Sensitivity analysis was also carried out by varying the average reservoir permeability. The formation permeability was reduced to 85%, 75%, 65%, and 50% of the original values. A case was also made to see the effect of having 25% more permeability in the formation. The goal was to determine the minimum permeability required for the formation to inject at least 50 million MT of CO_2

Lastly, another sensitivity analysis was carried out by varying the number of injection wells to determine the effect on the maximum CO_2 volume injected.

A comparison was also made to determine the effect of CO_2 solubility on the system by modelling a no-solubility case.

3.5.4 Exploring the Extent of Applicability of Mathias et al. (2011b) Analytical Model in Predicting Pressure Buildup

For this task, CMG GEMS simulation was done using a single well cylindrical model to match the assumptions in the semi-analytical models developed by Mathias et al. (2011b). The pressure buildup curves from the analytical model and the CMG GEMS model were compared in terms of slope. The reservoir radial extent was then varied, and the resulting curves were again compared for each case to identify and record any changes in the slope. The pore volume and the cumulative injection in reservoir conditions were obtained from CMG and the ratio was plotted against the change in slope.

Before the application of the solution of Mathias et al. (2011b), modifications to the numerical model were made to match some of the assumptions of their solution as follows:

1. Average permeability, porosity, and thickness values were used to run the simulation instead of the previously distributed values.
2. The shape of the grid was modified to be cylindrical with the injection well placed in the middle of the reservoir.
3. The model used one layer to obtain a single point value of pressure at any distance from the injection well.
4. A constant injection rate of 9.1 MMscfd of CO_2 was assumed.

All other parameters and the grid conditions remain the same. The modified model is a cylindrical model that has grid cell dimensions 10 x 150 x 1 with the injection well placed in the center grid cell (1, 1, 1)

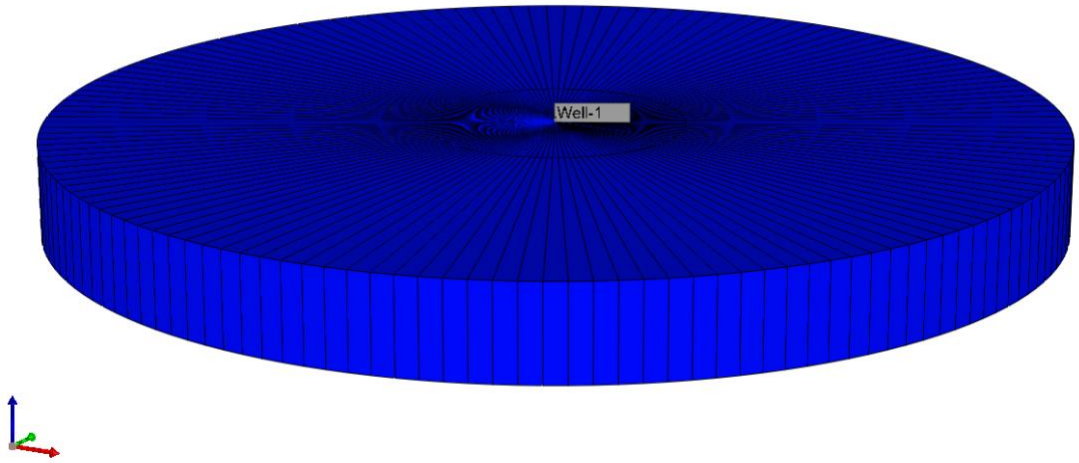

Figure 22: Cylindrical Osage Grid Model to match assumptions from Mathias et al. (2022) analytical solution.

Table 3 shows the parameters used to compute pressure build up using Mathias et al. (2022) analytical solution. The injection time was 30 years. Pressure buildup was calculated at the same point for all variations of reservoir radial extent (750ft from the injection well). The results were then compared to the results from the numerical simulation.

Table 3: Parameters for Mathias et al. (2011b) analytical solution

Parameter	**Value (Field units)**	**Value (S.I. units)**
Radial Extent	varied	varied
Porosity	0.09	0.09
Residual Brine Saturation	0.018	0.018
Endpoint Relative Permeability for CO_2	0.7	0.7
Well radius	0.25ft	0.0762 m
Rock Compressibility	3.02×10^{-7} Psi^{-1}	4.38×10^{-11} Pa^{-1}
Water compressibility	Calculated as described in Mathias et al. (2011b)	Calculated as described in Mathias et al. (2011b)
Injection rate, Mo	9.1 MMscfd	5.464 kg/s
Initial Pressure	1500 Psi	10342117 Pa
Temperature	120 ºF	40 ºC
Salinity	100,000 ppm	0.0999 kg/L
Formation Thickness	400 ft	121.92 m
Permeability	170 mD	1.67×10^{-13} m^2
Gas Density	Calculated as described in Mathias et al. (2011b)	Calculated as described in Mathias et al. (2011b)
Viscosity	Calculated as described in Mathias et al. (2011b)	Calculated as described in Mathias et al. (2011b)
Water viscosity	Calculated as described in Mathias et al. (2011b)	Calculated as described in Mathias et al. (2011b)

3.6 Pressure Buildup Analytical Solution of Mathias et al. (2011b)

Mathias et al. (2011b) developed a method to solve the pressure buildup for two-phase flow with a constant CO_2 injection rate in both closed and open brine aquifers. Numerical models are often costly and computationally expensive, creating a need for a quick and timely solution when carrying out initial CO_2 storage risk analysis where resources might be limited. Usually, a constant mass injection rate is employed to inject CO_2 into target reservoirs via injection wells. (Bai et al., 2017; Wu et al., 2017; Wu et al., 2018). Their research builds upon the assumptions made in Nordbotten et al.'s (2005) study, which postulates that a distinct interface exists between CO_2 and stagnant brine on one side, and flowing brine on the other. This interface is located at a certain elevation, h, above the formation's base. Since CO_2 typically has a lower density than brine, it is presumed that CO_2 exists above the interface. The pressure in the restricted porous formation with a vertical extent H (also known as the reservoir thickness) was assumed to be in vertical equilibrium over the entire thickness, while disregarding capillary pressure. Fig. 23 illustrates how the density of CO_2 is lower than that of brine. The fundamental principle of two-phase flow was deemed necessary to adhere to. Additionally, they assumed that saturation, viscosity, and relative permeability were uniformly constant in both the CO_2 and brine zones. The usual assumption made in order to solve the pressure distribution is that the compressibility of both fluids and the porous formation are very small and do not vary with pressure. (Mathias et al., 2009).

The method of Mathias et al. (2011b) for circular closed aquifer of radial extent is discussed in full.

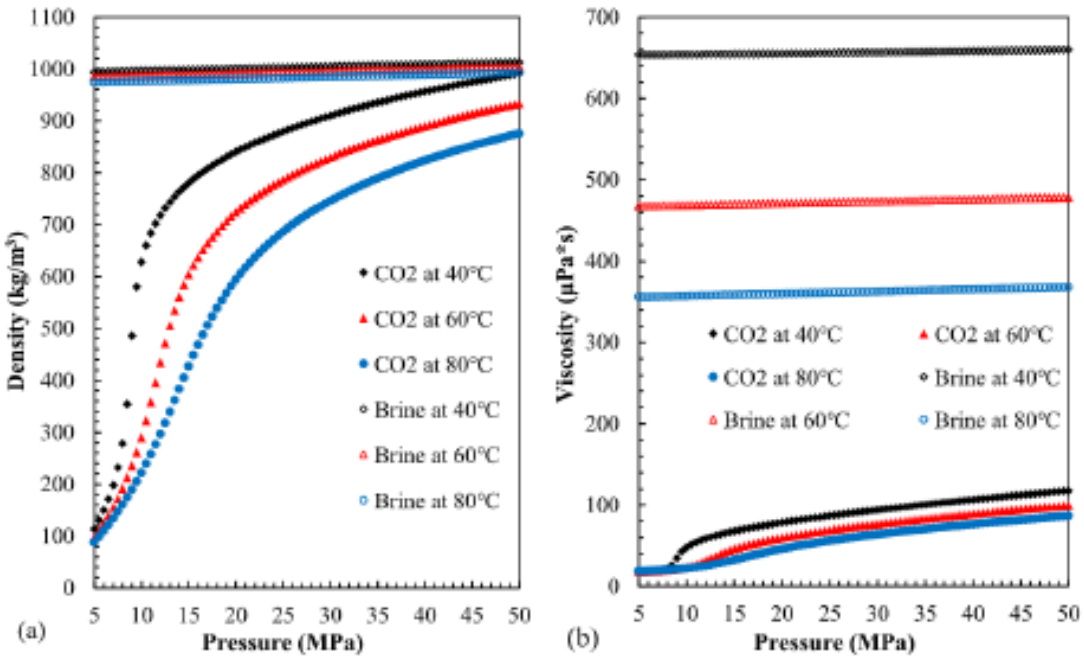

Figure 23: State curves showing CO_2 and Brine physical properties ((a): density; (b): viscosity against pressure) (Data obtained from the NIST (National Institute of Standards and Technology, USA) Chemistry Webbook (2016)) via (Wu et al., 2018).

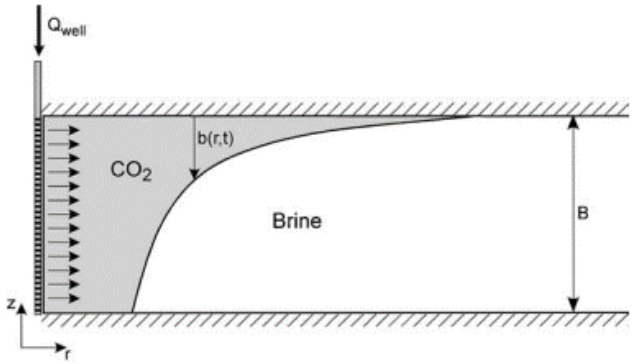

Figure 24: Diagram of the reservoir's CO_2 and brine flow.

3.6.1 Fundamentals of Two-Component, Two-Phase Flow

This solution closely follows the assumptions of two-component and two-phase flow as seen in the work of Zeidouni et al. (2009). The equation for mass continuity for a 1-dimensional system of radial symmetry for an incompressible 2-phase, CO_2 and water radial flow system was written as:

$$\phi \frac{\partial}{\partial t}(\omega_{ca}\rho_a S_a + \omega_{cg}\rho_g S_g) = -\frac{1}{r}\frac{\partial}{\partial r}[r(\omega_{ca}\rho_a q_a + \omega_{cg}\rho_g q_g)] \quad (1)$$

$$\phi \frac{\partial}{\partial t}(\omega_{wa}\rho_a S_a + \omega_{wg}\rho_g S_g) = -\frac{1}{r}\frac{\partial}{\partial r}[r(\omega_{wa}\rho_a q_a + \omega_{wg}\rho_g q_g)] \quad (2)$$

Where ø = porosity

t = time

r = radial distance

ω = mass fraction (Subscripts c, w, a, and g indicate CO2, water, aqueous phase, and gas phase respectively.

q = volumetric flux (subscript a and g represents aqueous phase and gas phase respectively

S = volumetric saturation.

The mass fractions and saturations are related as follows:

$$\omega_{ca} + \omega_{wa} + \omega_{sa} = 1 \quad (3)$$

$$\omega_{cg} + \omega_{wg} = 1 \quad (4)$$

$$S_a + S_g + S_s = 1 \quad (5)$$

They introduced a similarity transform z as follows:

$$z = \frac{\pi\phi\rho_c H r^2}{M_0 t} \quad (6)$$

Where M_0 = constant CO_2 mass injection rate

ρ_c = density of CO_2

H = formation thickness.

This similarity transforms in equation 6 reduces equation 1 and 2 to (Orr, 2007):

$$z = \frac{dH_c}{dG_c} = \frac{dH_w}{dG_w} \tag{7}$$

Where the G and H functions were defined as:

$$G_c = c_{ca}S_a + c_{cg}S_g, \qquad H_c = q_D a_c \tag{8}$$

$$G_w = c_{wa}S_a + c_{wg}S_g, \qquad H_w = q_D a_w \tag{9}$$

Where,

$$a_c = c_{ca}f_a + c_{cg}f_g, \qquad a_w = c_{wa}f_a + c_{wg}f_g, \tag{10}$$

And f_a and f_g indicate the aqueous phase and the gas phase fractional flows respectively, such that,

$$f_a = \frac{q_a}{q_a + q_g}, \qquad f_g = \frac{q_g}{q_a + q_g} \tag{11}$$

Also,

$$c_{ca} = \frac{\omega_{ca}\rho_a}{\rho_c}, \qquad c_{wa} = \frac{\omega_{wa}\rho_a}{\rho_c} \tag{12}$$

$$c_{cg} = \frac{\omega_{cg}\rho_g}{\rho_c}, \qquad c_{wg} = \frac{\omega_{wg}\rho_g}{\rho_c} \tag{13}$$

$$q_D = \frac{2\pi\rho_c Hr(q_a + q_g)}{M_0} \tag{14}$$

3.6.2 Determination of Shock Location and Evaluating q_D

Both trailing and leading shocks are produced by the two-phase, two-component system. (Noh et al., 2007; Zeidouni et al., 2009; Orr, 2007). Mathias et al. (2011b) proposed finding the locations of the trailing and leading shocks (z_T and z_L) using mass balance equations such that:

$$H_{c1} - H_{c3} = G_{c1}z_T + \int_{z_T}^{z_L} G_c dz - G_{c3}z_L, \quad (15)$$

$$H_{w1} - H_{w3} = G_{w1}z_T + \int_{z_T}^{z_L} G_w dz - G_{w3}z_L \quad (16)$$

Where,

$Gc1 = Gc(z = 0)$, $Gw1 = Gw\ (z = 0)$, $Hc1 = Hc\ (z = 0)$ and $Hw1 = Hw\ (z = 0)$, are descriptions of the physical state of the injection fluid,

and,

$Gc3 = Gc(z \to \infty)$, $Gw3 = Gw\ (z \to \infty)$, $Hc3 = Hc\ (z \to \infty)$ and $Hw3 = Hw\ (z \to \infty)$, represent the physical state of the brine in the aquifer at the initial.

They applied the chain rule on equations 15 and 16 to get:

$$\int_{z_T}^{z_L} G_c dz = \int_{G_{cT}}^{G_{cL}} G_c \frac{dz}{dG_c} dG_c, \quad (17)$$

Where,

$G_{cT} = Gc(z = z_T)$ and $G_{cL} = Gc(z = z_L)$

Integrating equation 17 by parts gave:

$$\int_{G_{cT}}^{G_{cL}} G_c \frac{dz}{dG_c} dG_c = [G_c z]_{G_{cT}}^{G_{cL}} - \int_{G_{cT}}^{G_{cL}} z dG_c \quad (18)$$

Which on substituting equation 7, similarly to Welge (1952),

$$[G_c z]_{G_{cT}}^{G_{cL}} - \int_{G_{cT}}^{G_{cL}} z dG_c = [G_c z - H_c]_{G_{cT}}^{G_{cL}} \quad (19)$$

From equation 19, it was derived that:

$$\int_{z_T}^{z_L} G_c dz = G_{cL} z_L - H_{cL} - G_{cT} z_T + H_{cT} \quad (20)$$

Where,

$H_{cT} = Hc(z = z_T)$ and $H_{cL} = Hc(z = z_L)$.

Substituting equation 20 into equation 15 gave:

$$H_{c1} - H_{c3} = G_{c1} z_T + G_{cL} z_L - H_{cL} - G_{cT} z_T + H_{cT} - G_{c3} z_L \quad (21)$$

Also,

$$H_{w1} - H_{w3} = G_{w1} z_T + G_{wL} z_L - H_{wL} - G_{wT} z_T + H_{wT} - G_{w3} z_L \quad (22)$$

Where,

$G_{wT} = Gw(z = z_T)$, $G_{wL} = Gw(z = z_L)$, $H_{wT} = Hw(z = z_T)$ and $H_{wL} = Hw(z = z_L)$

Thus, they derived an expression for the location of z_T by considering the equation of mass conservation for CO_2 and brine (water) within the area bounded by: $0 \leq z < z_T$, such that,

$$H_{c1} - H_{cT} = (G_{c1} - G_{cT}) z_T \quad (23)$$

$$H_{w1} - H_{wT} = (G_{w1} - G_{wT}) z_T \quad (24)$$

This reorders to:

$$z_T = \frac{H_{c1} - H_{cT}}{G_{c1} - G_{cT}} = \frac{H_{wT} - H_{w1}}{G_{wT} - G_{w1}} \quad (25)$$

Putting equation 25 into equations 21 and 22 results in:

$$z_L = \frac{H_{cL} - H_{c3}}{G_{cL} - G_{c3}} = \frac{H_{w3} - H_{wL}}{G_{w3} - G_{wL}} \quad (26)$$

With this, q_D was evaluated by dividing the system into three regions:

$$q_D = \begin{cases} q_{D1}, & 0 \le z < z_T \\ q_{D2}, & z_T \le z \le z_L \\ q_{D3}, & z > z_L \end{cases} \quad (27)$$

From equation 25 and 26, it was found that:

$$\frac{q_{D2}a_{cL} - q_{D3}a_{c3}}{G_{cL} - G_{c3}} = \frac{q_{D3}a_{w3} - q_{D2}a_{wL}}{G_{w3} - G_{wL}} \quad (28)$$

$$\frac{q_{D1}a_{c1} - q_{D2}a_{cT}}{G_{c1} - G_{cT}} = \frac{q_{D2}a_{wT} - q_{D1}a_{w1}}{G_{wT} - G_{w1}} \quad (29)$$

Using methods described in Orr (2007) and Zeidouni et al. (2009), q_{D2} and q_{D3} were derived as:

$$q_{D3} = q_{D2}\left[\frac{a_{wL}(G_{cL} - G_{c3}) + a_{cL}(G_{w3} - G_{wL})}{a_{w3}(G_{cL} - G_{c3}) + a_{c3}(G_{w3} - G_{wL})}\right] \quad (30)$$

$$q_{D2} = q_{D1}\left[\frac{a_{w1}(G_{c1} - G_{cT}) + a_{c1}(G_{wT} - G_{w1})}{a_{wT}(G_{c1} - G_{cT}) + a_{cT}(G_{wT} - G_{w1})}\right] \quad (31)$$

For the dry out zone (where $z < z_T$), the volumetric flow rate is not different from what was being injected thus making q_{D1}= 1.

The spreading wave was described as the area where f_g changes with gas saturation S_g, such that:

$$z = \frac{dH_c}{dG_c} = q_D\frac{df_g}{dS_g} \quad (32)$$

Thus, as long as a spreading wave is either trailing or leading the shocks z_T and z_L, we have:

$$z_L = q_{D2}\frac{df_g}{dS_g}\Big|_{S_g = S_{gL}} \quad \text{and} \quad z_T = q_{D2}\frac{df_g}{dS_g}\Big|_{S_g = S_{gT}} \quad (33)$$

Substitution the formulas in equation 33 into equations 25 and 26 and using the definitions in equations 8 and 9 gave:

$$\left.\frac{df_g}{dS_g}\right|_{S_g=S_{gs}} = \frac{A_1 + A_2 f_g(S_g = S_{gs})}{A_3 + A_2 S_{gs}} \tag{34}$$

Where:

$$A_1 = c_{ca} - (q_{D3}/q_{D2})a_{c3}, \quad A_2 = c_{cg} - c_{ca}$$
$$A_3 = c_{ca} - G_{c3}, \quad S_{gs} = S_{gL} \tag{35}$$

$$A_1 = (q_{D3}/q_{D2})a_{w3} - c_{wa}, \quad A_2 = c_{wa} - c_{wg}$$
$$A_3 = G_{w3} - c_{wa}, \quad S_{gs} = S_{gL} \tag{36}$$

$$A_1 = (q_{D1}/q_{D2})a_{c1} - c_{ca}, \quad A_2 = c_{ca} - c_{cg}$$
$$A_3 = G_{c1} - c_{ca}, \quad S_{gs} = S_{gT} \tag{37}$$

$$A_1 = c_{wa} - (q_{D1}/q_{D2})a_{w1}, \quad A_2 = c_{wg} - c_{wa}$$
$$A_3 = c_{wa} - G_{w1}, \quad S_{gs} = S_{gT}. \tag{38}$$

Mathias et al. (2011b) noted that it q_{D2} and q_{D3} had to be estimated iteratively except in the cases where the injection fluid has no water, and the reservoir fluid has no CO_2. This is a fundamental assumption of this model.

When this happens, we have:

$$G_{c1} = 1 - S_s, \quad a_{c1} = 1, \quad G_{w1} = 0, \quad a_{w1} = 0 \tag{39}, \text{ and}$$

$$G_{c3} = 0, \quad a_{c3} = 0, \quad G_{w3} = \omega_{wb}\rho_b/\rho_c, \quad a_{w3} = \omega_{wb}\rho_b/\rho_c \tag{40}$$

ρ_b is the water (brine) density while ω_{wb} is the mass fraction of pure water (no CO_2).

Also, $\omega_{wb} + \omega_{sb} = 1$ (ω_{sb} is the mass fraction of salt in the brine).

Having, $a_{w1} = G_{w1} = 0$, it is possible to calculate S_{gT} using equation 38 even when q_{D2} is unknown. The value of q_{D2} could then be calculated from equation 31. Also, $a_{c3} = G_{c3} = 0$ implies that S_{gL} can be estimated in a similar way as S_{gT} only using equation 35 and calculating q_{D3} from equation 30.

The volumetric saturation of salt that precipitates from brine using the method of Zeidouni et al. (2009) to give:

$$S_s = \frac{\omega_{sb}\rho_b(1 - S_{gT})}{\rho_s} \quad (41)$$

3.6.3 Applying Darcy's Law

From Darcy's law,

$$q_a = -\frac{kk_{ra}}{\mu_a}\frac{dP}{dr} \quad (42)$$

$$q_g = -\frac{kk_{rg}}{\mu_g}\frac{dP}{dr} \quad (43)$$

Where, k is the reservoir permeability,

μ_g is the dynamic viscosity of the gas phase

μ_a is the dynamic viscosity of the aqueous phase

$k_{ra}\ and\ k_{rg}$ are the relative permeabilities for the aqueous and gas phases respectively.

Thus, the equation of gas phase fractional flow f_g was derived as:

$$f_g = \left(1 + \frac{\mu_g k_{ra}}{\mu_a k_{rg}}\right)^{-1} \quad (44)$$

Assuming that the relative permeability functions are written in the form of power laws as:

$$k_{ra} = k_{ra0}\left(\frac{1 - S_g - S_{ar}}{1 - S_{gc} - S_{ar}}\right)^m \quad (45)$$

$$k_{rg} = k_{rg0}\left(\frac{S_g - S_{gc}}{1 - S_{gc} - S_{ar}}\right)^n \quad (46)$$

Where S_{ar} is the residual saturation of the aqueous phase and S_{gc} is the critical gas saturation

k_{ra0} and k_{rg0} are the endpoint relative permeabilities for the aqueous phase and the gas phase respectively.

The exponents m and n are the aqueous phase and gas phase power law exponents respectively.

Substituting equations 45 and 46 into equation 44 results in:

$$f_g = \left[1 + \gamma\left(\frac{1 - S_g - S_{ar}}{1 - S_{gc} - S_{ar}}\right)^m \left(\frac{S_g - S_{gc}}{1 - S_{gc} - S_{ar}}\right)^{-n}\right]^{-1} \quad (47)$$

Where,

$$\gamma = \frac{\mu_g k_{ra0}}{\mu_a k_{rg0}} \quad (48)$$

The differential of equation 47 w.r.t S_g led to:

$$\frac{df_g}{dS_g} = f_g(1 - f_g)\left[\frac{n(1 - S_g - S_{ar}) + m(S_g - S_{gc})}{(S_g - S_{gc})(1 - S_g - S_{ar})}\right] \quad (49)$$

In Fig. 25, Mathias et al. (2011b) plotted $\frac{df_g}{dS_g}$ versus S_g for different values of m and n. Where relative permeability is a nonlinear function of S_g, there are a range of values of $\frac{df_g}{dS_g}$ (Buckley and Leverett, 1942). In the specific cases where there is a linear relative permeability function, S_g has a single value.

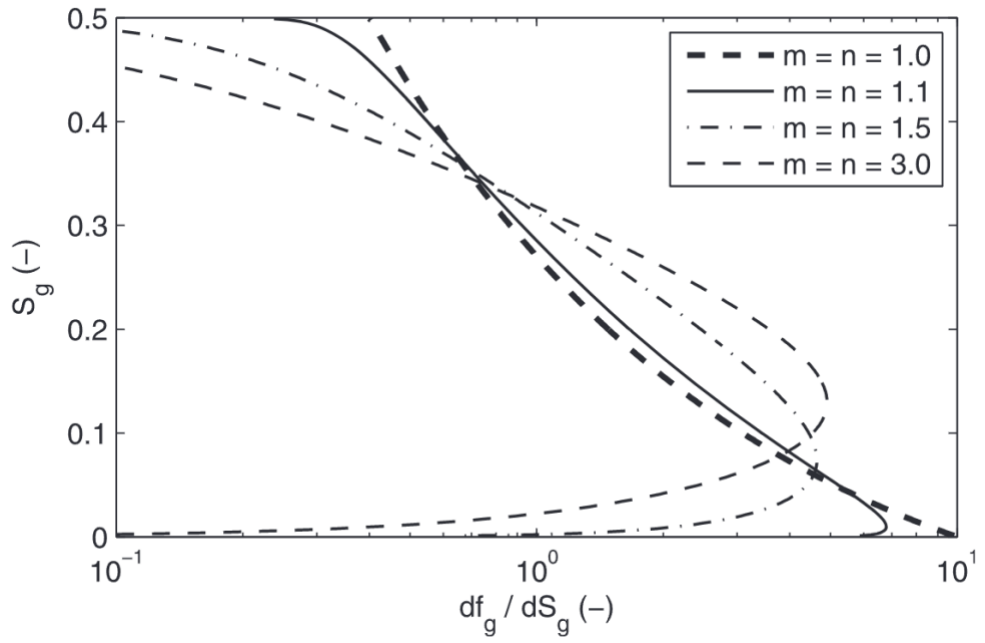

Figure 25: Plot of S_g against $\frac{df_g}{dS_g}$ for different values of m and n assuming γ= 0.2, S_{gc}= 0 and S_{ar}=0.5. (Mathias et al. (2011b).

For nonlinear relative permeability functions, getting closed-form solutions for S_{gT} and S_{gL} is infeasible using equation 34. In the special linear case, m = n = 1, and thus equations 47 and 49 reduce to:

$$f_g = \left[1 + \gamma\left(\frac{1 - S_g - S_{ar}}{S_g - S_{gc}}\right)\right]^{-1} \quad (50) \text{ and}$$

$$\frac{df_g}{dS_g} = \frac{\gamma(1 - S_{gc} - S_{ar})f_g^2}{(S_g - S_{gc})^2} \quad (51)$$

Putting this in equation 34 and calculating for S_{gs} gave:

$$S_{gs} = A_4 + \left\{\frac{\gamma(1 - S_{gc} - S_{ar})(A_4A_2 + A_3)}{(1 - \gamma)[(1 - \gamma)A_1 + A_2]}\right\}^{\frac{1}{2}} \quad (52)$$

Where:

$$A_4 = \frac{S_{gc}(A_1 + A_2) - \gamma(1 - S_{ar})A_1}{(1 - \gamma)A_1 + A_2} \tag{53}$$

With this, gas saturation at the leading and trailing shocks could be directly calculated making use of equations 35 and 38.

Equation 51 can be rearranged by combining equation 32 with equation 39 and 40 to give:

$$S_g = \begin{cases} 1 - S_s, & 0 \le z < z_T \\ 1 - S_{ar}, & z_T \le z \le z_C \\ S_{gc} + \frac{(1 - S_{gc} - S_{ar})}{(1 - \gamma)} \left[\left(\frac{z_C}{z} \right)^{\frac{1}{2}} - \gamma \right], & z_C < z \le z_L \\ 0, & z > z_L, \end{cases} \tag{54}$$

Where,

$$z_C = \frac{q_{D2}\gamma}{(1 - S_{gc} - S_{ar})} \tag{55}$$

When $z < z_c, S_g = 1 - S_{ar}$. Also note that when $z_T < z_c, z_T$ is no longer at the point where the spreading wave begins and thus, equation 34 is valid. When $z_T < z_c, S_{gT} = 1 - S_{ar}$ and $f_{gT} = 1$. Thus,

$$z_T = \frac{q_{D2}c_{wg}}{c_{wa}S_{ar} + c_{wg}(1 - S_{ar})}, \qquad z_T < z_C \tag{56}$$

q_{D2} is obtained from equation 31.

3.6.4 Pressure Buildup Equation

In solving for pressure, Mathias et al. (2011b) used Darcy's law as follows:

$$q_a + q_g = -k\left(\frac{k_{ra}}{\mu_a} + \frac{k_{rg}}{\mu_g}\right)\frac{dP}{dr} \tag{57}$$

Using the similarity transform z (6), and the q_D relationship (14) in equation 57 and rearranging led to:

$$\frac{dP}{dz} = -\frac{M_0}{4\pi\rho_c Hk}\left(\frac{k_{ra}}{\mu_a} + \frac{k_{rg}}{\mu_g}\right)^{-1}\frac{q_D}{z} \tag{58}$$

Using the description of shock fronts, z_T and z_L, earlier discussed,

$$\frac{dP}{dz} = -\frac{M_0}{4\pi\rho_c Hk}\begin{cases}\dfrac{\mu_c q_{D1}}{k_{rs} z}, & 0 \le z < z_T \\ \left(\dfrac{k_{ra}}{\mu_a} + \dfrac{k_{rg}}{\mu_g}\right)^{-1}\dfrac{q_{D2}}{z}, & z_T \le z \le z_L \\ \dfrac{\mu_b q_{D3}}{z}, & z > z_L, \end{cases} \tag{59}$$

Where,

k_{rs} is the permeability reduction factor caused by salt precipitation and μ_b and μ_c are the dynamic viscosity of pure brine and CO_2, respectively. Upon integrating, the pressure buildup equation was given as:

$$P - P_o = \frac{M_c}{4\pi\rho_c Hk}\begin{cases}\dfrac{\mu_c q_{D1}}{k_{rs}}\ln\left(\dfrac{z_T}{z}\right) + \mu_g q_{D2} F_2(z_T) + \mu_b q_{D3} F_1(z_L), & 0 \le z < z_T \\ \mu_g q_{D2} F_2(z) + \mu_b q_{D3} F_1(z_L), & z_T \le z \le z_L \\ \mu_b q_{D3} F_1(z), & z > z_L \end{cases} \tag{60}$$

Where P_o is the initial pressure, M_c is the mass injection rate of CO_2, ρ_c and μ_c are the density and dynamic viscosity of water-free CO_2, H is the formation thickness, k is the reservoir permeability, μ_b is the dynamic viscosity of CO_2-free brine and μ_g is the dynamic viscosity of the gas phase. The functions $F_1(z)$ and $F_2(z)$ were given as:

$$F_1(z) = \begin{cases} E_1(\alpha_1 z), \ z_E > \frac{0.5615}{\alpha_1} \\ (\alpha_1 z_E)^{-1} - \frac{3}{2} + \ln\left(\frac{z_E}{z}\right) + \frac{z - z_L}{z_E}, \ z_E < \frac{0.5615}{\alpha_1} \end{cases} \quad (61)$$

And for a circular closed aquifer of radial extent r_E, using the matched asymptotic expansions approach in Mathias et al (2009c, 2011),

$$F_2(z) = -\frac{1}{\mu_g}\int_z^{z_L}\left(\frac{k_{ra}}{\mu_a} + \frac{k_{rg}}{\mu_g}\right)^{-1}\frac{1}{z}dz$$

Where:

$$\alpha_1 = \frac{M_c \mu_b (c_r + c_b)}{4\pi H \rho_c k}, \ z = \frac{\pi \emptyset \rho_c H r^2}{M_c t}, \ z_E = \frac{\pi \emptyset \rho_c H r_E^2}{M_c t} \quad (62)$$

E_1 is the En function with n = 1 that is related to the exponential integral function, $E_i(x)$, such that $E_1(x) = -E_i(-x)$. $c_r \ and \ c_b$ are the rock and brine compressibilities, respectively, μ_a is the dynamic viscosity of the gas phase, $k_{ra} \ and \ k_{rg}$ are the relative permeabilities for the aqueous and gas phases respectively, $\emptyset$ is porosity and r_E is the reservoir's radial extent.

The fluid properties were calculated using the Hassanzadeh et al. (2008) equations of state (EOS) that utilized the work of Batzle and Wang (1992), Fenghour et al. (1998), Spycher et al. (2003) and Spycher and Pruess (2005) (Mathias et al., 2011b). The calculation uses a specified pressure value to estimate fluid properties, which Mathias et al. (2011b) recommend as a final estimate of pressure. However, this is infeasible in many practical applications, as the point of using models is to predict the pressure buildup. If the estimate of the final pressure used is far too small compared to the final pressure, the method will be inaccurate. This is one avenue for inaccuracy as the fluid properties influence the estimation of $\alpha_1 = \frac{M_c \mu_b (c_r + c_b)}{4\pi H \rho_c k}$ which determines what section of equation 61 to use. If the value of α_1 is too large, the fraction $\frac{0.5615}{\alpha_1}$ becomes small

leading to an underestimation of pressure buildup. When α_1 is too small, $\frac{0.5615}{\alpha_1}$ becomes large leading to an overestimation of pressure buildup. This is especially important in small aquifers (smaller radial extent). For very large systems, z_E is almost always greater than $\frac{0.5615}{\alpha_1}$ and thus, $F_1(z)$ is computed correctly.

In this thesis, a different approach was proposed to address this flaw in the model using slope correction factors that was born from "what-if" data analysis such that a factor was calculated to multiply time. This factor will affect the similarity transform z and force the value of pressure calculated at a particular time to its actual value when the same model was built using CMG GEMS. This eliminates the need for guessing the final pressure with which to calculate fluid properties. The fluid properties could instead be calculated using initial reservoir pressure, but these factors could be applied to time and thus the similarity transform (z) to calculate pressure.

In summary, the method of Mathias et al. (2011b) used in this thesis makes the following assumptions:

1. Circular closed aquifer of radial extent.
2. Constant fluid properties estimated at an arbitrary pressure.
3. Linear relative permeability
4. Constant rate injection.

This method's benefit is that it considers the influence of partial miscibility, including CO_2 solubility, on pressure buildup.

Chapter 4: Results and Discussion

4.1 Introduction

This chapter shows the results obtained from using Milad et al.'s (2022) geological model to verify the 100-psi maximum historical pressure buildup from water disposal reported by the operator. It also shows the results of simulating CO_2 sequestration using 1 injection well as highlighted in section 3.5.2 and 3.5.3 in the Arbuckle Group and the accompanying sensitivity analyses. To determine how well the analytical model of Mathias et al. (2011b) does in predicting pressure buildup, results from the CMG GEMS simulation of CO_2 sequestration using 1 injection well at constant flow rate was used and compared against the results from applying the semi-analytical solution while varying pore volume using the reservoir's radial extent

4.2 Verification of 100 Psi Maximum Historical Pressure Buildup from Water Disposal

The maximum historical pressure buildup from water disposal was verified as highlighted in sections 3.5.1. Open flow boundary was simulated using a horizontal well in the northwest boundary of the Osage Arbuckle set to produce at a minimum bottomhole pressure of 1500 psi (initial pressure at that depth).

The simulation was run using the injection history. The pressure evolution is shown in Fig. 26. Fig. 27 shows the pressure evolution with increasing distance from the injection well.

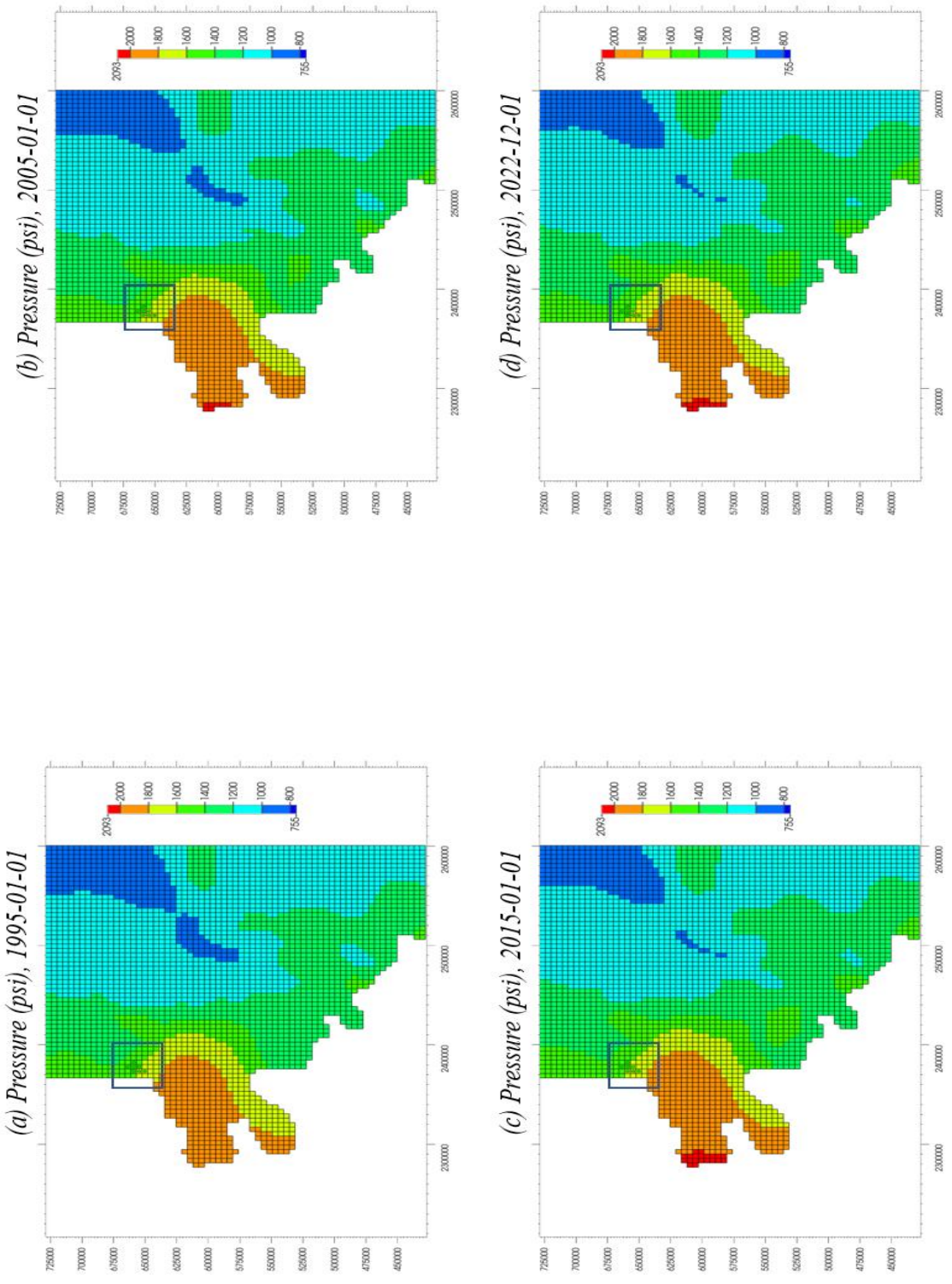

Figure 26: Simulation of Pressure evolution in Arbuckle using Milad et al. (2022) Permeabilities. (Blue box indicates North Burbank Unit injection region). Red indicates higher pressure and blue lower pressure.

Fig. 26 shows that there was little change in pressure from water injection. This was further highlighted in Fig. 27. The deep blue patches in the earlier frames become lighter in latter frames indicating a slight increase in pressure and the red patch on the west side ("panhandle") expanded slightly.

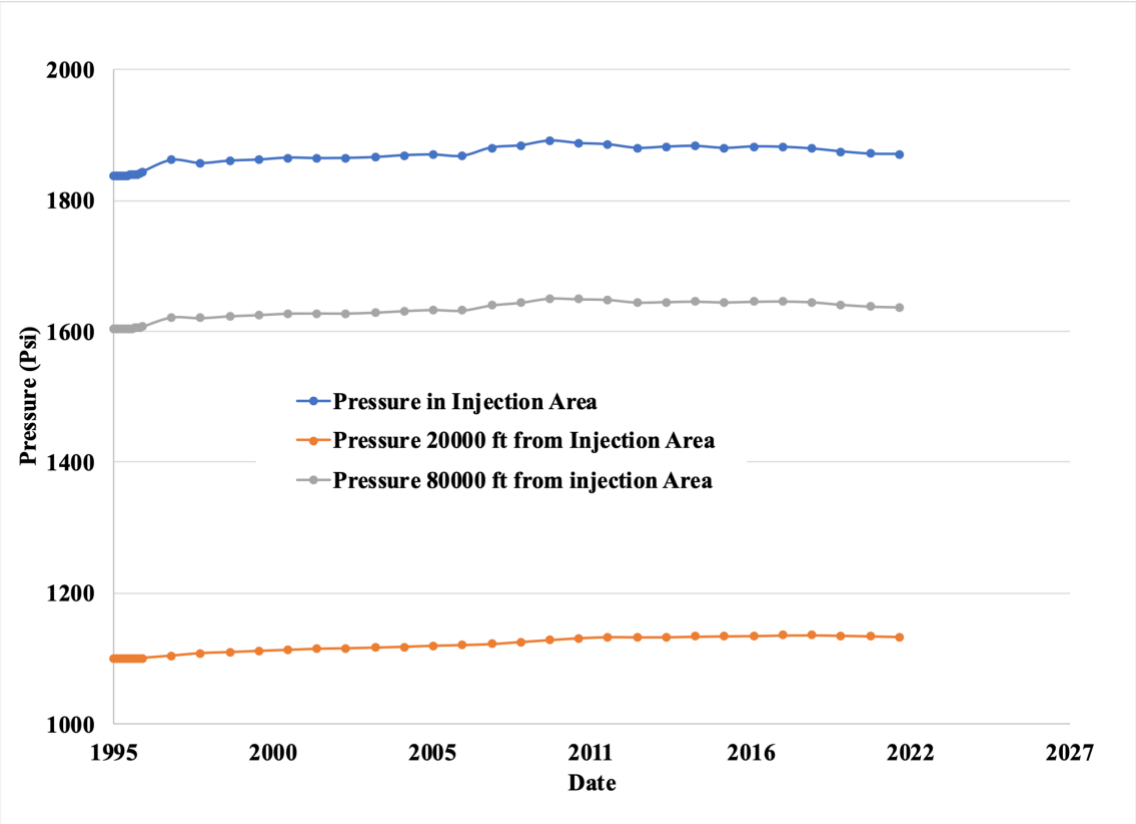

Figure 27: Pressure evolution with increasing distance from Injection Area.

From Fig. 27, it was implied that the pressure at all points never exceeds 100 psi more than the initial pressure matching the operator's observations as highlighted in section 3.4. This provides evidence that affirms the geological model in Milad et al. (2022). Fig. 27 also shows that the pressure reduced with increasing distance from the injection point and the rate of variation significantly reduces further away from the injection site.

4.3 CO_2 Simulation and Sensitivity Analysis

4.3.1 Simulation of the Injection of CO_2 for 30 years and 50 years of monitoring at the end of injection Using Coarse Grids.

The simulation of the injection of at least 50 million metric tons (964 Bcf) of CO_2 into the Arbuckle Saline aquifer was attempted using the reservoir and well characteristics as highlighted in Chapter 3. The simulation was run for 30 years after injection and 50-years post-injection. Fig. 28 shows the placement of the well in the coarse grid. Open flow boundary was again simulated using a horizontal well in the northwest boundary of the Osage Arbuckle set to produce at a minimum bottomhole pressure of 1500 psi (initial pressure at that depth).

Fig. 29 shows the cumulative injection trend for the entire field. The plot in Fig. 29 shows the injection of 39.6 million metric tons (737 Bcf) of CO_2 in this reservoir with one injection well and the outlined reservoir properties and constraints. This does not meet the set requirement for the injection of 50 million metric tons in this formation.

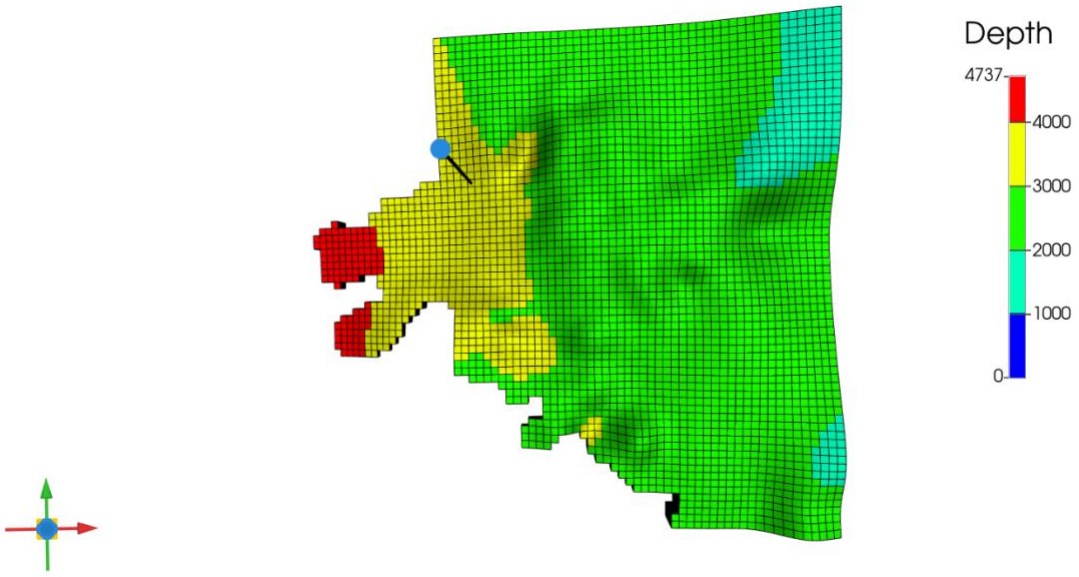

Figure 28: Well Arrangement in Grid for CO_2 Simulation (Black dots in square indicate injection wells)

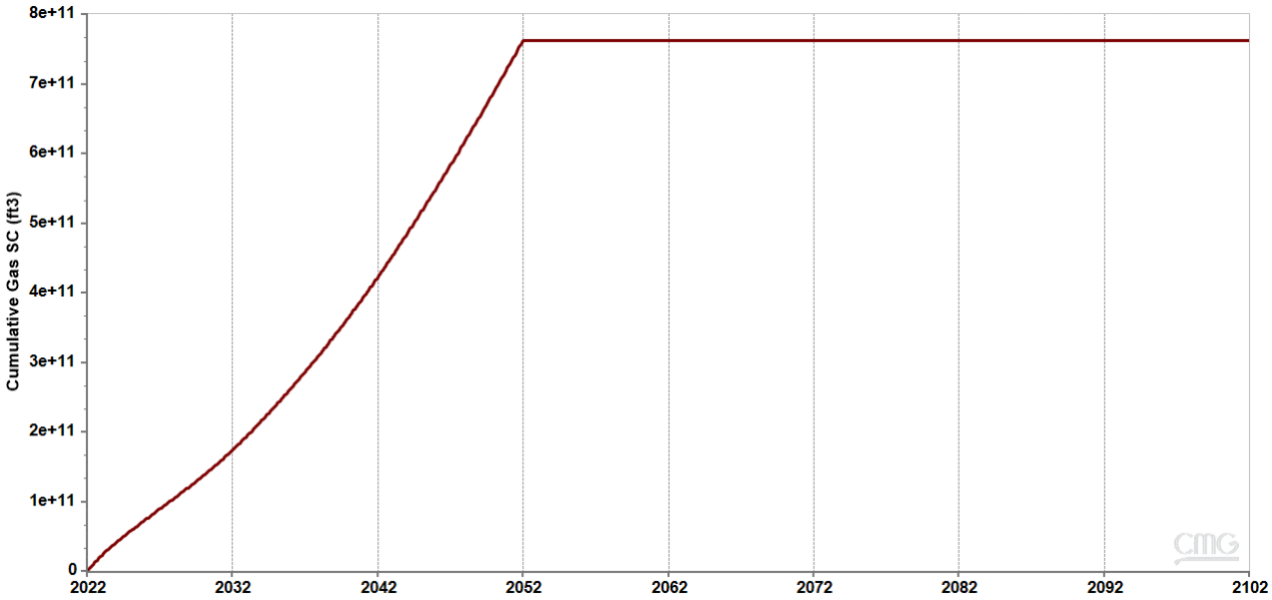

Figure 29: Field Cumulative Injection showing the injection of 737 Bcf (39.6 million MT) of CO_2 in 30 years

Fig. 30 shows the evolution of the pressure in the injection well block with time. The pressure in the block peaked at 2040 psi from the initial 1800 psi, an increase of about 240 psi from injection in this well. The pressure falls after injection was concluded to about 1700 psi after 50 years post-injection.

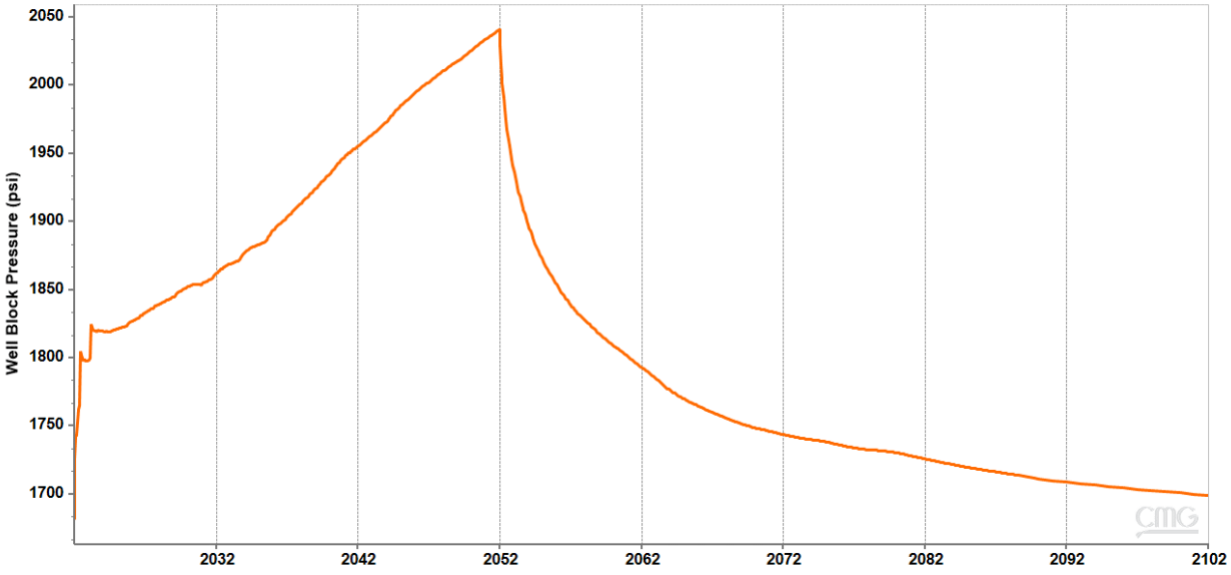

Figure 30: Injection well block pressure evolution

For the base case constraint (maximum bottomhole pressure = 90% of fracture pressure), Fig. 31 shows the average pressure in the system. Fig. 32 shows the pressure evolution over time in the formation. The blue box indicates the North Burbank region where the injection wells were drilled. From Fig. 31, it was found that pressure gradually increases across the formation as injection proceeded. The maximum pressure in any grid block is 2274 psi in the year 2052 found in the horn of the Osage Arbuckle where formation depth is 4825 ft and $fracture\ pressure = 0.6 \times 4825 = 2895\ psi$. In other words, the maximum pressure is below 90% of the fracture pressure (2606 psi) in that block reducing the risk of fracture or induced seismicity in the region. On conclusion of injection, average pressure in the formation started to reduce. The peak average pressure was 1388 psi (from 1280 psi), an increase of just over 100 psi in the system overall.

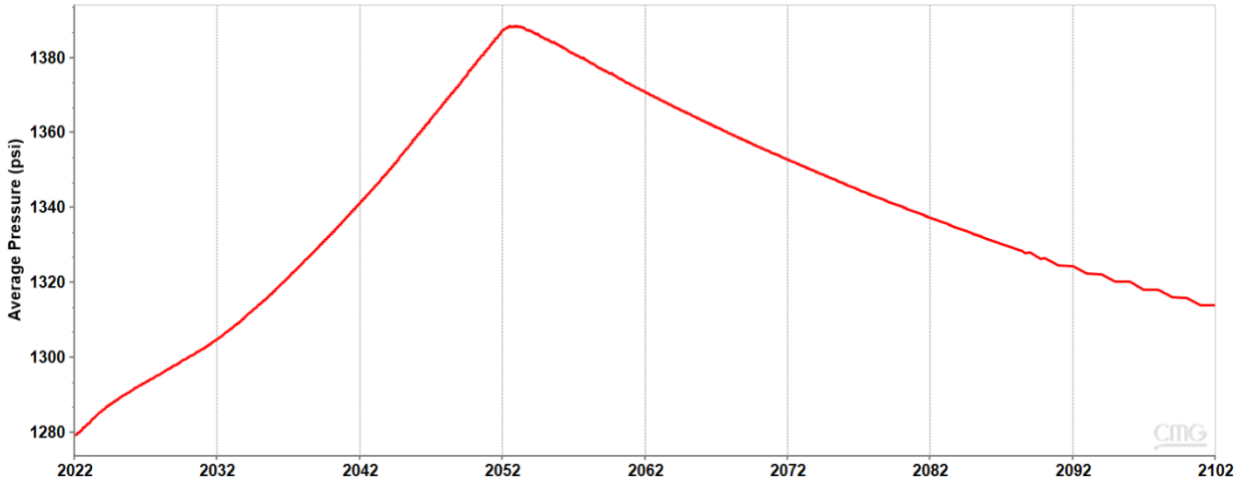

Figure 31: Average Pressure in the formation for 30 years injection and 50 years post-injection

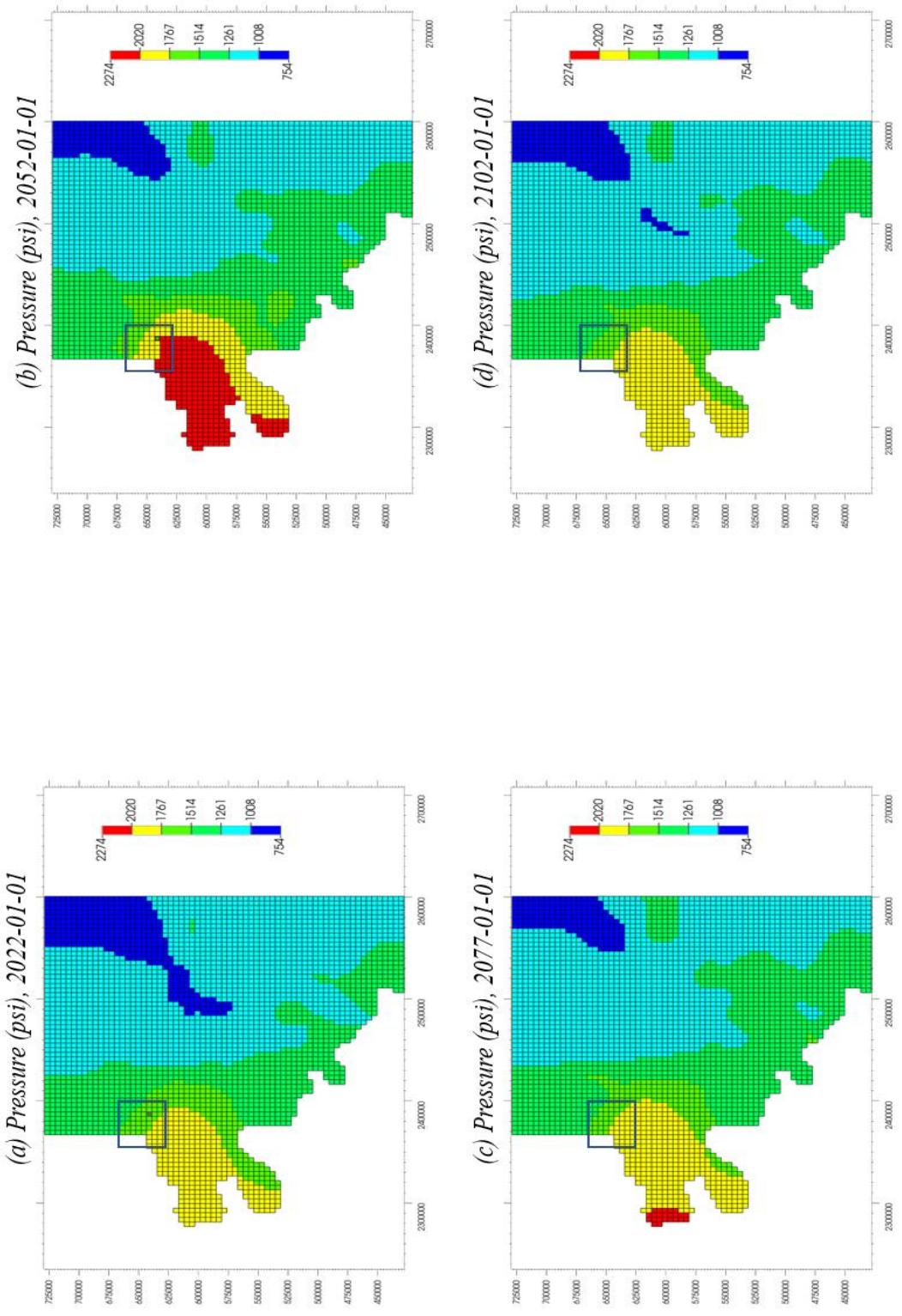

Figure 32: Pressure evolution in Arbuckle with CO_2 injection. (Blue box indicates North Burbank Unit injection region). Red indicates high pressure; blue indicates low pressure and green represents moderate pressure.

As seen in Fig. 33, of the total mass of CO_2 injected, most (33 million MT) was trapped hydrologically in supercritical condition as at the end of injection (2052). Residual trapping starts to occur on completion of injection with about 14 million MT stored residually as at 50 years post-injection.

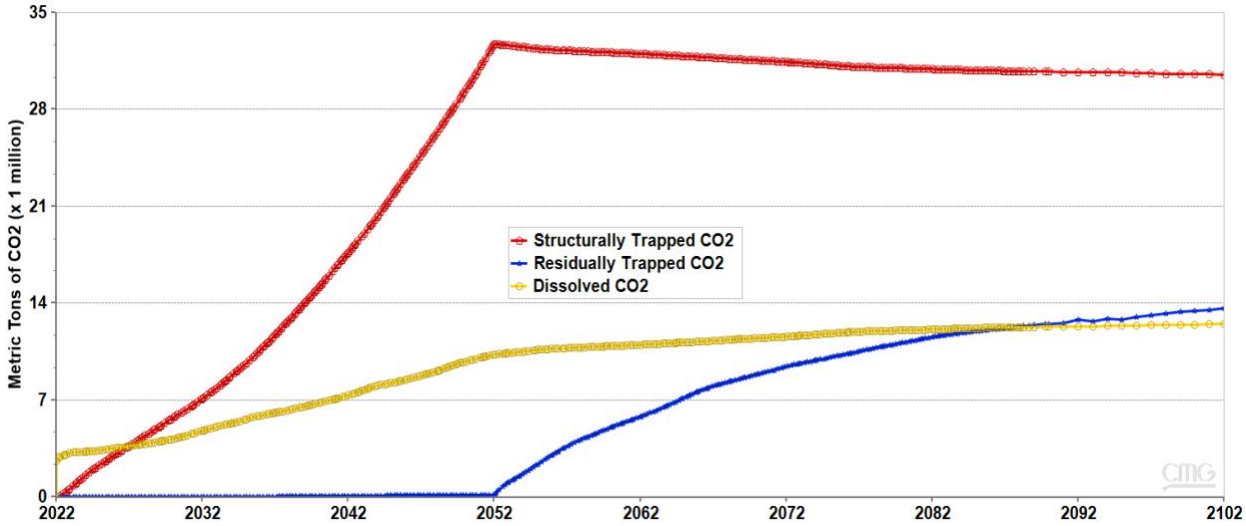

Figure 33: Proportions of CO_2 stored by various mechanisms.

Fig. 34 shows the CO_2 plume evolution overtime in the reservoir's 7th layer. The 7th layer was chosen because it has the highest CO_2 saturation of all layers during injection. It was observed that the size of the plume and the gas saturation around the area of injection in layer 7 gradually increased during the 30 years of injection (2022 – 2052). Beyond the period of injection, this trend reversed, and the CO_2 plume gradually migrated upwards as the initially displaced brine starts to fill back into the pore spaces. This was visualized in Fig. 35 which shows the CO_2 plume (saturation) evolution along the injection well. In general, the CO_2 plume never migrates beyond the North Burbank Injection Region and is some distance away from the Ada-Vamoosa underground sources of drinking water (USDW) in the area. The CO_2 plume was not well defined due to some numerical dispersion that amounts from using coarse grids.

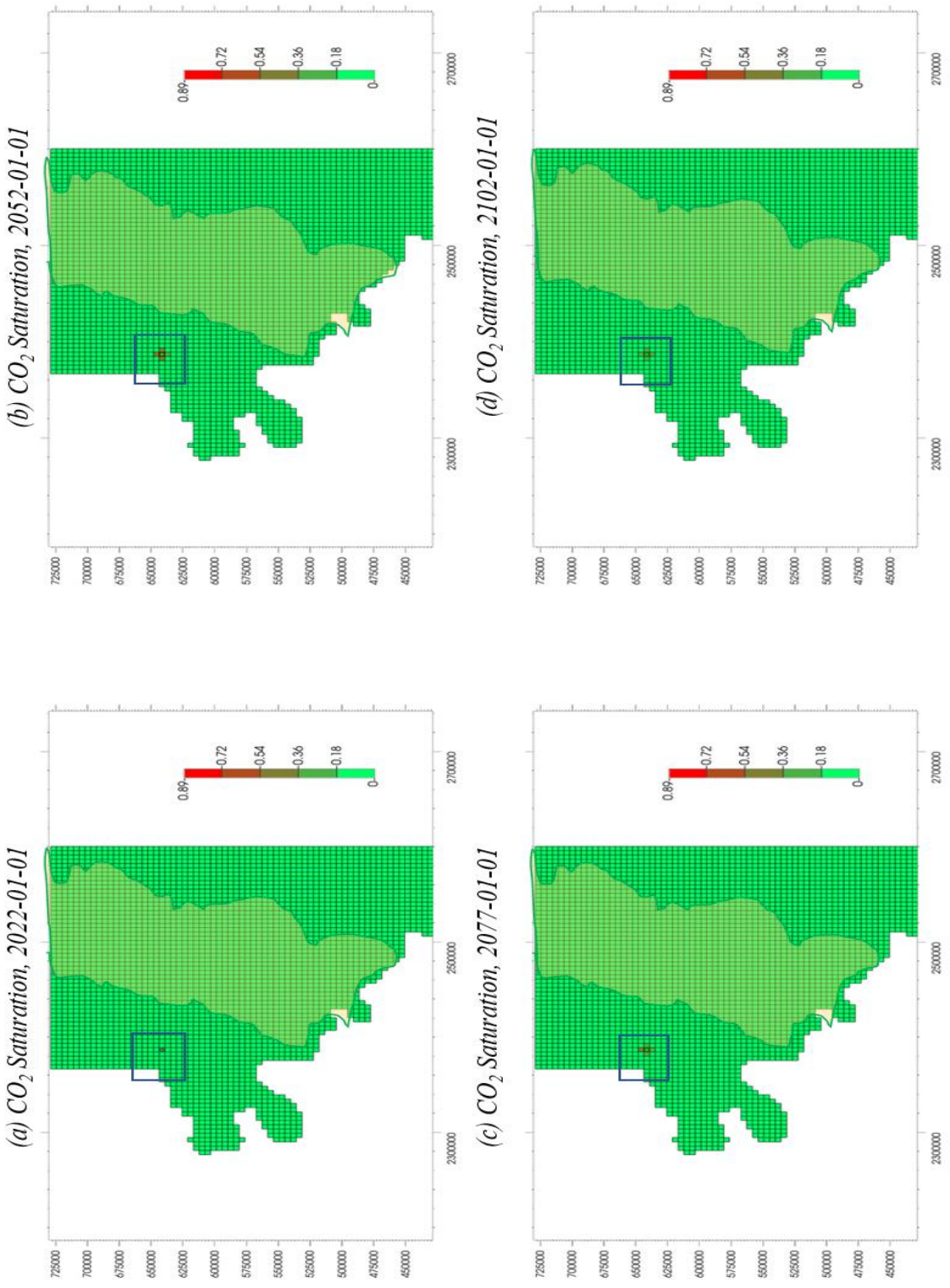

Figure 34: Areal map showing CO_2 plume evolution in Layer 7 of the Arbuckle with CO_2 injection. (Blue box indicates North Burbank Unit injection region, orange polygon indicates Ada-Vamoosa USDW aquifer). Red indicates higher plume saturation.

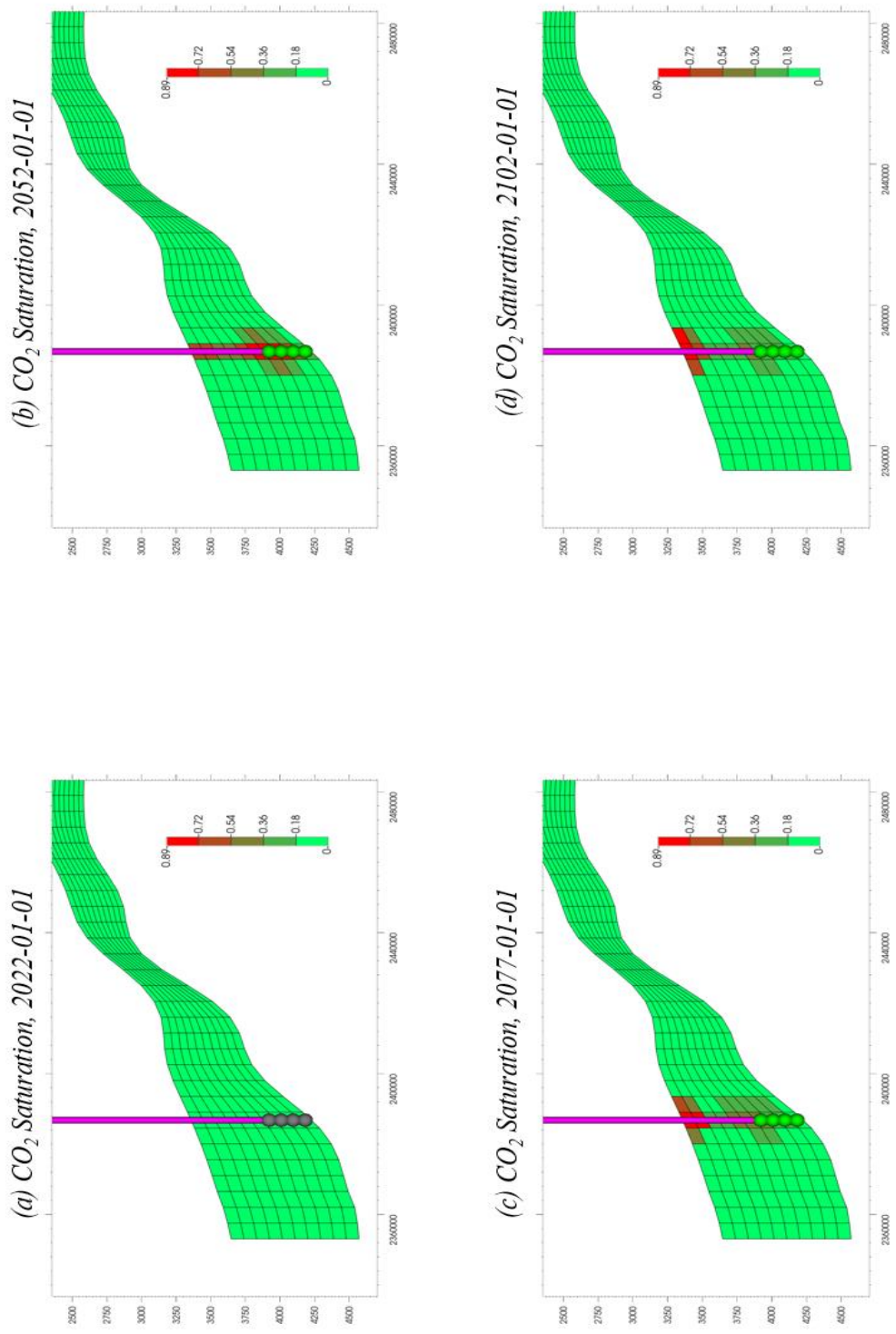

Figure 35: View of CO_2 plume evolution through the injection well showing the plume migrate to the top of the formation as residual gas trapping causes the brine to imbue back into the pore spaces it was displaced from.

4.3.2 Simulation of the Injection of CO_2 for 30 years and 50 years of monitoring at the end of injection Using Local Grid Refinement (LGR) around Injection Site.

To obtain a higher level of detail and accuracy in simulation results, local grid refinement was done around the injection site. To determine the optimal grid size in the "x" and "y" directions, sensitivity analysis was carried out using the cumulative injection as the objective function. The results were shown in table 4 below. Below 224.8 ft x 224.8 ft, there was little change in the predicted cumulative injection from the simulations. Thus, grid dimensions of 224.8 ft x 224.8 ft was used for simulation to balance computational time with accuracy. The grid size in the "z" direction remained the same with 10 layers, each with an average thickness of 40 ft.

Table 4: Sensitivity analysis to determine optimum grid dimension to balance accuracy and runtime with LGR around injection well

Dx x Dy	Cumulative Injection (Bcf)	Cumulative Injection (million MT)
4495 ft x 4495 ft	737	39.6
449.7 ft x 449.7 ft	1575	81.7
224.8 ft x 224.8 ft	1699	88.1
112.4 ft x 112.4 ft	1710	88.7
89.9 ft x 89.9 ft	1715	88.9

The grid cell dimension in the area around the injection well was reduced from 4497 ft x 4497 ft to 224.8 ft x 224.8 ft on the "x-y" axis to optimize accuracy and runtime. The injection well remained at the same location as in section 4.3.1.

Fig. 36 shows the cumulative injection for the entire field. The plot in Fig. 36 shows the injection of 88.1 million metric tons (1699 Bcf) of CO_2 in this reservoir with one injection well and the outlined reservoir properties and constraints. This was more than double the cumulative

injection obtained from running the simulation with coarse grids at every point (39.6 million MT). In other words, simulating with coarse grids caused a large underestimation of the injection capacity of this formation.

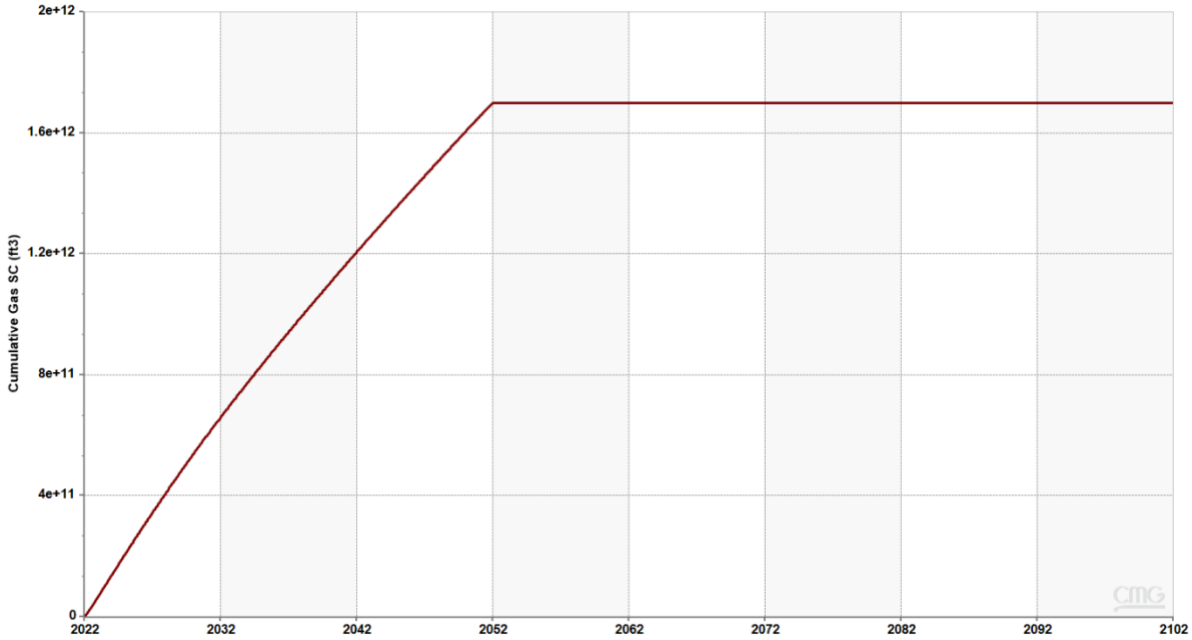

Figure 36: Field Cumulative Injection showing the injection of 1699 Bcf (88.1 million MT) of CO_2 in 30 years.

Fig. 37 shows the comparison of the pressure buildup at the injection well block with time. The pressure in the well block was very close to the bottom hole pressure of the well during injection thus highlighting the much-reduced numerical dispersion in the simulation.

Fig. 38 shows the pressure evolution over time in the formation. The blue box indicates the North Burbank region where the injection wells were drilled. The maximum pressure in any grid block is 2491 psi in the year 2052 found in the horn of the Osage Arbuckle where formation depth is 4825 ft and $fracture\ pressure\ = 0.6 \times 4825 = 2895\ psi$. In other words, the maximum pressure is below 90% of the fracture pressure (2606 psi) in that block reducing the risk of fracture or induced seismicity in the region.

Fig. 39 gives a closer look at the pressure plume evolution in the refined grid region around the injection well. It shows the overall increase in the pressure during injection when the pressures peak before they start reducing as once the injection well is shut in and liquid continues to move through the formation's open boundary.

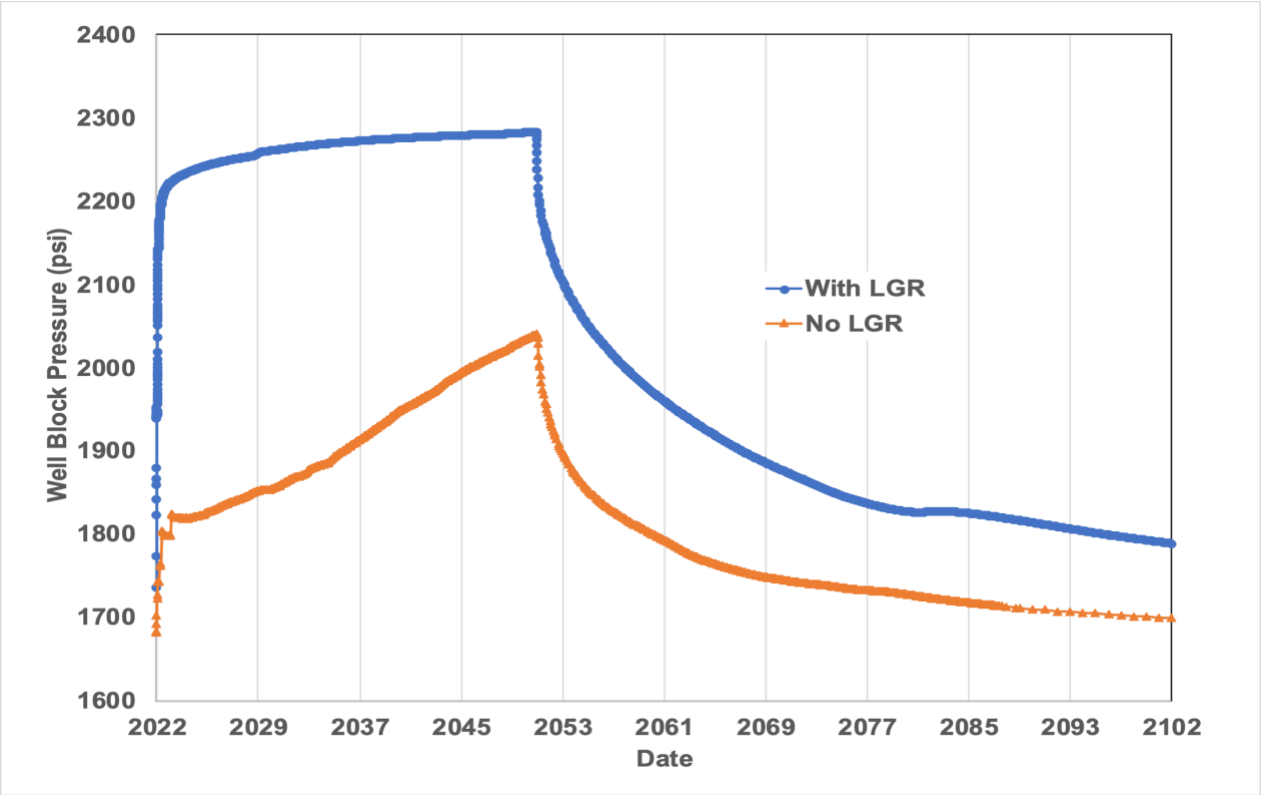

Figure 37: Comparison of Injection well block pressure evolution with and without local grid refinement

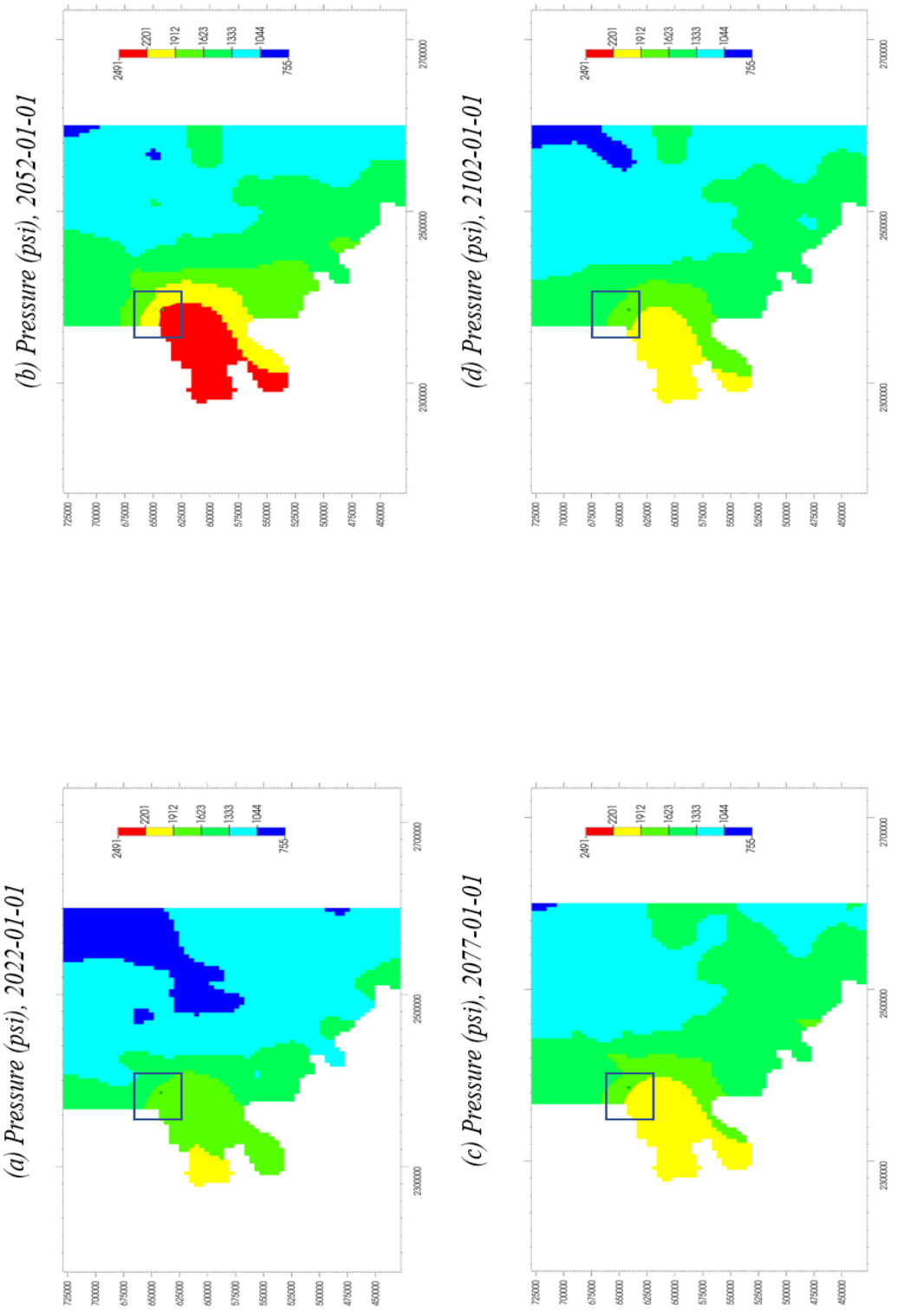

Figure 38: Pressure evolution in Arbuckle with CO_2 injection using local grid refinement around the injection well. (Blue box indicates North Burbank Unit injection region). Red indicates high pressure; blue indicates low pressure and green represents moderate pressure.

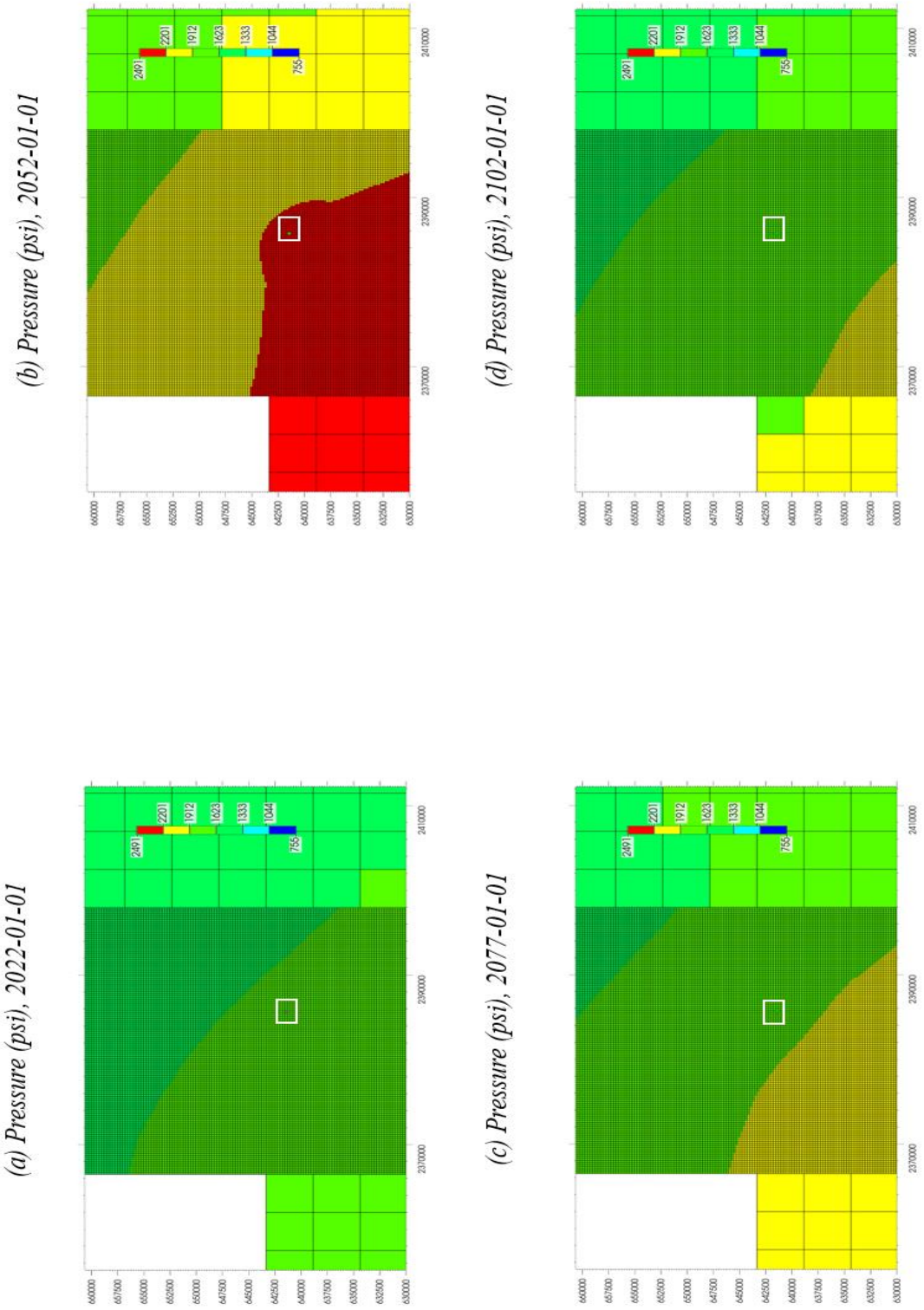

Figure 39: Pressure evolution in Arbuckle with CO_2 injection using local grid refinement around the injection well. (Blue box indicates North Burbank Unit injection region). Red indicates high pressure; blue indicates low pressure and green represents moderate pressure.

As seen in Fig. 40, of the total mass of CO_2 injected, most (85 million MT) was trapped hydrologically in supercritical condition as at the end of injection (2052). Residual trapping starts to occur on completion of injection with about 22 million MT stored residually as at 50 years post-injection. There was also about 10 million MT of dissolved CO_2 at the end of the 80-year observation period.

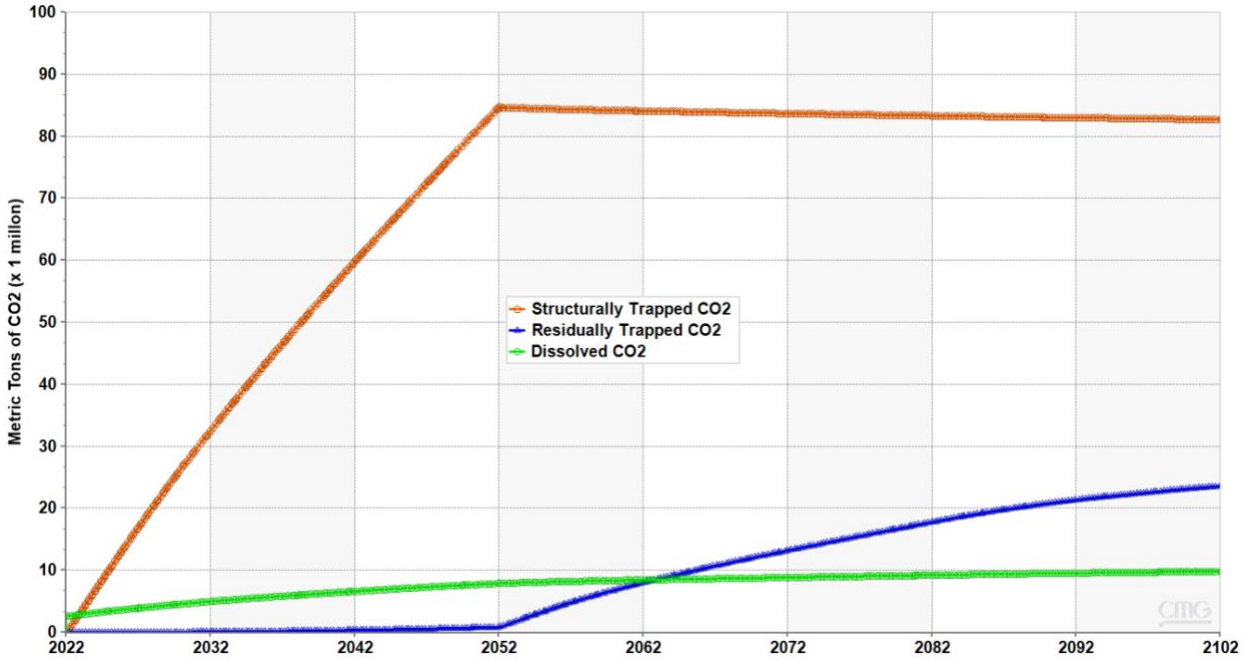

Figure 40: Proportions of CO_2 stored by various mechanisms with refined grid blocks around injection area.

To better appreciate the effect of the dissolution of CO_2 on carbon sequestration, a sensitivity case was run without accounting for CO_2 dissolution. Fig. 41 shows the comparison of cumulative injection for the solubility and no solubility cases. In Fig. 42, a comparison of the well block pressure is shown. CO_2 dissolution allowed for the injection of about 50 Bcf (2 million MT) more CO_2. Dissolution also slightly reduced the pressure around the well bore

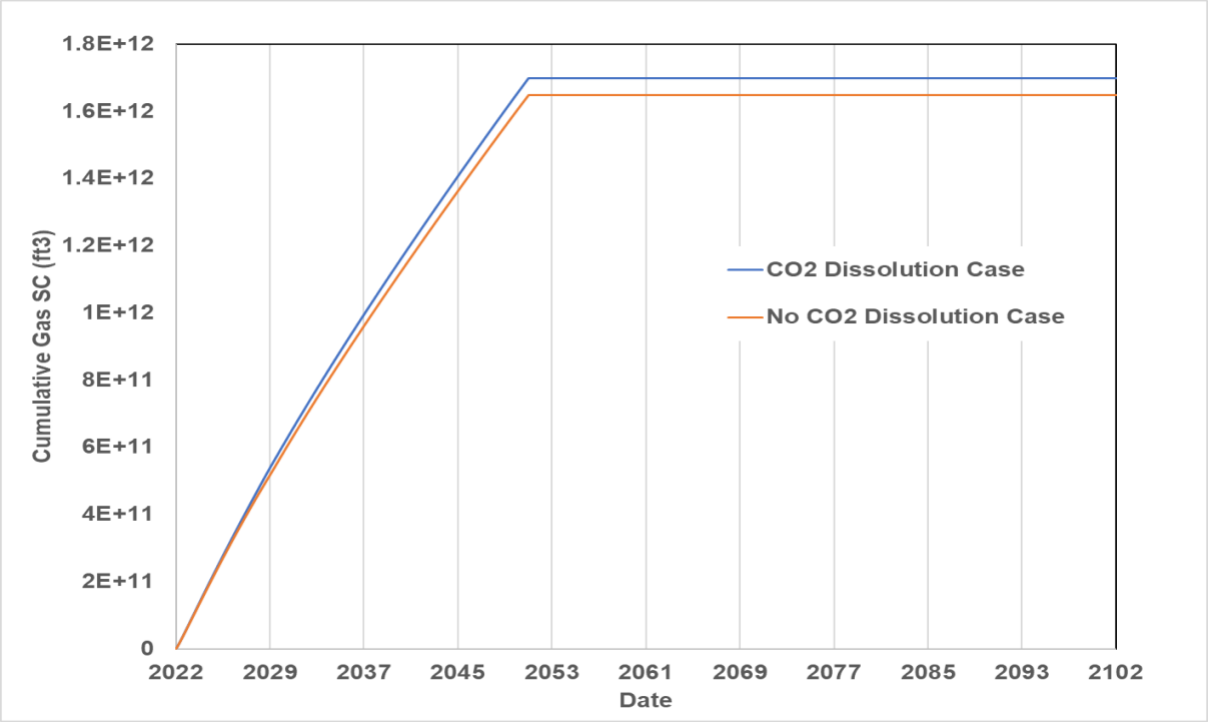

Figure 41: Comparison of cumulative gas injection with and without CO_2 dissolution

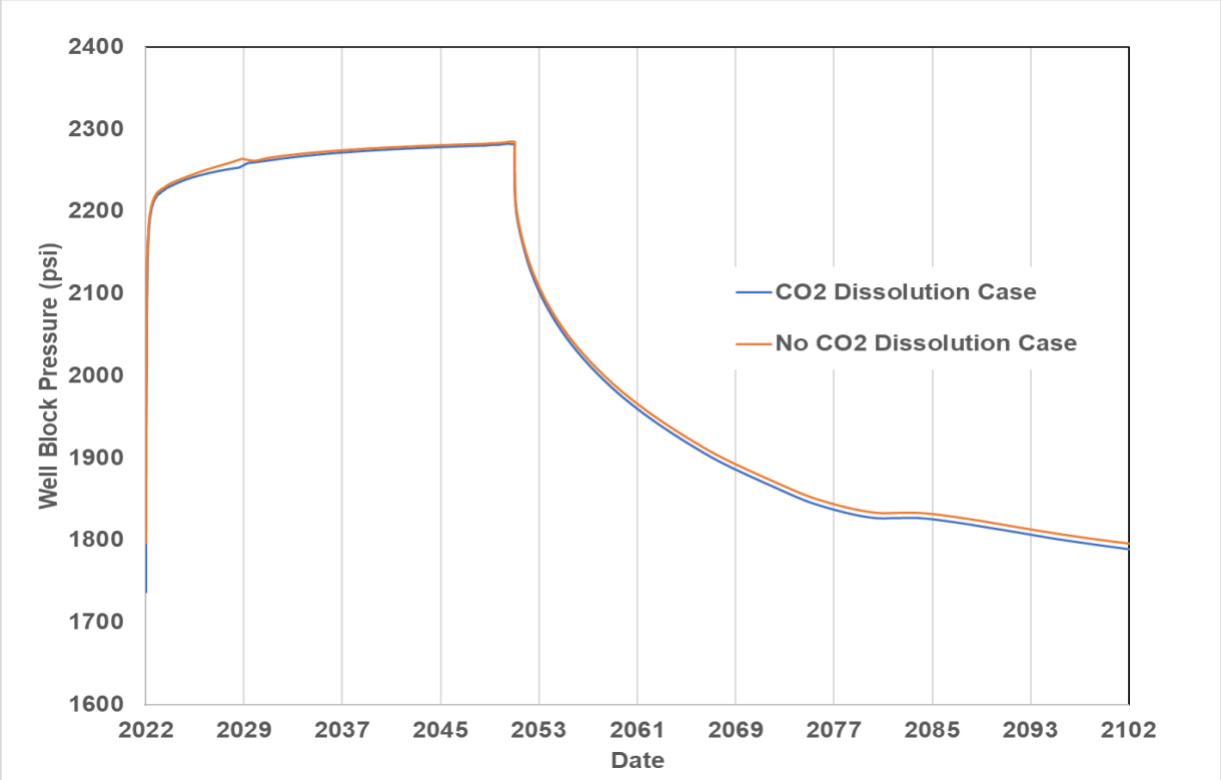

Figure 42: Comparison of injection well block pressure evolution with and without CO_2 dissolution

Fig. 43 and Fig. 44 shows the CO_2 plume evolution over time in the 7th layer of the formation. The 7th layer was chosen because it has the highest CO_2 saturation (98%) of all layers during injection. It was observed that the size of the plume and the gas saturation around the area of injection in layer 7 gradually increased during the 30 years of injection (2022 – 2052). Beyond the period of injection, this trend reversed, and the CO_2 plume gradually migrated upwards as the brine started to imbue back into the pore spaces it was originally displaced from. This was visualized in Fig. 46 which shows the CO_2 plume (saturation) evolution along the injection well. In general, the CO_2 plume never migrates beyond the North Burbank Injection Region and is some distance away from the Ada-Vamoosa underground sources of drinking water (USDW) in the area. The CO_2 plume was not well defined due to the effect of using coarse grids.

The gas plume covered a diameter of 17979 ft in both the x and y directions on the 7th layer covering an area of about 5287 acres. The areal extent was slightly larger at the end of 50-years post injection at the top of the formation in layer 1 covering 22470 ft in the x and y directions and an area of 9103 acres (visualized in Fig. 45).

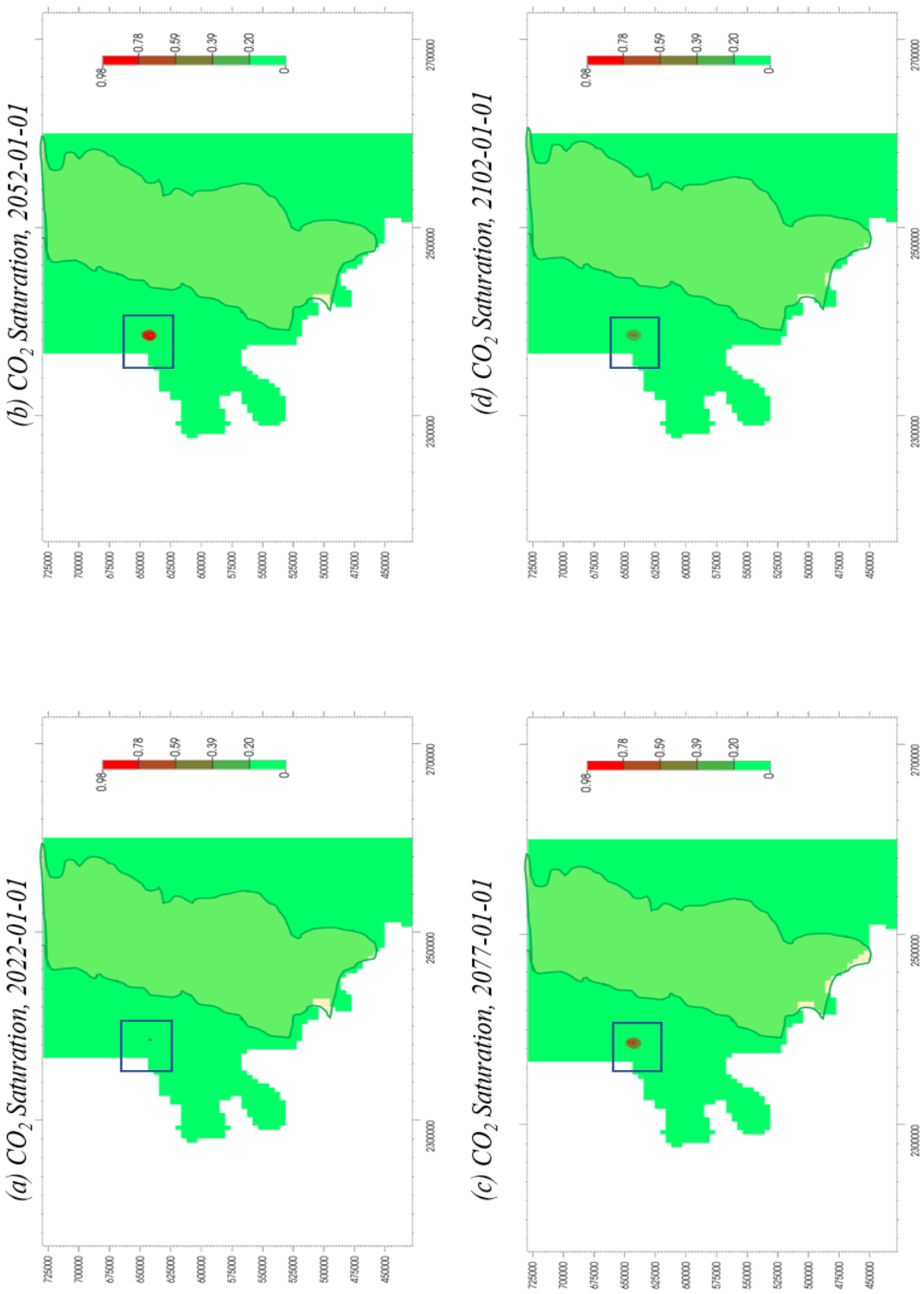

Figure 43: Areal map showing CO2 plume evolution in Layer 7 of the Arbuckle with CO_2 injection using refined grid blocks around injection well. (Blue box indicates North Burbank Unit injection region, orange polygon indicates Ada-Vamoosa USDW aquifer). Red indicates higher plume saturation.

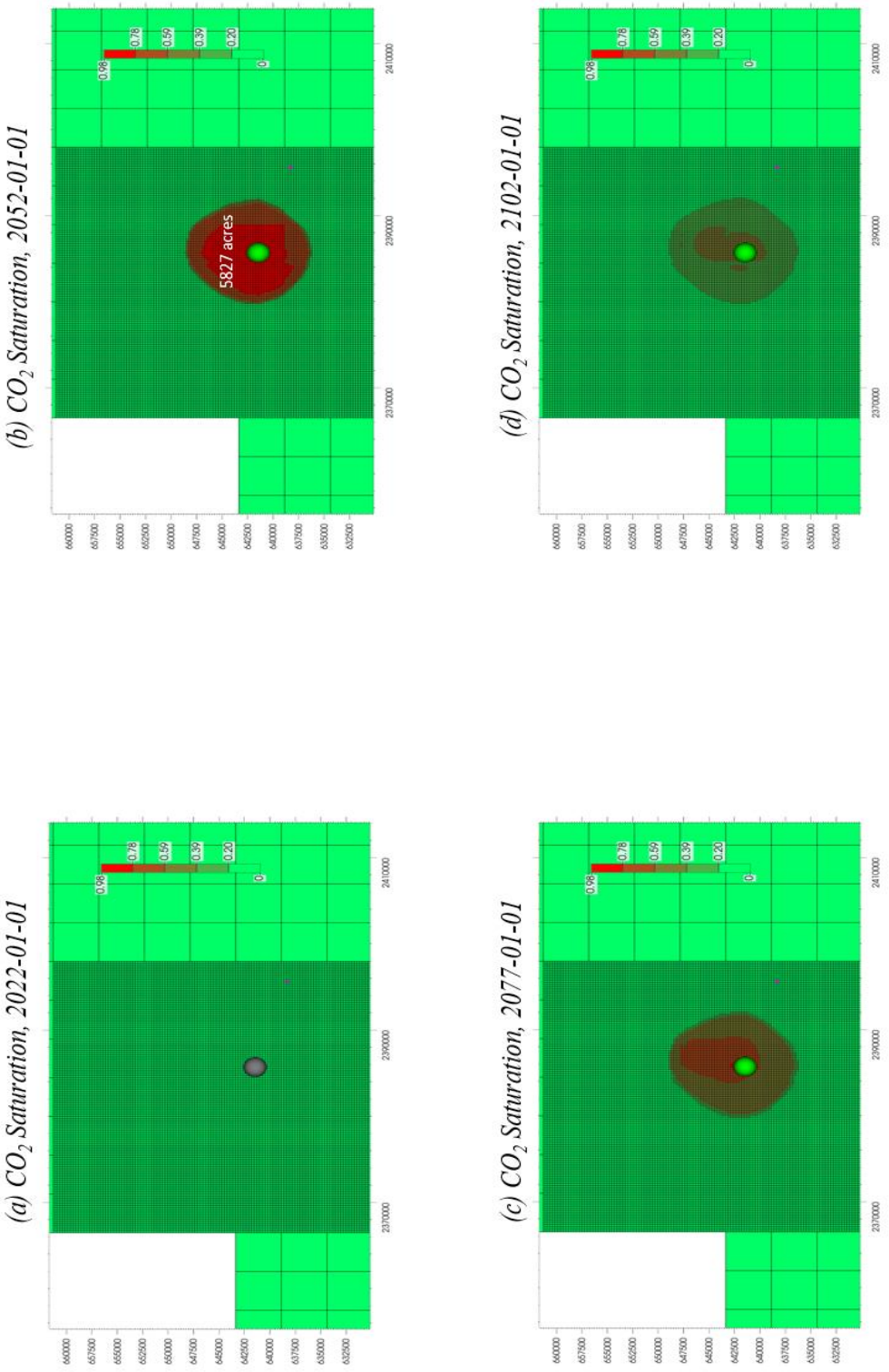

Figure 44: Areal map showing CO2 plume evolution in Layer 7 of the Arbuckle with CO2 injection in refined grid blocks around injection well. Red indicates higher plume saturation.

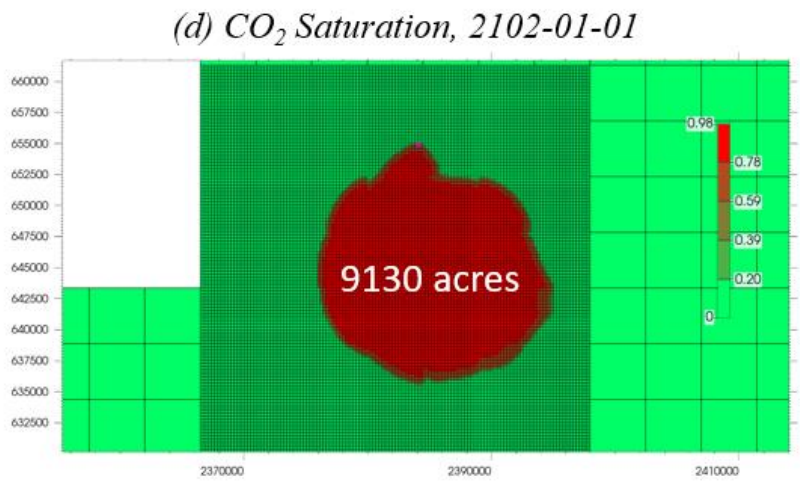

Figure 45: Areal map showing CO_2 plume evolution in Layer 1 of the Arbuckle with CO_2 injection in refined grid blocks around injection well. Red indicates higher plume saturation.

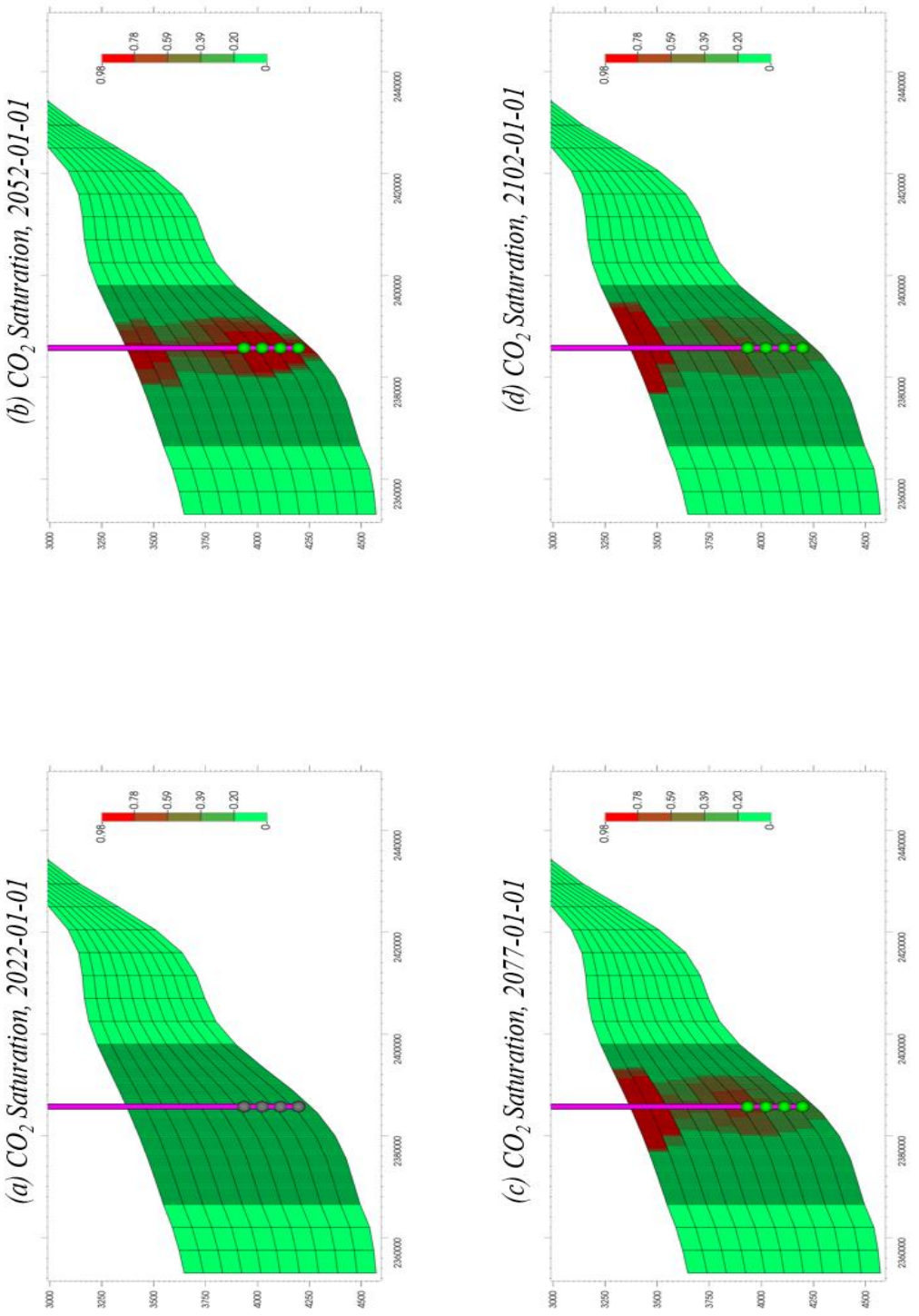

Figure 46: View of CO_2 plume evolution through the injection well showing the plume migrate to the top of the formation as residual gas trapping causes the brine to imbue back into the pore spaces it was displaced from.

4.3.3 Sensitivity Analysis

The result of the sensitivity of the injected mass to the maximum bottomhole pressure obtained by setting to varying percentages of fracture pressure (90%, 80% and 70%) is shown in table 5 below. It was observed that the total injected mass reduced as the maximum injection pressure reduces. The sensitivity analysis indicated that to reach a target of at least 50 million metric tons of injected CO_2 per Department of Energy guidelines (Hamzat et al., 2022), using 1 injection well in the North Burbank injection area, the maximum bottomhole injection pressure would have to be set to at least 80% of the fracture pressure. This is safe regarding fracture risks and induced seismicity (Ochie, 2022).

Table 5: Sensitivity Analysis of Injected Volume and Mass to Maximum Bottomhole Pressure

% of Fracture Pressure	Maximum Bottomhole Pressure (psi)	Injected Volume (Bcf)	Injected Mass (million metric tons)
90	2300	1699	88.1
80	2044	970	50.3
70	1789	291	15.1

Table 6 presents the outcomes of the sensitivity study performed by varying the average permeability value. The formation permeability was modified to 65%, 75%, 85% and 125% of the original values. As seen from table 6 and Fig. 47, the total mass of CO_2 injected after 30 years increased following a polynomial function from about 49.4 million metric tons with 85mD permeability to 100 million metric tons at 200mD permeability. To inject exactly 50 million metric tons in 30 years, the average permeability required is about 86 mD.

Table 6: Sensitivity Analysis of Injected Volume and Mass to Average Permeability

% of Original Formation Permeability	Average Permeability (mD)	Injected Volume (Bcf)	Injected Mass (million Metric Tons)
50	85	952	49.4
65	110.5	1182	61.2
75	127.5	1328	68.9
85	144.5	1494	77.5
100	170.0	1699	88.1
125	212.5	2014	104.5

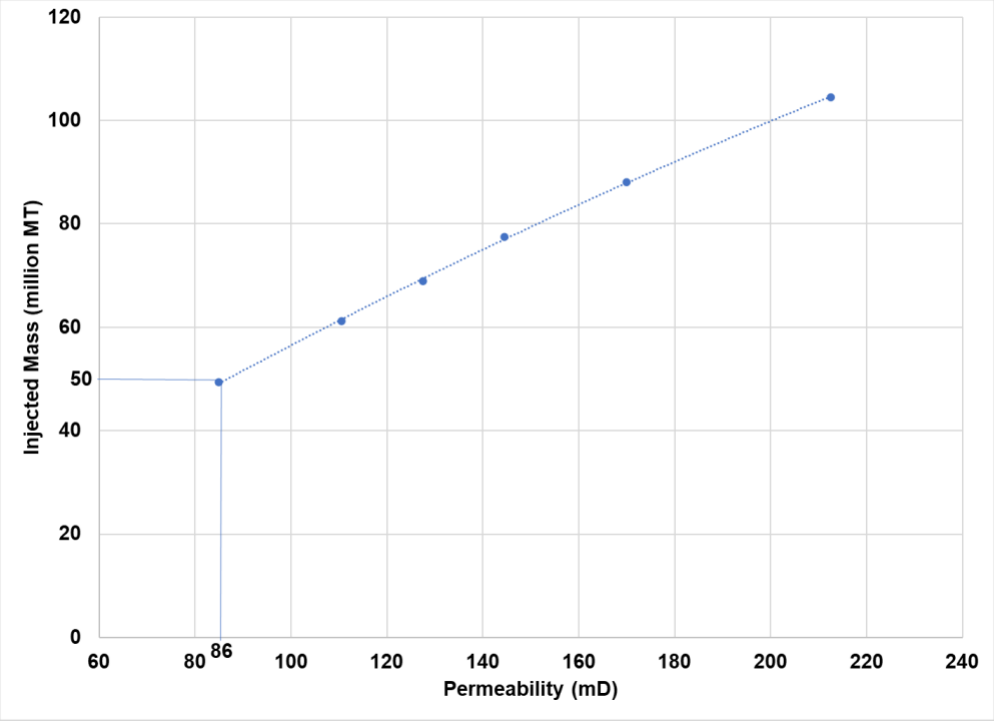

Figure 47: Comparing permeability to injected mass (million MT). 86mD permeability required to inject 50 million MT

With these results, the Arbuckle of Osage County can still take 50 million metric tons of CO_2 in 30 years even if the average permeability from Milad et al. (2022) is overestimated by up to 84 mD (almost half the initial value).

Table 7 shows the results from the sensitivity study performed by varying the number of injection wells. The wells were spaced 800 ft apart linearly in the x-direction. All the injection wells were constrained to operate at a bottomhole pressure equal to 90% of the fracture pressure in the block it was perforated in. The results suggest that there was some benefit to having additional injection wells as it increases the cumulative injection in 30 years. A cost-benefit analysis would however need to be carried out in deciding whether to injecting with more wells makes economic sense.

Table 7: Sensitivity of Injected Mass to Number of Injected Wells

Number of Injection Wells	Injected Volume (Bcf)	Injected Mass (million Metric Tons)
1	1699	88.1
2	1766	91.6
3	1804	93.6

4.4 Exploring the Extent of Applicability of Mathias et al. (2011b) Analytical Model in Predicting Pressure Buildup

In this section, the analytical solution of Mathias et al. (2011b) was tested using the assumptions made in section 3.6 and for different reservoir radial extents.

The fundamental difference between the analytical model and the numerical model was the assumption of constant fluid properties and the use of linear relative permeability functions.

Table 8 shows the values of reservoir radial extent, the pore volume, the cumulative injected volume (at reservoir conditions), the ratio of cumulative injected volume to pore volume,

and the slope correction factor (determined using a what-if analysis in MATLAB) that were used to determine the extent of applicability of Mathias et al. (2011b) analytical model.

Table 8: Results of Comparing Pressure buildup Curve of Analytical Model to CMG model.

Reservoir Radial Extent (ft)	Pore Volume (10^{11} ft^3)	Cumulative Injection (10^{11} ft^3 at res. condition)	Ratio of Cumulative Injection to Pore Volume	Slope Correction Factor
227933	58.7	0.00389	6.63×10^{-5}	1.000
112838	14.4	0.00381	2.65×10^{-4}	1.000
59682	4.03	0.00377	1.02×10^{-3}	1.000
45587	2.35	0.0034	1.44×10^{-3}	0.910
32822	1.22	0.003	2.44×10^{-3}	0.840
29081	0.95	0.0028	3.11×10^{-3}	0.810
14244	0.023	0.00255	1.11×10^{-1}	0.67

The slope correction factor was found by calculating the slope (assumed linear) of the pressure buildup curve in CMG GEMS and comparing against the slope of the pressure buildup from the analytical model (also assumed linear). The ratio of the slope of the analytical model to that of the numerical CMG model was calculated and that number was used as the slope correction factor. This factor was then applied to the time "t" in the analytical model to obtain a new pressure buildup curve.

Fig. 48 shows the plot of the slope correction factor against the ratio of cumulative injection (reservoir conditions) to pore volume. It was found that there was significant variation between the slopes of the pressure buildup curve from analytical solution in Mathias et al (2011b) and that obtained from CMG GEMS, when the cumulative injection at reservoir condition exceeded 0.1% of pore volume. Beyond 0.1%, the analytical model of Mathias et al. (2011b) was found to not be as accurate in estimating the pressure buildup from continuous CO_2 injection in this system. This is likely because of the assumption of constant fluid properties as smaller systems will get higher

pressures than the pressure used in estimating the fluid properties in the analytical model. Correcting the slope using the slope correction factors in Fig. 48 could potentially solve this problem as shown in Fig. 50

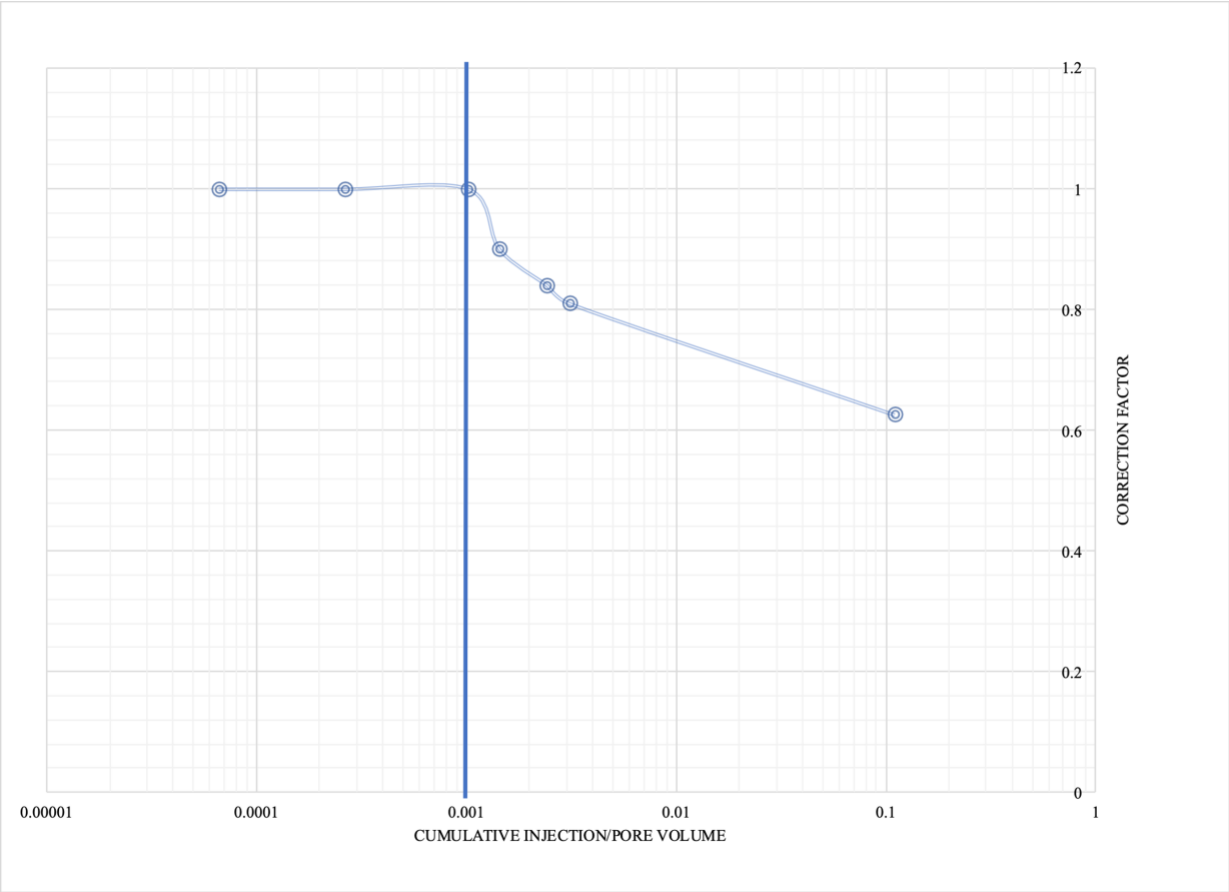

Figure 48: Plot of correction factor against the ratio of cumulative injection (reservoir conditions) to pore volume

Fig. 49 is an example of the difference in slope observed for the case where radial extent is 227933 ft. From this, it is obvious that the analytical model does a great job predicting pressure buildup for this size of reservoir.

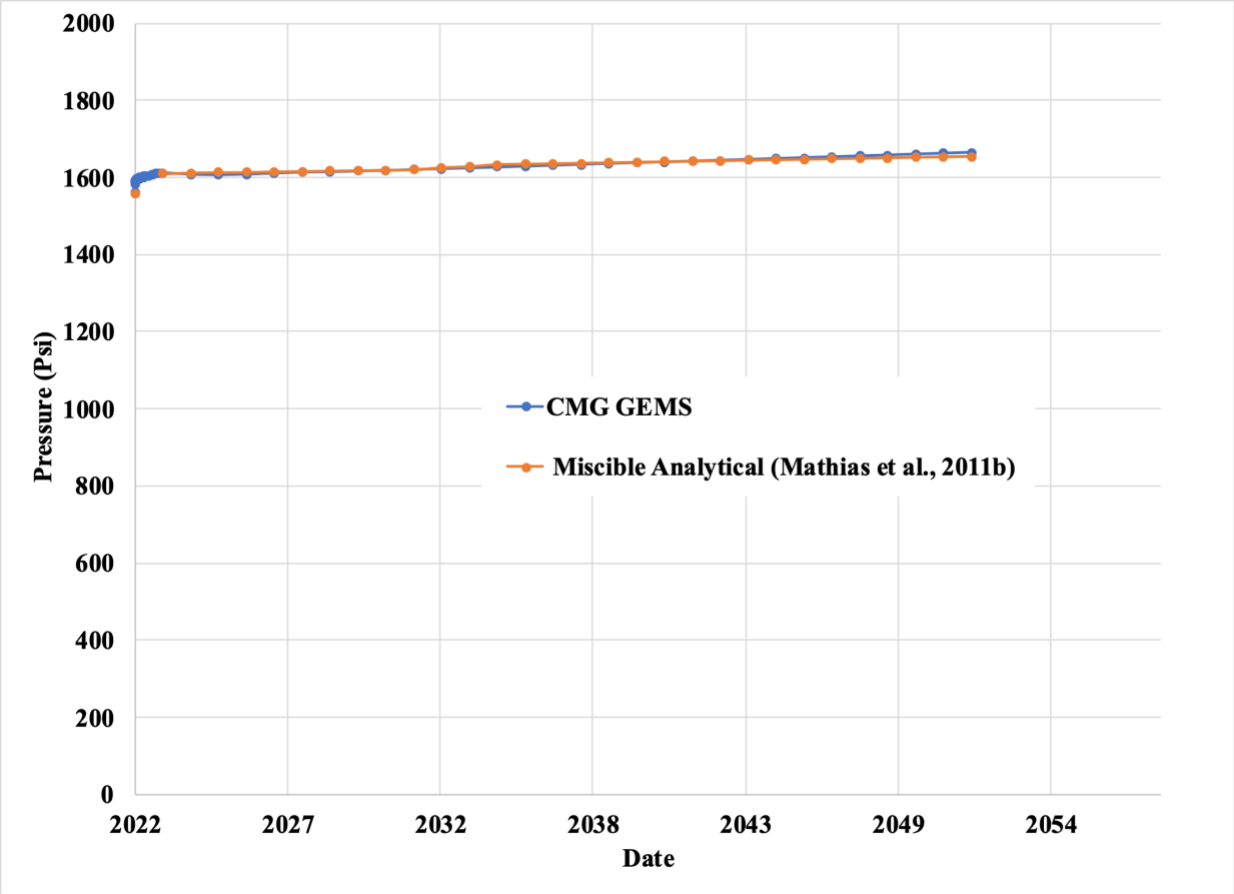

Figure 49: Pressure buildup comparison between analytical and numerical methods at 750ft from injection well site for 227933ft radial extent

Fig. 50 shows an example of the difference in slope observed for the case where the radial extent is 14244 ft. The original calculations from the analytical model deviate significantly from what was obtained from the CMG GEMS. The slope was corrected by multiplying time with a slope correction factor (0.67) determined by comparing the slope of the analytical model to that of the numerical CMG model. Similar plots for each case are included in the Appendix.

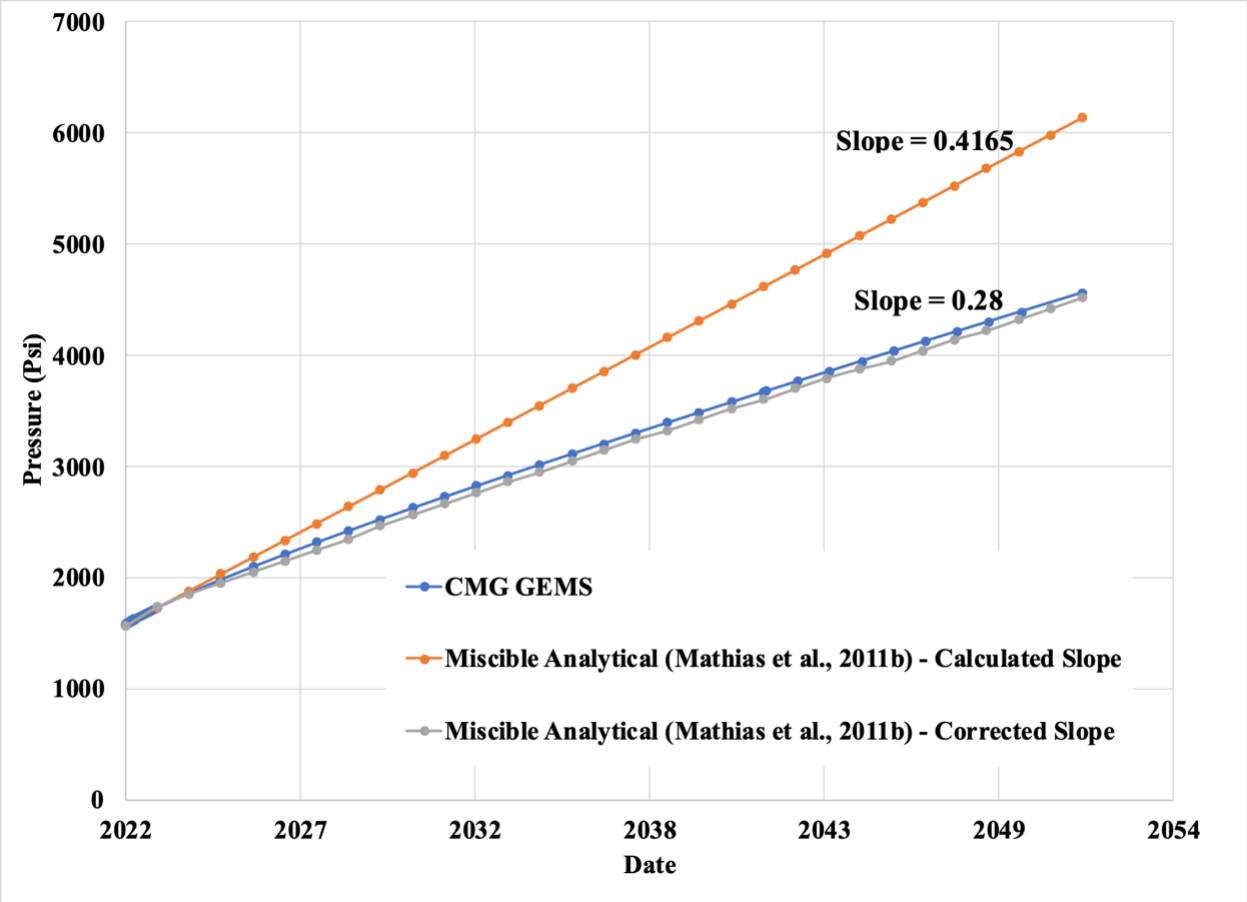

Figure 50: Pressure buildup comparison between analytical and numerical methods at 750ft from injection well site for 14244ft radial extent

Chapter 5: Conclusion

5.1 Conclusion and Recommendations

A numerical simulation model of the Arbuckle group of Osage County, Oklahoma was built and developed using CMG GEMS with one injection well and reservoir characterization data obtained from literature and the current field operator in the North Burbank Region of the formation.

- The results from numerical simulation showed that it is possible to meet the Department of Energy Requirements of 50 million metric tons of injected CO_2 in the formation with minimal risk of reservoir fracturing or induced seismicity following guidelines in Ochie (2022).
- Sensitivity analysis also showed that the maximum injection pressure and the average permeability affect the amount of CO_2 that could be injected into the formation.
- The maximum amount of gas that can be injected with 1 injection well without damaging or fracturing the system is 88.1 million metric tons. To inject any more, there would be a need to increase the number of injection wells.
- To meet the required target, an average permeability of about 86mD is required to operate at 90% of the Fracture Pressure. If the geological model by Milad et al. (2022) overestimated permeability by almost 2 times the actual value, the injection of 50 million metric tons of CO_2 would still be feasible.
- The results also showed that most of the gas was trapped structurally with some amount dissolved in the brine and minimal residual trapping post-injection. The dissolution of CO_2 in brine also allowed for the injection of an additional 50 Bcf (2

million MT) of CO_2 in 30 years while marginally reducing the pressure around the wellbore.

These results should encourage investment into the execution of a CO_2 sequestration project in the Arbuckle Group of Osage County. It has the requisite storage capacity and possesses minimal environmental risks. More analysis would need to be done to evaluate the project's socio-economic impact.

Using a single well cylindrical model of the reservoir, the semi-analytical solution of Mathias et al. (2011b) was tested against CMG GEMS numerical simulation.

- It was found to perform well if the cumulative volume of CO_2 injection in this system is less than 0.1% of the pore volume. In other words, the analytical model of Mathias et al. (2011b) performs well when the injection of CO_2 in an aquifer can be likened to “a tiny drop of water in a mighty ocean”.
- To use the analytical model to predict pressure buildup when injecting the same quantity of CO_2 in a smaller system, it would be necessary to correct the derived slope of the curve using a correction factor as described in Fig. 48 using the applicable ratio of cumulative injection volume at reservoir conditions to pore volume.

5.2 Future Work

Future area of research entails carrying out further simulation sensitivity analysis by varying more parameters such as porosity and reservoir anisotropy (kv/kh). More work should also be done observe longer-term (>100 years) impact of sequestration on the formation. Sensitivity should also be carried out to determine the effect of well-spacing on the cumulative injection volume using more than one (1) well. It would also be useful to carry out more sensitivity analysis

on the analytical model of Mathias et al. (2011b) by varying other parameters as an accurate analytical model could be useful where there is little or no access to numerical methods when evaluating the potential for CO_2 storage in saline aquifers. Further investigation should also be carried out into why Mathias et al. (2011b) analytical fails when cumulative injection is beyond 0.1% of the pore volume in this system and ways to improve the accuracy beyond what has been proposed in this thesis.

Nomenclature

Bcf	Billion cubic feet
CMG	Computer Modelling Group
CO_2	Carbon dioxide
CUSP	Carbon, Utilization and Storage Partnership
EOR	Enhanced oil recovery
GCS	Geological carbon storage
LGR	Local grid refinement
MMscf	Million standard cubic feet
MT	Metric tons
Psi	Pound per square inch
USDW	Underground Source of Drinking Water

References

Alzayer, H., Zahrani, T., & Shubbar, A. (2022). Modeling CO_2 Sequestration in Deep Saline Aquifers – Best Practices. Day 2 Tue, February 22, 2022. https://doi.org/10.2523/iptc-22423-ea

Anchliya, A. (2009). Aquifer Management for CO_2 Sequestration. College Station, Texas: Texas A&M University.

Anchliya, A., Economides, C. A., & Jafarpour, B. (2012). Aquifer Management to Accelerate CO2 Dissolution and Trapping. Society of Petroleum Engineers Journal, 805-816. doi: http://dx.doi.org/10.2118/126688-PA

Anderson, S. T. (2017). Risk, liability, and economic issues with long-term CO2 storage—a review. Natural Resources Research, 26(1), 89–112. https://doi.org/10.1007/s11053-016-9303-6

Ashfaq, M. J. (2017). Investigation of CO2 Sequestration for the Assessment of the Impact on Resource Storage with Co-production of Brine. Graduate Theses, Dissertations, and Problem Reports. 5127. https://researchrepository.wvu.edu/etd/5127

Ayash, S.C., Nakles, D. V., Wildgust, N., Peck, W. D., Sorensen, J. A., Glazewski, K. A., Aulich, T. R., Klapperich, R. J., Azzolina, N. A., and Gorecki, C. D. (2017). Best practice for the commercial deployment of carbon dioxide geologic storage—the adaptive management approach: Plains CO2 Reduction (PCOR) Partnership Phase III Task 13 Deliverable D102/Milestone M59 for U.S. Department of Energy National Energy Technology

Laboratory Cooperative Agreement No. DE-FC26-05NT42592, EERC Publication 2017-EERC-05-01, Grand Forks, North Dakota, Energy & Environmental Research Center, May.

Bakker, R. J. (2003). Package fluids 1. computer programs for analysis of fluid inclusion data and for modelling bulk fluid properties. Chemical Geology, 194(1-3), 3–23. https://doi.org/10.1016/s0009-2541(02)00268-1

Bandilla, K. W., Celia, M. A., Birkholzer, J. T., Cihan, A., & Leister, E. C. (2015). Multiphase Modeling of Geologic Carbon Sequestration in Saline Aquifers. NATIONAL GROUNDWATER ASSOCIATION. doi: https://doi.org/10.1111/gwat.12315

Barrufet, M. A., Bacquet, A., & Falcone, G. (2010). Analysis of the Storage Capacity for CO2 Sequestration of a Depleted Gas Condensate Reservoir and a Saline Aquifer. The Journal of Canadian petroleum technology, 49, 23-31. doi: https://doi.org/10.2118/139771-PA

Battelle, I. (2018, June 5). Energy & Environment. Retrieved from Inside Battelle: https://inside.battelle.org/blog-details/carbon-capture-sequestration-is-worth-pursuing?keyword_session_id=vt~adwords|kt~|mt~b|ta~496274902983&_vsrefdom=wordstream&gclid=Cj0KCQjwiNSLBhCPARIsAKNS4_dlFUVoYbcC0mSgrfXK4_uxMsRaPRpHD8iUx9DhVJTJe_sVgosxz4gaAqq2E.

Batzle, M. and Wang Z. (1992). Seismic properties of pore fluids, Geophysics, 57, 1396-1408

Bennion, D. B., & Bachu, S. (2008). Drainage and imbibition relative permeability relationships for supercritical CO2/Brine and H2S/brine systems in intergranular sandstone, carbonate,

shale, and Anhydrite Rocks. SPE Reservoir Evaluation & Engineering, 11(03), 487–496. https://doi.org/10.2118/99326-pa

Birdie, T., Holubnyak, E., Watney, L., Bidgoli, T., Hollenbach, J., & Fazelalavi, M. (2022). Assessing Induced Seismicity Risk at the Wellington Geologic Sequestration Site.

Birkholzer, J., Zhou, Q., & Tsang, C. (2009). Large-scale impact of CO_2 storage in deep saline aquifers: A sensitivity study on pressure response in Stratified Systems. International Journal of Greenhouse Gas Control, 3(2), 181–194. https://doi.org/10.1016/j.ijggc.2008.08.002

Buckley S. E. and Leverett M. C. (1942). Mechanism of fluid displacement in sands. Trans Am Inst Min Metall Pet Eng 146:107–116.

Burton, M., N. Kumar, and S. L. Bryant (2008), Time-dependent injectivity during CO2 storage in aquifers, 15 pp., SPE/DOE Improved Oil Recovery Symposium Tulsa, SPE 113937, doi:10.2118/113937-MS.

Chang, Y. B., Coats, B. K., & Nolen, J. S. (1996). A compositional model for CO2 floods including CO2 solubility in water. All Days. https://doi.org/10.2118/35164-ms

Chaves, G. (2011). Simulation of CO2 sequestration in deep saline aquifers Gordon Creek Field, Utah (thesis). New Mexico Institute of Mining and Technology, Socorro, NM.

Chiaramonte, L., Zoback, M. D., Friedmann, J., & Stamp, V. (2008). Seal integrity and feasibility of CO2 sequestration in the Teapot Dome EOR pilot: geomechanical site characterization. Environmental Geology, 54(8), 1667-1675. Retrieved from https://idp.springer.com/authorize/casa?redirect_uri=https://link.springer.com/article/10.10

07/s00254-007-0948-7&casa_token=RqQmuvF-YcYAAAAA:LSGfogyYy-j6rsjltAO9d13GGnjmOzcBCxluyhH6oO2Esl9731kAQqyHwDUUX82kdeOy6p_Sj9VWwmOzNw

Chidambaram, P., Tewari, R. D., Ali, S. S., Tan, C. P., & PETRONAS, R. S. (2021). Understanding the Effect of Rock Compressibility on CO2 Storage Capacity Estimation in a Depleted Carbonate Gas Reservoir. International Petroleum Technology Conference. Virtual: IPTC. Retrieved from https://onepetro.org/IPTCONF/proceedings-pdf/21IPTC/2-21IPTC/D021S003R001/2423471/iptc-21207-ms.pdf.

Ching, B. Y., & Friedman, G. M. (2000). Subsurface Arbuckle Group Cambro-Ordovician in the Bowman Well of the Wilburton Field in the Arkoma Basin, Oklahoma; depositional facies, diagenetic signatures, petrophysical aspects, and economic potential. Carbonates and Evaporites, 15(1), 49-80. doi:10.1007/bf03175648

Cihan, A., Birkholzer, J. T., & Zhou, Q. (2012). Pressure buildup and brine migration during CO2 storage in multilayered aquifers. Ground Water. https://doi.org/10.1111/j.1745-6584.2012.00972.x

CMG (Computer Modelling Group). (2011). GEM Advanced Compositional and GHG Reservoir Simulator, User's Guide. Calgary, Alberta, Canada.

Dixon, T., McCoy, S. T., & Havercroft, I. (2015). Legal and regulatory developments on CCS. International Journal of Greenhouse Gas Control, 40, 431–448.

Djebbas, F., Aziez, Z. & Cherif, K. (2015). Study of the fractures effect on the capacity and security geological storage of the CO2 in hydrocarbon reservoirs. INTERNATIONAL JOURNAL OF ENERGY and ENVIRONMENT, ISSN: 2308-1007.

Environmental Protection Agency. (2023). Climate Change Indicators: Sea Surface Temperature. EPA. Retrieved March 22, 2023, from https://www.epa.gov/climate-indicators/climate-change-indicators-sea-surface-temperature.

EPA. (2021). Subpart UU – Injection of Carbon Dioxide. Retrieved from United States Environmental Protection Agency: https://www.epa.gov/ghgreporting/subpart-uu-injection-carbon-dioxide#:~:text=This%20rule%20requires%20reporting%20of,purpose%20other%20than%20geologic%20sequestration.

ExxonMobil. (2022). Outlook for energy. ExxonMobil. Retrieved March 22, 2023, from https://corporate.exxonmobil.com/energy-and-innovation/outlook-for-energy

Fakher, S., & Imqam, A. (2020). A Review of Carbon Dioxide Adsorption to Unconventional Shale Rocks Methodology, Measurement, and Calculation. SN Applied Sciences, 2(1). doi: https://doi.org/10.1007/s42452-019-1810-8

Fakher, S., Abdelaal, H., Elgahawy, Y., & El-Tonbary, A. (2020). A Review of Long-Term Carbon Dioxide Storage in Shale Reservoirs. Unconventional Resources Technology Conference. Virtual: Society of Exploration Geophysicists. doi: https://doi.org/10.15530/urtec-2020-1074

Fazelalavi, M. (2015). Determination of Relative Permeability Curves in the Arbuckle. Kansas: Kansas Geological Survey Open-File Report 2017-6

Fenghour, A., Wakeham W. A., Vesovic, V. (1998). The viscosity of carbon dioxide, J. Phys. Chem. Ref. Data, 27, 31-44

Forchheimer, P. (1901). Wasserbewegung durch Boden Zeit, vol. 45. Ver. Deut. Ing.

Franseen, E. K., Byrnes, A. P., Cansler, J. R., Steinhauff, D. M., & Carr, T. R. (2004). The Geology of Kansas Arbuckle Group. Kansas; Kansas Geological Survey.

Frei-Pearson, A., & Bryant, S. (2014). The relationship between KH and achievable rates of injection, and repercussions for large scale storage. Energy Procedia, 63, 3041–3050. https://doi.org/10.1016/j.egypro.2014.11.327

Fritz, R. D., Medlock, P., Kuykendall, M. J., and Wilson, J. L., (2013). The Geology of the Arbuckle Group in the Midcontinent: Sequence Stratigraphy, Reservoir Development, and the potential for Hydrocarbon Exploration. AAPG extended abstract.

Glazewski, K. A., Aulich, T. R., Wildgust, N., Nakles, D. V., Azzolina, N. A., Hamling, J. A., Burnison, S. A., Livers-Douglas, A. J., Peck, W. D., Klapperich, R. J., Sorensen, J. A., Ayash, S. C., Gorecki, C. D., Steadman, E. N., Harju, J. A., Stepan, D. J., Kalenze, N. S., Musich, M. A., Leroux, K. M., and Pekot, L. J. (2018). Best practices manual – monitoring for CO2 storage: Plains CO2 Reduction (PCOR) Partnership Phase III Task 9 Deliverable D51 for U.S. Department of Energy National Energy Technology Laboratory Cooperative

Agreement No. DE-FC26-05NT42592, EERC Publication 2018-EERC-03-15, Grand Forks, North Dakota, Energy & Environmental Research Center, March.

Gorucu, F. B., Jikich, S. A., Bromhal, G. S., Sams, W. N., Ertekin, T., & Smith, D. H. (2005). Matrix shrinkage and swelling effects on economics of enhanced coalbed methane production and CO2 sequestration in coal. Society of Petroleum Engineers Eastern Regional Meeting. Morgantown, West VA, United States: Society of Petroleum Engineers. Retrieved from https://pennstate.pure.elsevier.com/en/publications/matrix-shrinkage-and-swelling-effects-on-economics-of-enhanced-co.

Gunter, W. D., Perkins, E. H., & Hutcheon, I. (2000). Aquifer disposal of acid gases: Modelling of water–rock reactions for trapping of acid wastes. Applied Geochemistry, 15(8), 1085–1095. https://doi.org/10.1016/s0883-2927(99)00111-0

Hamzat, A., Milad, B., Moghanloo, R., & Daneshfar, J. (2022). AGU Fall Meeting 2022. In Advances in CO2 Capture, Transport, Utilization, and Storage Technologies. Chicago; American Geophysical Union. ESS Open Archive DOI: 10.22541/essoar.168055205.56507814/v1

Hassanzadeh H., Pooladi-Darvish, M., Elsharkawy, A. M., Keith D. W. (2008). Predicting PVT data for CO_2-brine mixtures for black-oil simulation of CO_2 geological storage, Int J. Greenhouse Gas Control, 2, 65-77

Hitchon, B., Bachu, S., & Gunter, W., Perkins, E., Law, D. & Wiwchar, B. (1996). Aquifer Disposal of Carbon Dioxide: Hydrodynamic and Mineral Trapping - Proof of Concept.

Holubnyak, Y., Watney, L., Hollenbach, J., Birdie, T., Fazelalavi, M., Bidgoli, T., Schwab, D., Nolte, A., Tsoflias, G., Victorine, J., Graham, B., Doveton, J., Bruns, J., Blazer, B., & Wreath, D. (2017). (rep.). Small Scale Field Test Demonstrating CO2 Sequestration in Arbuckle Saline Aquifer and by CO2-EOR at Wellington Field, Sumner County, Kansas.

HOT: The Hawaii Ocean Time-series. (2023). Retrieved March 22, 2023, from https://hahana.soest.hawaii.edu/hot/

IEAGHG. (2022). A Brief History of CCS and Current Status. Retrieved from CCS Information Sheet: https://ieaghg.org/docs/General_Docs/Publications/Information_Sheets_for_CCS_2.pdf.

Intergovernmental Panel on Climate Change. (2005). IPSS Special Report onCarbon Dioxide Capture and Storage. New York: Cambridge University Press. Retrieved from https://www.google.com/url?sa=i&url=https%3A%2F%2Fwww.ipcc.ch%2Fsite%2Fassets%2Fuploads%2F2018%2F03%2Fsrccs_wholereport-1.pdf&psig=AOvVaw1RuofI65_dbVAXQFrgAFD-&ust=1667621358339000&source=images&cd=vfe&ved=0CA0QjhxqFwoTCIiRnOjTk_sCFQAAAAAdAAAAABAR

Jiang, K., Dou, H., Shen, P., & Sun, T. (2015). China's CCUS Progresses and a New Evaluation Method of CO2 Storage Capacity in Coalbed Reservoirs. Carbon Management Technology Conference. Sugar Land, Texas: Society of Petroleum Engineers. doi: https://doi.org/10.7122/440095-MS

Johnson, K. S., (1991). Geologic overview and economic importance of Late Cambrian and Ordovician rocks in Oklahoma, in K. S. Johnson, ed., Late Cambrian Ordovician geology of the southern Midcontinent, 1989 Symposium: Oklahoma Geological Survey Circular 92, 3–14.

Johnson, S., (2008). Geologic History of Oklahoma: Educational Publication, v. 9, p 3-8.

Joshi, A. (2014). Investigation of Multiple Well Injections for Carbon Dioxide Sequestration in Aquifers. Master's Thesis. Waterloo, Canada: University of Waterloo. Retrieved from https://uwspace.uwaterloo.ca/handle/10012/8754

Kartikasurja, D. O., Lin, T. G., Sukahar, M. W., & Viratno, B. (2008). Study of produced CO_2 Storage into aquifer in an offshore field, Malaysia. All Days. https://doi.org/10.2118/114553-ms

Kumar, A., Ozah, R., Noh, M., Pope, G. A., Bryant, S., Sepehrnoori, K., & Lake, L. W. (2005). Reservoir simulation of CO2 storage in deep saline aquifers. SPE Journal, 10(03), 336–348. https://doi.org/10.2118/89343-pa

Land, C. S. (1968). Calculation of imbibition relative permeability for two- and three-phase flow from rock properties. Society of Petroleum Engineers Journal, 8(02), 149–156. https://doi.org/10.2118/1942-pa

Li, Y. K., & Nghiem, L. X. (1986). Phase equilibria of oil, gas, and water/brine mixtures from a cubic equation of state and Henry's Law. The Canadian Journal of Chemical Engineering, 64(3), 486–496. https://doi.org/10.1002/cjce.5450640319

Mathias, S. A., & Todman, L. C. (2010). Step-drawdown tests and the Forchheimer equation. Water Resources Research, 46(7). https://doi.org/10.1029/2009wr008635

Mathias, S. A., Butler, A. P., & Zhan, H. (2008). Approximate solutions for Forchheimer flow to a well. Journal of Hydraulic Engineering, 134(9), 1318–1325. https://doi.org/10.1061/(asce)0733-9429(2008)134:9(1318)

Mathias, S. A., Gluyas, J. G., González Martínez de Miguel, G. J., & Hosseini, S. A. (2011). Role of partial miscibility on pressure buildup due to constant rate injection of CO2 into closed and open brine aquifers. Water Resources Research, 47(12). https://doi.org/10.1029/2011wr011051

Mathias, S. A., González Martínez de Miguel, G. J., Thatcher, K. E., & Zimmerman, R. W. (2011). Pressure buildup during CO2 injection into a closed brine aquifer. Transport in Porous Media, 89(3), 383–397. https://doi.org/10.1007/s11242-011-9776-z

Mathias, S. A., Hardisty, P. E., Trudell, M. R., & Zimmerman, R. W. (2008). Approximate solutions for pressure buildup during CO2 injection in brine aquifers. Transport in Porous Media, 79(2), 265–284. https://doi.org/10.1007/s11242-008-9316-7

McPherson, B. J., Lichtner, P. C., Forster, C. B., & Cole, B. S. (2001). Regional-scale permeability by heat flow calibration in the Powder River Basin, Wyoming. Geophysical Research Letters, 28(16), 3211–3214. https://doi.org/10.1029/2000gl012591

Milad, B., Daneshfar, J., & Moghanloo, R. G. (2022). CO2 storage potential in Arbuckle Reservoir: A case study in Osage County, Oklahoma. Energy in Data Conference, Austin, Texas, 20–23 February 2022. https://doi.org/10.7462/eid2022-07.1

Milad, B., Ghosh, S., & Slatt, R. M. (2018). Comparison of rock and natural fracture attributes in karsted and nonkarsted Hunton Group Limestone: Ada and Fittstown area, Oklahoma. The Shale Shaker Journal, Vol. 69, No. 2, Pages 70-86.

Mo, S., & Akervoll, I. (2005). Modeling long-term CO2 storage in aquifer with a black-oil reservoir simulator. All Days. https://doi.org/10.2118/93951-ms

Morgan, B. C. & Murray, K. E., (2015). Characterizing Small-Scale Permeability of the Arbuckle Group, Oklahoma: Oklahoma Geologic Survey Open-File Report OF2-2015

Murray, K. E., (2015). Class II saltwater disposal for 2009– 2014 at the annual-, state-, and county-scales by geologic zones of completion, Oklahoma: Oklahoma Geologic Survey Open-File Report OF5-2015

Nghiem L., S. P. (2004). Modeling CO2 Storage in Aquifers with a Fully Coupled Geochemical EOS Compositional Simulator. SPE/DOE Symposium on Improved Oil Recovery. Tulsa, Oklahoma: Society of Petroleum Engineers. doi: http://dx.doi.org/10.2118/89474-MS

Nghiem, L. S. (2009). Simulation of Trapping Processes for CO2 Storage in Saline Aquifers. Canadian International Petroleum Conference. Calgary, Alberta: Petroleum Society of Canada. doi:10.2118/2009-156

Nghiem, L., Sammon, P., Grabenstetter, J., & Ohkuma, H. (2004). Modeling CO2 storage in aquifers with a fully coupled geochemical EOS Compositional Simulator. All Days. https://doi.org/10.2118/89474-ms

Nghiem, L., Shrivastava, V., Tran, D., Kohse, B., Hassam, M., & Yang, C. (2009). Simulation of CO2 storage in Saline Aquifers. All Days. https://doi.org/10.2118/125848-ms

NIST Chemistry WebBook (2016) NIST Chemistry Webbook: http://webbook.nist.gov/chemistry/.

Noh, M., Lake, L. W., Bryant, S. L., and Araque-Martinez, A. (2007), Implications of coupling fractional flow and geochemistry for CO2injection in aquifers, SPE Reservoir Eval. Eng.,10, 406–414.

Nordbotten, J. M., Celia, M. A., & Bachu, S. (2005). Injection and storage of CO2 in deep saline aquifers: Analytical solution for CO2 plume evolution during injection. Transport in Porous Media, 58(3), 339–360. https://doi.org/10.1007/s11242-004-0670-9

Ochie, K. I. (2022). A Data-Driven Approach for the Evaluation of Seismicity Risks Associated with CO_2 Injection (thesis). Mewbourne School of Petroleum and Geological Enginering, University of Oklahoma, Norman, Oklahoma.

Orr, F. M., Jr. (2007), Theory of Gas Injection Processes, 381 pp., Tie-Line Publications, Copenhagen, Denmark.

Ortoleva, P., Merino, E., Moore, C., & Chadam, J. (1987). Geochemical self-organization I; reaction-transport feedbacks and Modeling Approach. American Journal of Science, 287(10), 979–1007. https://doi.org/10.2475/ajs.287.10.979

Oruganti, Y., & Bryant, S. L. (2008). Pressure Build-Up During CO2 Storage in Partially Confined Aquifers. 9th International Conference on Greenhouse Gas Control Technologies (GHGT-9) (pp. 3315-3322). Washington, DC: Greenhouse Gas Control Technologies. doi: 10.1016/j.egypro.2009.02.118

Ozah, R. C., Lakshminarasimhan, S., Pope, G. A., Sepehrnoori, K., & Bryant, S. L. (2005). Numerical simulation of the storage of pure CO2 and CO2-H2S gas mixtures in deep saline aquifers. All Days. https://doi.org/10.2118/97255-ms

Peng, D.-Y., & Robinson, D. B. (1976). A new two-constant equation of State. Industrial & Engineering Chemistry Fundamentals, 15(1), 59–64. https://doi.org/10.1021/i160057a011

Perilla-Castillo, P. J. (2017). Rock properties derived from analysis of Earth tide strain observed in continuous pressure monitoring of the Arbuckle Group of Oklahoma (thesis). University of Oklahoma.

Ragland, D. A., and Donovan, R. N. (1991). Sedimentology and diagenesis of the Arbuckle Group in outcrops of southern Oklahoma, in Arbuckle Group Core Workshop and Field Trip: Oklahoma Geological Survey, Special Publication 91-3, p. 9-30

Ringrose, P. S., Mathieson, A. S., Wright, I. W., Selama, F., Hansen, O., Bissell, R., Saoula, N., & Midgley, J. (2013). The in Salah CO2 Storage Project: Lessons Learned and Knowledge Transfer. Energy Procedia, 37, 6226–6236. https://doi.org/10.1016/j.egypro.2013.06.551

Rottmann K., Guttery B., Hadaway S. (2015). Potential diagenetic alteration of the Arbuckle Group and its impact to local structure within the Mid-Continent.

Rottmann, K., 2018, Well-Log Characterization of the Arbuckle Group in Central and Northern Oklahoma: Interpretation of the Impact of its Depositional and Post-Depositional History on Injection Induced Seismicity, Oklahoma Geological Survey, Open File Report 21-2018, Norman, Oklahoma.

Rubin, E., Booras, G., Davison, J., Ekstrom, C., Matuszewski, M., McCoy, S., & Short, C. (2013). Toward a common method of cost estimation for CO2 capture and storage at fossil fuel power plants—A white paper. Cheltenham: IEA Environmental Projects Ltd., Technical Report 2013/TR2, March.

Rutqvist, J., Birkholzer, J., Cappa, F., & Tsang, C.-F. (2007). Estimating maximum sustainable injection pressure during geological sequestration of CO2 using coupled fluid flow and geomechanical fault-slip analysis. Energy Conversion and Management, 48(6), 1798–1807. https://doi.org/10.1016/j.enconman.2007.01.021

Saripalli, P., & McGrail, P. (2002). Semi-analytical approaches to modeling deep well injection of CO2 for geological sequestration. Energy Conversion and Management, 43(2), 185–198. https://doi.org/10.1016/s0196-8904(01)00017-6

Sona, S., Sasaki, K., Sagai, Y., & Fujiwara, A. (2013, September). Numerical Simulation on Solubility of CO_2 in Aquifer. Paper presented at the SPWLA 19th Formation Evaluation Symposium of Japan, Chiba, Japan.

Spycher, N. and Pruess, K. (2005). CO_2-H_2O mixtures in the geological sequestration of CO_2. II. Partitioning in chloride brines at 12100^oC and up to 600 bar, Geochim. Cos-mochim. Acta 69, 3309–3320, DOI :10.1016/j.gca.2005.01.015

Spycher, N., Pruess, K., and Ennis–King, J. (2003). CO_2–H_2O mixtures in the geological sequestration of CO_2. I. Assessment and Calculation of Mutual Solubilities from 12 to 100

C and up to 600 bar, Geochim. Cos-mochim. Acta,67, 3015–3031, DOI :10.1016/S0016-7037(03)00273-4.

U.S. Environmental Protection Agency (U.S.EPA). (2010c). RIN 2040–AE98—Federal requirements under the Underground Injection Control (UIC) program for Carbon Dioxide (CO2) Geologic Sequestration (GS) wells. Washington, DC: Federal Register, 75(237), December 10, 77230–77303. http://www.gpo.gov/fdsys/pkg/FR-2010-12-10/pdf/2010-29954.pdf. Accessed 30 April 2015.

U.S. Environmental Protection Agency (U.S.EPA). (2011). Announcement of Federal Underground Injection Control (UIC) Class VI program for Carbon Dioxide (CO2) Geologic Sequestration (GS) wells. Washington, D.C.: Federal Register, 76(179), September 15, 56982–56983. http://www.gpo.gov/fdsys/pkg/FR-2011-09-15/pdf/2011-23662.pdf. Accessed 12 June 2015.

United Nations. (2023). Causes and effects of climate change. United Nations. Retrieved March 22, 2023, from https://www.un.org/en/climatechange/science/causes-effects-climate-change#:~:text=Fossil%20fuels%20%E2%80%93%20coal%2C%20oil%20and,they%20trap%20the%20sun's%20heat.

US Department of Commerce, NOAA. (2023). Global Monitoring Laboratory - Carbon Cycle Greenhouse Gases. GML. Retrieved March 22, 2023, from https://gml.noaa.gov/ccgg/trends/mlo.html.

Van der Meer, L., & Diederik van Wees, J. (2006). Limitations to Storage Pressure in Finite Saline Aquifers and the Effect of CO2 Solubility on Storage Pressure. SPE Annual Technical

Conference and Exhibition. San Antonio: Society of Petroleum Engineers. doi:10.2118/103342-MS

van Engelenburg, B. a. (1993). Disposal of Carbon Dioxide in Permeable Underground Layers: A Feasible Option? Climatic Change, 55-69.

Welge, H. J. (1952), A simplified method for computing oil recovery by gas or water drive, Trans. AIME,195, 91–98

Wilson, J. L., (1994). The Lower Ordovician Great American bank of the southwestern United States, in Keller, D. R., and Reed, C. L., eds., Paleokarst, karst-related diagenesis, reservoir development, and exploration concepts; examples from the Paleozoic section of the southern Mid-Continent: SEPM (Society for Sedimentary Geology), SEPM Guidebook 93-34, p. 35–43.

Wu, H., Bai, B., & Li, X. (2018). An advanced analytical solution for pressure build-up during CO2 injection into infinite sali6e aquifers: The role of compressibility. Advances in Water Resources, 112, 95–105. https://doi.org/10.1016/j.advwatres.2017.12.010

Wu, H., Bai, B., Li, X., Gao, S., Liu, M., & Wang, L. (2017). An explicit integral solution for pressure build-up during CO2 injection into infinite saline aquifers. Greenhouse Gases: Science and Technology, 6(5), 633–647. https://doi.org/10.1002/ghg.1601

Zeidouni, M., Pooladi-Darvish, M., & Keith, D. (2009). Analytical solution to evaluate salt precipitation during CO2 injection in Saline Aquifers. Energy Procedia, 1(1), 1775–1782. https://doi.org/10.1016/j.egypro.2009.01.232

Zhang, D., & Song, J. (2014). Mechanisms for geological carbon sequestration. Procedia IUTAM, 10, 319–327. https://doi.org/10.1016/j.piutam.2014.01.027

Zhou, Q., Birkholzer, J. T., Tsang, C. F., & Rutqvist, J. (2008). A method for quick assessment of CO2 storage capacity in closed and semi-closed saline formations. International Journal of Greenhouse Gas Control, 2(4), 626–639. https://doi.org/10.1016/j.ijggc.2008.02.004

Zoback, M. D., Barton, C. A., Brudy, M., Castillo, D. A., Finkbeiner, T., Grollimund, B. R., . . . Wiprut, D. J. (2003). Determination of stress orientation and magnitude in deep wells. International Journal of Rock Mechanics and Mining Sciences, 40(7-8), 1049-1076. Retrieved from https://www.sciencedirect.com/science/article/pii/S1365160903001175?casa_token=RYGyEByIyeQAAAAA:tEGwyhOEPIpfGp78Y-skeK_HH0Piy0wDSRIVzJJ2Flh0LQgXAbyG9a0rKw1Td30KaORdxJi_RVM.

Appendix

A. Well Grid Locations for verification of 100 Psi Maximum Pressure Buildup from Water Disposal

Well, 3430D – Lat 36.8163 Long -96.7146 (Grid Block 23,53,7:10)

Well, 2629D – Lat 36.81993 Long -96.7094 (Grid Block 23,53,7:10)

Well, 5031D – Lat 36.80147 Long -96.7191 (Grid Block 22,52,7:10)

Well, 10518D – Lat 36.75957 Long -96.6791 (Grid Block 25,48,7:10)

Well, 10217D – Lat 36.75864 Long -96.6985 (Grid Block 24,48,7:10)

Well, 5231D – Lat 36.80288 Long -96.7034 (Grid Block 23,52,7:10)

Well, 4429D – Lat 36.80599 Long -96.697 (Grid Block 24,52,7:10)

B. Well Grid Locations for Simulation of the Injection of CO_2 for 30 years and 50 years monitoring at the end of injection.

Injector 1 - Grid block 24,48,1

C. Comparing CMG GEMS To Analytical Model

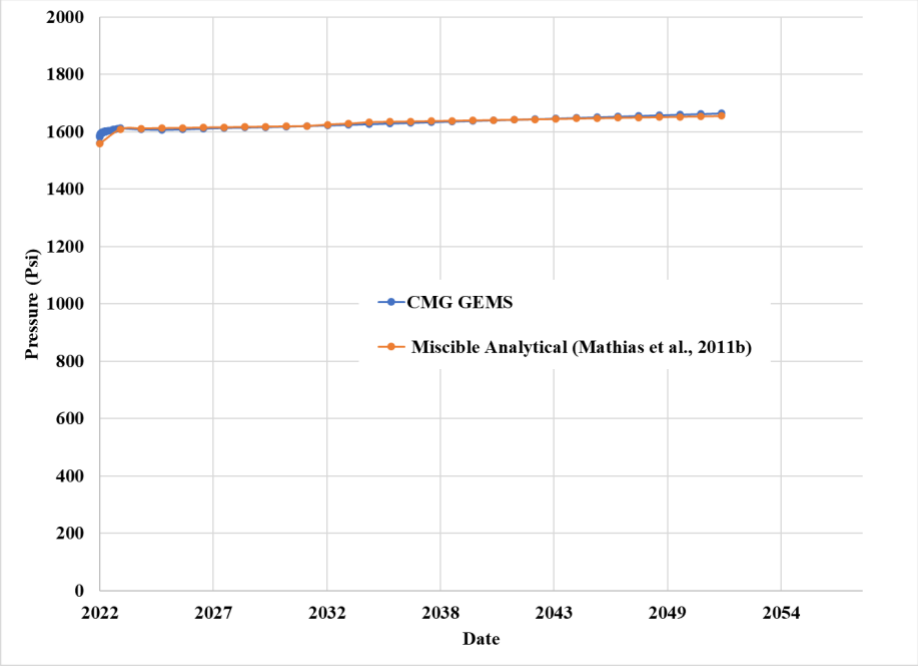

Figure 51: Pressure buildup comparison between analytical and numerical methods at 750ft from injection well site for 112838 ft radial extent

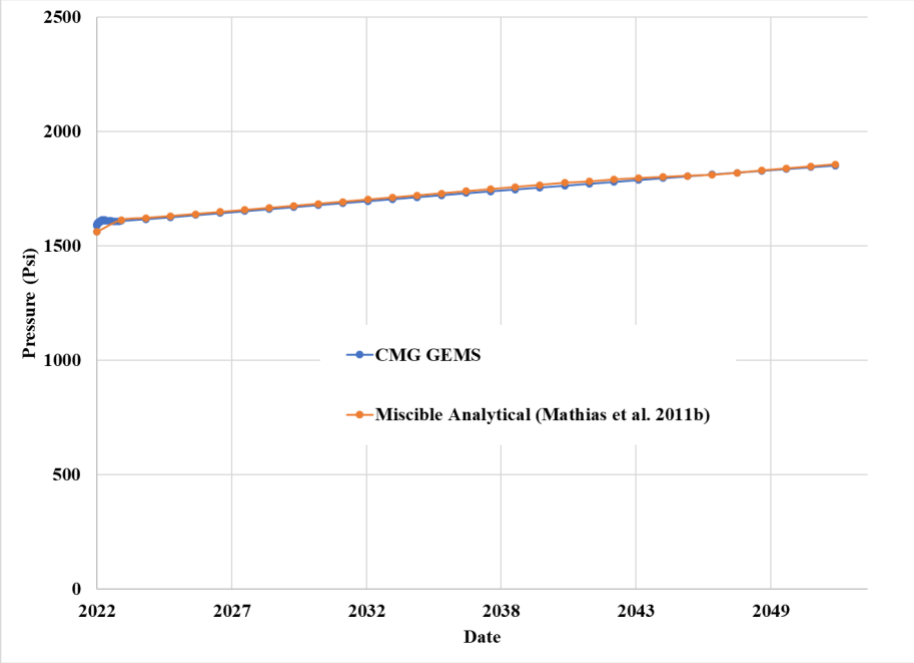

Figure 52: Pressure buildup comparison between analytical and numerical methods at 750ft from injection well site for 59682ft radial extent

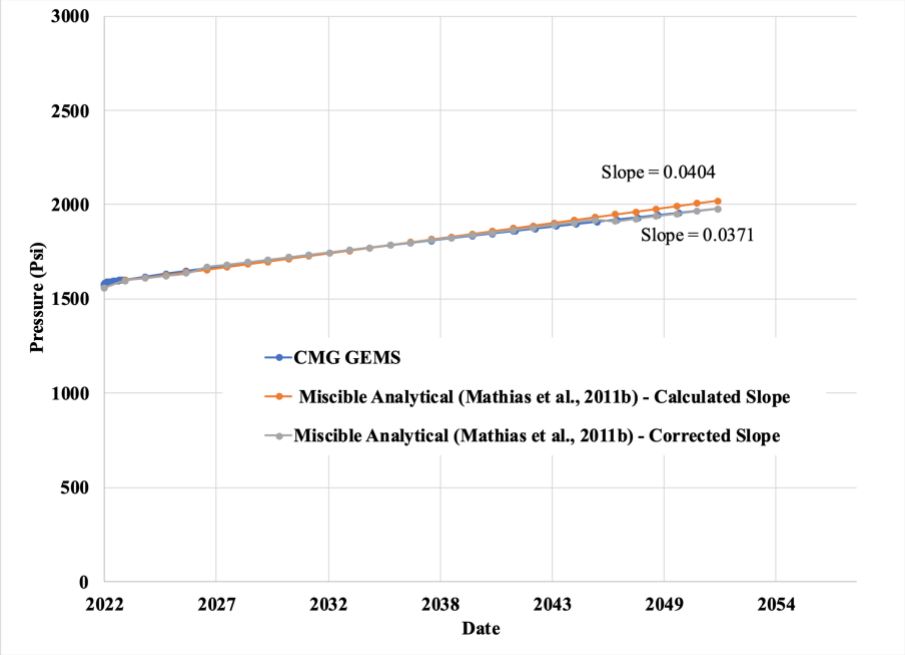

Figure 53: Pressure buildup comparison between analytical and numerical methods at 750ft from injection well site for 45587ft radial extent

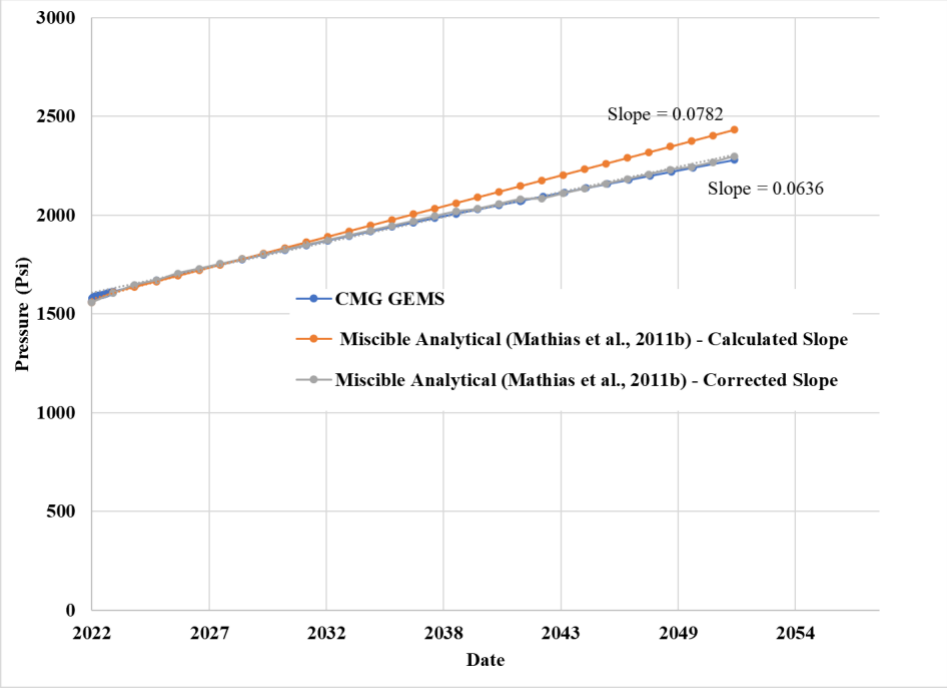

Figure 54: Pressure buildup comparison between analytical and numerical methods at 750ft from injection well site for 32822ft radial extent.